University of Windsor
Scholarship at UWindsor

Electronic Theses and Dissertations | Theses, Dissertations, and Major Papers

2005

Vehicle interior sound and vibration numerical estimation method based on engine radiated sound and mount vibration

Nikolina Kojovic
University of Windsor

Follow this and additional works at: https://scholar.uwindsor.ca/etd

Recommended Citation

Kojovic, Nikolina, "Vehicle interior sound and vibration numerical estimation method based on engine radiated sound and mount vibration" (2005). *Electronic Theses and Dissertations*. 4515.
https://scholar.uwindsor.ca/etd/4515

This online database contains the full-text of PhD dissertations and Masters' theses of University of Windsor students from 1954 forward. These documents are made available for personal study and research purposes only, in accordance with the Canadian Copyright Act and the Creative Commons license—CC BY-NC-ND (Attribution, Non-Commercial, No Derivative Works). Under this license, works must always be attributed to the copyright holder (original author), cannot be used for any commercial purposes, and may not be altered. Any other use would require the permission of the copyright holder. Students may inquire about withdrawing their dissertation and/or thesis from this database. For additional inquiries, please contact the repository administrator via email (scholarship@uwindsor.ca) or by telephone at 519-253-3000ext. 3208.

VEHICLE INTERIOR SOUND AND VIBRATION NUMERICAL ESTIMATION METHOD BASED ON ENGINE RADIATED SOUND AND MOUNT VIBRATION

by

Nikolina Kojovic

A Thesis
Submitted to the Faculty of Graduate Studies and Research
Through the Department of Mechanical, Automotive and Materials Engineering
In Partial Fulfillment of the Requirements for
The Degree of Master of Applied Science at the
University of Windsor

Windsor, Ontario, Canada
2005

Reproduced with permission of the copyright owner. Further reproduction prohibited without permission.

Library and Archives Canada

Published Heritage Branch

395 Wellington Street
Ottawa ON K1A 0N4
Canada

Bibliothèque et Archives Canada

Direction du Patrimoine de l'édition

395, rue Wellington
Ottawa ON K1A 0N4
Canada

Your file Votre référence
ISBN: 0-494-04982-0
Our file Notre référence
ISBN: 0-494-04982-0

NOTICE:
The author has granted a non-exclusive license allowing Library and Archives Canada to reproduce, publish, archive, preserve, conserve, communicate to the public by telecommunication or on the Internet, loan, distribute and sell theses worldwide, for commercial or non-commercial purposes, in microform, paper, electronic and/or any other formats.

The author retains copyright ownership and moral rights in this thesis. Neither the thesis nor substantial extracts from it may be printed or otherwise reproduced without the author's permission.

AVIS:
L'auteur a accordé une licence non exclusive permettant à la Bibliothèque et Archives Canada de reproduire, publier, archiver, sauvegarder, conserver, transmettre au public par télécommunication ou par l'Internet, prêter, distribuer et vendre des thèses partout dans le monde, à des fins commerciales ou autres, sur support microforme, papier, électronique et/ou autres formats.

L'auteur conserve la propriété du droit d'auteur et des droits moraux qui protège cette thèse. Ni la thèse ni des extraits substantiels de celle-ci ne doivent être imprimés ou autrement reproduits sans son autorisation.

In compliance with the Canadian Privacy Act some supporting forms may have been removed from this thesis.

While these forms may be included in the document page count, their removal does not represent any loss of content from the thesis.

Conformément à la loi canadienne sur la protection de la vie privée, quelques formulaires secondaires ont été enlevés de cette thèse.

Bien que ces formulaires aient inclus dans la pagination, il n'y aura aucun contenu manquant.

Canada

Reproduced with permission of the copyright owner. Further reproduction prohibited without permission.

1021843

© Nikolina Kojovic 2005

Reproduced with permission of the copyright owner. Further reproduction prohibited without permission.

ABSTRACT

A study was undertaken to develop a numerical estimation method for vehicle interior sound and vibration based on 5.4L V8 engine radiated sound and mount vibration and to quantify the contributions of vibroacoustic paths to vehicle interior sound and vibration. The modal analysis included acoustic and mechanical excitation of the frame and body assembly of a light truck. It was performed to estimate the sound and vibration transmission characteristics from the engine compartment to vehicle interior. The respective frequency response functions were then combined with frequency based source (engine radiated sound and forces transmitted through the mounts) data to estimate the response at the receivers. The response was characterized as the binaural sound pressure and driver's seat track triaxial acceleration. The results were verified by actual vehicle interior sound and vibration measurements and subjective (jury) evaluations at relevant operating conditions.

The subjective evaluations indicated that despite similar overall levels measured the differences in perceived sound may still exist and are due to differences in transfer path contribution to interior sound, as seen from interaural sound measurements (between left and right ear). The adverse changes in interior vibration comfort were related to the change in rate of change of acceleration known as jerk. The Z-direction acceleration of the seat was found to be sufficient in describing interior vibration; the directions of vibration were indiscernible by the jury in subjective evaluations.

Although there were slight differences in transfer path contribution the effect of using a more production efficient cast iron crank engine compared to a more durable steel crank

Reproduced with permission of the copyright owner. Further reproduction prohibited without permission.

engine, both used in the study, is negligible in terms of interior sound and vibration as indicated in estimated, objective and subjective results.

Reproduced with permission of the copyright owner. Further reproduction prohibited without permission.

DEDICATION

This work is dedicated to my parents.

Reproduced with permission of the copyright owner. Further reproduction prohibited without permission.

ACKNOWLEDGEMENTS

The author would like to express her appreciation to Dr. Jimi Tjong for his dedication, guidance and encouragement throughout the duration of this study. Thanks are also due to Dr. M. Ahmadi, Dr. E. K. L. Tam and Dr. R. G. S. Gaspar for their assistance and comments.

The author would also like to thank the members of Powertrain Engineering Research and Development Centre and Rose City Ford Sales Limited and dynamometer technicians at Ford Essex Engine Plant for their assistance in experimental set up and data collection.

Reproduced with permission of the copyright owner. Further reproduction prohibited without permission.

TABLE OF CONTENTS

ABSTRACT iv
DEDICATION vi
ACKNOWLEDGEMENTS vii
LIST OF TABLES xi
LIST OF FIGURES xii
NOMENCLATURE xiv

CHAPTER 1: INTRODUCTION 1

CHAPTER 2: LITERATURE SURVEY 3
2.1 Vehicle Interior Sound and Vibration 3
2.2 Transfer Path Analysis 5
2.2.1 Air-borne Sound Pressure Inputs 6
2.2.2 Air-borne Frequency Response Function Measurements 7
2.2.3 Structure-borne Operating Force Inputs 8
2.2.3.1 Direct Method 8
2.2.3.2 Indirect Method 9
2.2.3.2.1 Mount Stiffness Method 9
2.2.3.2.2 Matrix Inversion 10
2.2.4 Structure-borne Frequency Response Function Measurements 11
2.3 Finite Element Analysis 12
2.4 Interior Sound and Vibration Measurement and Analysis Techniques 13
2.4.1 Interior Sound and Vibration Objective Evaluation 13
2.4.1.1 Sound Pressure and Acceleration Measurements 15
2.4.1.1.1 Binaural Recordings 16
2.4.1.1.2 Monaural Recordings 17
2.4.1.1.3 Equalization 18
2.4.1.2 Sound Quality Metrics 18
2.4.2 Interior Sound and Vibration Subjective Evaluation 19
2.5 Conclusions 20

CHAPTER 3: THEORY 21
3.1 Sound and Vibration Transducers 21
3.1.1 Microphones 22
3.1.1.1 Free Field Microphones 22
3.1.1.2 Diffuse Field Microphones 23
3.1.1.3 Binaural Head 23
3.1.2 Accelerometers 23
3.1.2.1 Integrated Circuit Piezoelectric Accelerometers 24
3.1.2.2 Charge Amplified Accelerometers 24
3.2 Structural Excitation Signal Sources 25
3.2.1 Impact Hammers 25

Reproduced with permission of the copyright owner. Further reproduction prohibited without permission.

3.2.2 Loudspeakers 26
3.3 Analog to Digital Conversion 26
3.3.1 Fixed Sampling 26
3.3.1.1 Sampling Frequency Considerations 28
3.3.1.1.1 Aliasing 29
3.3.1.1.2 Filtering 30
3.3.1.2 Sampling Period Considerations 31
3.3.1.2.1 Leakage 31
3.3.1.2.2 Windowing 31
3.3.2 Variable Sampling Frequency 32
3.3.2.1 Tracking Trace Acquisition and Resampling Techniques 32
3.3.3 Quantization Concepts 34

CHAPTER 4: EXPERIMENTAL DETAILS 35
4.1 Interior Sound and Vibration Numerical Estimation Method 35
4.2 Powertrain Sources of Vehicle Interior Sound and Vibration 37
4.2.1 Semi-Anechoic Engine Dynamometer Test Cell 38
4.2.1.1 Powertrain Radiated Sound 38
4.2.1.2 Mount Vibration 41
4.2.2 Operating Conditions 42
4.3 Frequency Response Function Measurements 43
4.3.1 Acoustic Excitation 44
4.3.2 Impact Excitation 46
4.4 Interior Sound and Vibration Measurements 48
4.5 Subjective Evaluation of Interior Sound and Vibration 49

CHAPTER 5: DATA ANALYSIS METHODS 50
5.1 Analysis Overview for Estimated Interior Sound and Vibration 50
5.2 Time Domain Analysis 52
5.2.1 Root Mean Square 53
5.3 Frequency Domain Analysis 53
5.3.1 Fourier Analysis 54
5.3.1.1 Fourier Transform 56
5.3.1.2 Tracked Spectral Processing 56
5.4 Integration of Acceleration Signal to Obtain Displacement 58
5.5 Frequency Response Functions 59
5.5.1 Coherence 62

CHAPTER 6: RESULTS AND DISCUSSION 64
6.1 Engine Radiated Sound and Mount Vibration 64
6.2 Frequency Response Functions 66
6.2.1 Coherence 67
6.3 Vehicle Interior Sound and Vibration Evaluation 73
6.3.1 Objective Evaluation 73
6.3.2 Subjective Evaluation 81
6.3.2.1 Binaural Replay 84

Reproduced with permission of the copyright owner. Further reproduction prohibited without permission.

CHAPTER 7: CONCLUSIONS AND RECOMMENDATIONS 86
7.1 Conclusions 86
7.1.1 Significant Contributions to Research 87
7.2 Recommendations 88

REFERENCES 89

BIBLIOGRAPHY 93

APPENDICES 94
A. SUMMARY CHART OF THE REFERENCES 95
B. FREQUENCY RESPONSE FUNCTIONS 97
C. INTERIOR SOUND AND VIBRATION RECEIVER RESULTS 117
D. EQUIPMENT SPECIFICATIONS 135

VITA AUCTORIS 142

Reproduced with permission of the copyright owner. Further reproduction prohibited without permission.

LIST OF TABLES

Table 4.1: Air-borne and Structure-borne Sources Considered..... 37

Table 6.1: Transfer Path Contribution Ranking..... 81

Reproduced with permission of the copyright owner. Further reproduction prohibited without permission.

LIST OF FIGURES

Figure 3.1: Fixed Sampling Frequency (uniform sample spacing) 27

Figure 3.2: The Effect Aliasing in the Time Domain - a. Analog Signal, fm = 10 Hz, b. Sampled Signal, fs = 50 Hz, c. Sampled Signal, fs = 15 Hz. 28

Figure 3.3: The Effect Aliasing in the Frequency Domain 30

Figure 3.4: Raw, time domain CID signal (a) and corresponding resampled, averaged CID signal (b). 34

Figure 4.1: Transfer Path Sign and Naming Convention 36

Figure 4.2: Air-borne Source Measurements - Location of Transducers (a) and Experimental Setup (b). 40

Figure 4.3: Structure-borne Sources Measurements - Location of Engine and Transmission Mounts (a) and Left Engine Mount Transducers (b). 42

Figure 4.4: Acoustic Excitation in the Engine Compartment - Front Direction. 46

Figure 4.5: Hammer Impact Excitation, Right Mount, X-direction. 47

Figure 4.6: Interior Noise (a) and Vibration (b) Measurement Sensors and Locations.... 48

Figure 5.1: Vehicle Interior Sound and Vibration Numerical Estimation Method Overview 51

Figure 5.2: Example of Inertance FRF (a) and Corresponding Coherence Function (b). 62

Figure 6.1: Right Engine Radiated Sound [Pa], Steel Crank Engine 65

Figure 6.2: Left Mount, Z-direction Force [N], Steel Crank Engine. 65

Figure 6.3: Frequency Response Function, Right Mount, Y-direction Input, Triaxial Acceleration Output. 69

Figure 6.4: Coherence, Right Mount, Y-direction Input, Triaxial Acceleration Output. . 69

Figure 6.5: Frequency Response Function, Right Mount, Y-direction Input, Binaural Sound Pressure Output. 70

Reproduced with permission of the copyright owner. Further reproduction prohibited without permission.

Figure 6.6: Coherence, Right Mount, Y-direction Input, Binaural Sound Pressure Output. 70

Figure 6.7: Frequency Response Function, White Noise Left Input, Triaxial Acceleration Output. 71

Figure 6.8: Coherence, White Noise Left Input, Triaxial Acceleration Output. 71

Figure 6.9: Frequency Response Function, White Noise Left Input, Binaural Sound Pressure Output..... 72

Figure 6.10: Coherence, White Noise Left Input, Binaural Sound Pressure Output..... 72

Figure 6.11: Estimated Interior Sound Pressure [Pa], Right Ear, Steel Crank Engine..... 74

Figure 6.12: Actual Interior Sound Pressure [Pa], Right Ear, Steel Crank Engine. 74

Figure 6.13: Estimated and Actual Interior Sound, Right Ear, Steel Crank Engine..... 77

Figure 6.14: Estimated and Actual Interior Sound, Left Ear, Steel Crank Engine..... 77

Figure 6.15: Estimated and Actual Interior Vibration, Z-direction, Steel Crank Engine. 78

Figure 6.16: Transfer Path Contribution to Interior Sound - Right Ear, Steel Crank Engine. 79

Figure 6.17: Transfer Path Contribution to Interior Sound - Left Ear, Steel Crank Engine. 80

Figure 6.18: Interior Sound, Subjective Evaluation - Average..... 82

Figure 6.19: Overall Perception of Interior Sound, Subjective Evaluation - Average..... 83

Figure 6.20: Overall Perception of Seat Vibration, Subjective Evaluation - Average..... 83

Reproduced with permission of the copyright owner. Further reproduction prohibited without permission.

NOMENCLATURE

ACT	Active Path Tracking
ASQ	Air-borne Source Quantification
CID	Cylinder Identification
CPS	Crankshaft Position Sensor
dB	decibel
F	operating force
$F(\omega)$	operating mount force function
f_m	maximum signal frequency
f_s	sampling frequency
FEA	Finite Element Analysis
FFT	Fast Fourier Transform
$H(\omega)$	frequency response function
i	data index
j	data index
K_i	elastic rate of an isolator
$k(\omega)$	(complex) mount stiffness function
L	sound pressure level
M	number of air-borne paths
N	number of structure-borne paths
NVH	Noise, Vibration and Harshness
P	sound pressure
P_{air}	air-borne sound pressure contribution to interior sound
P_i	partial contribution to interior sound pressure
P_0	reference rms sound pressure
$P_{structure}$	structure-borne sound pressure contribution to interior sound
P_t	total interior sound pressure
PCA	Principal Component Analysis
$\dot{Q}$	volume acceleration
$r(\omega)$	magnitude of receiver (sound or vibration) function for a single transfer path
$R(\omega)$	total magnitude of receiver function due to all transfer paths
rms	root mean square
$s(\omega)$	magnitude of source (sound or vibration) function
S_i	surface area of a patch
$S_{xx}(\omega)$	autopower spectrum
$S_{xy}(\omega)$	crosspower spectrum
SDF	Standard Data Format
t	time
T	period of measurement
TDF	Test Data File
TPA	Transfer Path Analysis

Reproduced with permission of the copyright owner. Further reproduction prohibited without permission.

ω	frequency
X	displacement
$\ddot{X}$	acceleration
$X_a(\omega)$	displacement of the active side of mount
$X_p(\omega)$	displacement of the passive side of mount
γ^2	coherence function

Reproduced with permission of the copyright owner. Further reproduction prohibited without permission.

CHAPTER 1: INTRODUCTION

One of the main areas of consideration in defining vehicle customer satisfaction is vehicle interior sound and vibration. Engine radiated sound and mount vibration are significant contributors to vehicle interior sound and vibration. Characterizing their contribution requires a detailed and methodical analysis that may be used to establish baseline levels, identify manufacturing deficiencies, and influence design changes for baseline improvements of vehicle interior sound and vibration.

Component-level testing such as engine sound and vibration testing is performed frequently because it is more practical and less costly compared to similar vehicle-level testing. Thus, estimating vehicle performance based on engine performance can potentially provide cost reduction benefits at all stages of vehicle design and manufacturing. One of the goals of this study is to implement this estimation method in a major powertrain research facility. This can be undertaken by utilizing the available data acquisition and processing resources and optimizing the analysis parameters in order to estimate vehicle interior sound and vibration. In addition, the individual transfer path contributions to interior sound and vibration that are obtained by using this method may be used to justify possible structural design modifications for improved vibroacoustic sensitivity of the vehicle. In this study, a practical example is used to demonstrate the application of the method. This was done by investigating and comparing vehicle interior sound and vibration by switching between a cast iron crankshaft and a steel crankshaft. Both crankshafts are currently used in production. The cast iron crankshaft offers improved productivity and a reduced cost; however, it does not provide the same

Reproduced with permission of the copyright owner. Further reproduction prohibited without permission.

durability performance as the steel version. The cast iron crankshaft is used on a needs-only basis.

The research objectives of this study are to:

1. Develop a vehicle interior sound and vibration numerical estimation method based on engine radiated sound and mount vibration and verify the estimations by actual vehicle interior sound and vibration measurements at all operating conditions under investigation.
2. Evaluate the contribution of individual engine air-borne and structure-borne sources of sound and vibration to the total vehicle interior sound and vibration.
3. Obtain relationships between objective measurements and subjective evaluations of interior sound and vibration.
4. Investigate the effect of using a more cost-effective cast iron crankshaft on the vehicle interior sound and vibration, compared to a more durable steel crankshaft currently used in production.

Reproduced with permission of the copyright owner. Further reproduction prohibited without permission.

CHAPTER 2: LITERATURE SURVEY

A customer's assessment of vehicle quality is strongly dependent on the vehicle interior sound and vibration (vibroacoustic) characteristics. In order to achieve improvements to vibroacoustic quality, it is necessary to first identify the relevant sources, paths and receivers of sound and vibration. The next steps are to quantify them through measurements and to assess their impact to vibroacoustic quality through data analysis, the results of which are then used to modify their properties through product or process design changes. This chapter is a literature review of analytical, numerical and experimental methods and analysis techniques currently used to quantify contributions and investigate the effect of sound and vibration sources on vehicle interior sound and vibration. Their advantages and disadvantages are emphasized as they pertain to testing, processing and analysis parameters chosen for this study.

2.1 Vehicle Interior Sound and Vibration

There are numerous sound and vibration sources that contribute to the overall level and quality of sound and vibration perceived in the vehicle interior. It is important to identify these sources and understand their causes and transfer mechanisms in order to reduce their undesirable effects. The goal is often to establish vibroacoustic baselines in order to detect causes of deviations from the baselines, such as quality issues, by finding the most effective data collection and analysis method. In certain cases, the sound and vibration studied at a component level, such as a cylinder block or a cylinder head [34], may provide insight to a possible interior sound and vibration issue. For an in-depth

Reproduced with permission of the copyright owner. Further reproduction prohibited without permission.

understanding of causes of undesirable interior sound and vibration, both sources and transfer paths must be considered. The complexity of sound and vibration transfer mechanisms from the sources to the receiver locations points to a need for careful assessment.

The vehicle interior sound and vibration is a combination of air-borne and structure-borne transfer paths. The behaviour of principal sources of sound and vibration are dependant on the vehicle design and its operating conditions. Examples of vibroacoustic sources include wind and road, powertrain, intake and exhaust systems and others. The total sound and vibration level in the vehicle interior is a sum of partial pressures and accelerations caused by all air-borne and structure-borne delivery paths from the sources of sound and vibration. For the case of total interior sound, for M air-borne paths and N structure-borne paths, the total interior sound pressure (equation 2.1) can be expressed as:

$$P = \sum_{i=1}^{M} (P_{air})_i + \sum_{j=1}^{N} (P_{structure})_j \qquad (2.1)$$

In order to identify the most significant vibroacoustic sources according to their contribution to the interior sound and vibration levels a method known as Principal Component Analysis (PCA) is often used. Unruh et al [40] used PCA to identify interior noise contributions of engine vibration and air-borne propeller and engine exhaust noise in propeller driven aircraft. The most common method used to estimate the interior sound and vibration is known as the Transfer Path Analysis.

Reproduced with permission of the copyright owner. Further reproduction prohibited without permission.

2.2 Transfer Path Analysis

The Transfer Path Analysis (TPA) is an experimental technique used to establish the effect of individual air-borne and structure-borne paths on the interior sound and vibration. The TPA method requires the vibroacoustic source and the transfer function data. A target response due to a single path, $r(\omega)$, is a combination of frequency response function, $H(\omega)$, and the magnitude of the source or excitation, $s(\omega)$, as shown in equation 2.2:

$$r(\omega) = H(\omega) \cdot s(\omega) \tag{2.2}$$

The total receiver sound pressure level, $R(\omega)$, is the sum of n partial pressures of the individual transfer paths, i, (equation 2.3).

$$R(\omega) = \sum_{i=1}^{n} \frac{r(\omega)}{s_i(\omega)} \cdot s_i(\omega) \tag{2.3}$$

The transfer function form depends on whether the sources and targets are pressures, accelerations, or combinations of both pressures and accelerations. Lee et al [20], for example, used TPA method to find the contribution of a shock absorber structure-borne noise to the driver seat sound pressure.

Other methods may be used in conjunction with TPA to estimate transfer path contributions to interior sound or vibration. Rust and Elinger [32] identified the structure-borne noise paths by the Active Path Tracking (APT) method. Here, the mount input forces are modeled and ranked in terms of their relative importance related to their ability to recreate the vehicle interior sound field that is under investigation. Typically,

Reproduced with permission of the copyright owner. Further reproduction prohibited without permission.

this method considers air-borne sound contributions up to 12 kHz and structure-borne contributions up to 2 kHz. In addition, Haste and Nachimuthu [17], established that the partial contribution to the total interior sound of an elastic isolator such as an engine mount is directly proportional to the sensitivity of the total acoustic pressure to a change in the elastic rate of the isolator in that path as shown in equation 2.4:

$$P_i = \Delta P_t \cdot \frac{K_i}{\Delta K_i} \tag{2.4}$$

Therefore, if an engine mount is replaced, the partial interior sound contribution of path corresponding to the mount may be calculated based on the mount stiffness and the measured total acoustic pressure before and after the change is implemented.

2.2.1 Air-borne Sound Pressure Inputs

The air-borne sound implies that the perceived sound is not transferred as a result of interacting mechanical parts between the source and the receiver. The contribution of air-borne transfer paths dominates at frequencies above 1.5 kHz [5]. The radiated sound is usually measured in terms of sound pressures from the direction of the source. An alternative method called Air borne Source Quantification (ASQ) may also be used and is described by Van Der Linden et al [41]. This method assumes that the contribution of a sound-radiating surface to the sound pressure at a particular location in the sound field is equivalent to the sum of contributions of equivalent point sources that can be modelled as vibrating patches or areas on the sound-radiating surface. The sound pressure at a particular location (i.e. sound pressure at one meter around an engine) can be estimated from the volume accelerations of the surfaces. The volume accelerations of these point

Reproduced with permission of the copyright owner. Further reproduction prohibited without permission.

sources are determined from the integral of accelerations normal to the surface over the surface area of the patch (see equation 2.5).

$$\dot{Q}_j = \int_S \ddot{X}_j \cdot dS \approx \ddot{X}_j \cdot S_i \tag{2.5}$$

Where $\dot{Q}_j$ is volume acceleration of surface i, $\ddot{X}_j$ is surface centre acceleration and S_i is surface area of patch. An important conclusion from this study is that a free field point source sound pressure can be approximated on the basis of surface vibration.

2.2.2 Air-borne Frequency Response Function Measurements

Air-borne frequency response functions measurements are performed in the engine compartment (with the powertrain removed) and receiver locations in the passenger compartment. Bocksch et al [5] used an engine noise simulator. It is a rectangular engine model with loudspeaker cones on its faces, and it is placed in the engine compartment after removal of the engine. An input signal with a frequency up to 12 kHz is commonly used as the test source [14]. Alternatively, a reciprocal method may be used to obtain air-borne frequency response functions. According to Lord Rayleigh's reciprocity law, the transmitter and receiver may be exchanged in order to determine the transfer behaviour of a system [1]. This implies that the excitation may be performed from the passenger compartment and the response measured in the engine compartment on all sides of the powertrain simultaneously.

Reproduced with permission of the copyright owner. Further reproduction prohibited without permission.

2.2.3 Structure-borne Operating Force Inputs

The structure-borne sound is transferred to the interior of a vehicle through forces caused by the interaction of mechanical parts. Common examples include connecting components such as engine mounts. The basic principle accounts for the vibrations produced by the source (for example an engine) that excites the supporting structure of a vehicle whose surfaces radiate sound perceived in the vehicle interior. The structure-borne sound up to approximately 800 Hz is a major contributor to interior sound quality [32]. This low frequency structure-borne sound up to 50 Hz can be estimated numerically, using a Finite Element Analysis method [25], or experimentally using transfer path analysis, as explained in the following sections.

The structure-borne sound and vibration operating forces may be measured directly, or determined indirectly. Both methods may be used and compared to verify the accuracy of the results [36]. It is also possible to use different methods on different paths. The choice of a method for a particular path depends on operating conditions and availability of data for that path.

2.2.3.1 Direct Method

The direct method implies that the forces are measured directly, in all three directions, possibly with a load cell. This method is not commonly used in practice since the measuring locations are often not easily accessible. Also, the lack of space between the engine and the engine mount, for example, makes it impractical to use force transducers. Thus, forces are usually estimated indirectly using the mount stiffness and matrix inversion methods as outlined in the following sections.

Reproduced with permission of the copyright owner. Further reproduction prohibited without permission.

2.2.3.2 Indirect Method

The indirect experimental or analytical methods are convenient when direct measurements are impractical. Hoffman and Dowling [19] used an analytical model to simulate engine dynamics and vibration, including forces transmitted through the mounts; however, this method is limited to low frequency vibration. Thus, experimental models are most commonly used. They employ measurements of transfer functions, physical characteristics of the mounts, and mathematical operations such as matrix inversion, as described in the next sections.

2.2.3.2.1 Mount Stiffness Method

The resulting force acting on the mount in a specific direction or path is a function of the stiffness of the mount and the difference in displacement between active and passive sides of the mount. Usually, the acceleration signals are obtained from the source and the body side of the mount and results are integrated twice to obtain the displacements. The relative displacement is the difference in displacement between the active and passive sides of the mount, and is proportional to the operating force, for a specific range of frequencies. The proportionality constant is the mount stiffness (see equation 2.6).

$$F(\omega) = k(\omega) \cdot (X_a(\omega) - X_p(\omega)) \tag{2.6}$$

Consequently, the mount stiffness is a function of rotational speed (frequency) of the engine, as well as the direction of motion. This function is also known as the complex stiffness function. Each path requires a stiffness function in order to obtain an estimate of its operating force. The accuracy of this estimate is a strong function of the stiffness

Reproduced with permission of the copyright owner. Further reproduction prohibited without permission.

function accuracy. The stiffness function is determined experimentally, using hydraulic high frequency rate testing machines that apply a sinusoidal excitation of varying frequency to the mount, while controlling variables such as temperature and preload. The engine mount stiffness must be optimized such that it provides adequate rigidity to reduce the interior vibration amplitudes but enough softness to ensure desired level of comfort [30]. Diemer et al [7] provided guidelines to reduce the effect of mount bracket resonance on the interior vehicle noise, such that the resonance is above approximately 700 Hz, and thus, above low frequencies characteristic of structure-borne vibration. Muller et al [27] designed an active engine mount. It was a combination of a classical hydromount and an electromagnetic actuator, in order to reduce sound and vibration levels from the engine to vehicle structure and into the passenger compartment.

In order to obtain valid results using the mount stiffness method the difference in displacement of the active and passive sides of the mounts must be significant. Generally, if this difference is smaller than approximately ten decibels, or if an accurate estimate of mount stiffness is unavailable, the mount stiffness method is no longer adequate and the matrix inversion method must be used.

2.2.3.2.2 Matrix Inversion

The cross-coupling effect is the interaction between different paths. In most practical situations it is present and needs to be considered. It is taken into account by performing a full matrix inversion, as opposed to a point inversion, which neglects cross-coupling effects. The information required for the matrix inversion method includes transfer functions and acceleration measurements between sources and receiver locations. The

Reproduced with permission of the copyright owner. Further reproduction prohibited without permission.

accelerations are measured at the receiver side, under operating conditions. In addition, it is necessary to remove the source prior to obtaining measurements using the matrix inversion method. The method is illustrated by matrix equation 2.7.

$$\begin{bmatrix} F_1 \\ F_2 \\ F_3 \\ \cdots \\ F_i \end{bmatrix} = \begin{bmatrix} \frac{\ddot{X}_{11}}{F_1} & \frac{\ddot{X}_{12}}{F_2} & \frac{\ddot{X}_{13}}{F_3} & \cdots & \frac{\ddot{X}_{1i}}{F_i} \\ \frac{\ddot{X}_{21}}{F_1} & \cdot & & & \cdot \\ \frac{\ddot{X}_{31}}{F_1} & & \cdot & & \cdot \\ \cdots & & & \cdot & \cdot \\ \frac{\ddot{X}_{j1}}{F_1} & \cdot & \cdot & \cdot & \frac{\ddot{X}_{ij}}{F_n} \end{bmatrix}^{-1} \cdot \begin{bmatrix} \ddot{X}_1 \\ \ddot{X}_2 \\ \ddot{X}_3 \\ \cdots \\ \ddot{X}_i \end{bmatrix} \tag{2.7}$$

If the cross-coupling effect is neglected, only diagonal elements of the above matrix are considered. The effectiveness the matrix inversion method depends on the accuracy of frequency response function measurements.

2.2.4 Structure-borne Frequency Response Function Measurements

The relationship between the force input and acoustic (sound) or tactile (acceleration) output is expressed in terms of structure-borne frequency response function. The required triaxial force excitation may be applied by an electro-dynamic shaker or an impact hammer. Although shakers provide a more controlled input at low frequencies, they require more space for application than most impact test devices, and they are often impractical to use [14]. If hammer excitation is used, the hammer tip material must be properly selected. Ferraz and Cherman [11] used impact hammer excitation to acquire frequency response functions in the range of 10 to 600 Hz. The measurement required a plastic-nylon tip to obtain high frequency information and a soft rubber tip to obtain low

Reproduced with permission of the copyright owner. Further reproduction prohibited without permission.

frequency information. Alt et al [1] experimented with steel and rubber hammer materials and determined that the lowest possible frequency resulting in sufficient correlation between inputs and outputs occurred only above 100 Hz for a steel tip, and above 30 Hz for a rubber tip.

In addition, it is important to ensure controlled test conditions and to identify parameters that introduce variability. Liu and Frenz [21] identified the structural non-linearity causing automotive seat free-play and affecting the quality of the frequency response function measurements, particularly for hammer impact applications. In this case, shaker inputs must be used to keep the force levels within the linear region of the structure. When accessibility is an issue such as the case when a powertrain is not removed for the purposes of FRF measurements, a high performance hand-held miniature shaker is recommended due to the limited available space in the engine compartment [32]. The structure-borne frequency response function methodology may also be used to determine optimum seat system design for desirable level of ride comfort. Boardman and Paddan [4] estimated, using multiple test occupants, the occupied seat transfer function between the shaker force input and seat cushion surface acceleration output. Madjlesi et al [24] used an FRF-based model in conjunction with optimization algorithms for mount system design in order to reduce vibration levels.

2.3 Finite Element Analysis

The numerical computations using finite element analysis (FEA) can also be used to estimate the interior noise levels at lower frequencies, typically up to 50 Hz. Unfortunately, the number of nodes and the computing power required for this type of analysis are rather large. In addition, the model accuracy is uncertain, as the properties of

Reproduced with permission of the copyright owner. Further reproduction prohibited without permission.

interior materials such as seats are difficult to model [25]. The analysis that considers higher frequencies is computationally intensive and thus impractical. For simple geometries and loading conditions, such as a uniformly loaded plate, the FEA method may be used to optimize the design to minimize noise radiation efficiency and reduce the sound power [28]. In addition, the FEA methodology has been successfully implemented for a component level design optimization. For example, Wang et al [44] used a full vehicle system finite element model, parameterized mount stiffness and location to obtain an optimum set of parameters for idle shake performance improvement, measured in terms of seat track vibration levels.

2.4 Interior Sound and Vibration Measurement and Analysis Techniques

Sound is transmitted as small pressure fluctuations in a fluid medium. The undesirable sound is classified as noise. This classification is often determined subjectively, or objectively, by calculating sound quality metrics based on measured data. The acceptable correlation between the two methods is a strong indicator of a complete assessment of sound quality. A similar argument is valid for vibration measurements and ride comfort. The following sections summarize the available methods for both, subjective and objective evaluations of interior sound and vibration.

2.4.1 Interior Sound and Vibration Objective Evaluation

The objective indicators of quality of interior sound and vibration are obtained by post processing sound pressure and acceleration measurements. Pinto et al [30], for example, used kurtosis in conjunction with spectral analysis based on raw, time data to establish acceptable limits of sound and vibration and detect excessive noise, mechanical impulses

Reproduced with permission of the copyright owner. Further reproduction prohibited without permission.

and collisions felt by the driver, caused by a specific quality issue such as an engine shaking phenomenon. Silveira et al [35] presented a general overview of vibroacoustic theory, mainly frequency domain analysis, and its applications to seat track acceleration and driver's outer ear sound pressure measurements processing. Alternative methods of sound and vibration data analysis for a system or component diagnostic purposes include Wavelet analysis [37], Statistical Energy Analysis [43], component and operational variability analysis [29] and crank angle domain analysis [38].

The noise reduction and sound quality in the vehicle interior are important aspects of vehicle design. Numerous applications of design of components for reduced noise or improved sound quality are continuously researched. For example, Esposito and Freeman [9] studied the effect of laminated side windows on the overall noise reduction in the critical frequency range for human conversation, by quantifying transmission loss of different window side glass designs. The objective parameters may also be used for component design improvements at the powertrain level. For example, Grasso et al [15] used "engine presence" (sound pressure in the range of 220 to 700 Hz) and booming noise (rapid rise in second engine order) as objective parameters to optimize NVH of engine oil sump, torsional damper and flexible flywheel. Also, Hemingray [18] related the balancing limits of rotating components, such as engine crankshafts, brake drums, tire and wheel assemblies to the human perception of vibration. Other examples of objective parameters include the following research. Gu [16] investigated human seat ride comfort for vibration at low frequency in the vertical direction using a spring-mass dummy, and related the results to tests with human occupants using transmissibility as a comparison criterion. Amman et al [2] incorporated weighing factors to root mean square (RMS)

Reproduced with permission of the copyright owner. Further reproduction prohibited without permission.

accelerations (typically used to quantify interior vibration) in three orthogonal directions (vertical, lateral and longitudinal), due to the difference in human sensitivity to vibration in different axis directions. Verver and Van Hoof [42] used a human and seat mathematical model (based on FEA and multibody techniques) to estimate comfort based on a series of transmissibility functions, coupled with a human model validation. Lastly, the objective parameters may also be based on studies with large groups of people whose perception of different sounds is used to calculate various psychoacoustic metrics. For example, Renzo et al [31] developed acoustic and vibrational quality indices by correlating results from experimental road tests and jury testing.

2.4.1.1 Sound Pressure and Acceleration Measurements

In order to evaluate sound quality parameters objectively, sound pressure measurements are required. Sound pressure measurements are only a starting point and are inadequate for comprehensive description of perceived sound quality. Different methods exist and are used to measure the sound pressure level in the vehicle interior, depending on the type of sensor (i.e. microphone) and its orientation with respect to the source. The choice of a method is dependent on the purpose of the experiment. Dumbacher et al [8] described the appropriate measurement parameters such as microphone spacing and placement from the test surface, and number of microphones for correct application of acoustic holography techniques. Schroeder [33] estimated interior sound pressure at driver's ear for a heavy commercial truck using thirty-four surface patches (interior noise sources) surrounding the driver space and both, free field and diffuse field models in conjunction with sound intensity measurements. The visualization of interior sound using the sound

Reproduced with permission of the copyright owner. Further reproduction prohibited without permission.

intensity techniques is also important in selecting an optimum placement for a sound absorber or insulator in the vehicle [26].

2.4.1.1.1 Binaural Recordings

The perceived sound quality is a function of both, physical and psychological characteristics of human hearing. Thus, sole free field sound pressure measurements are not adequate in describing sound quality. The human ear is a nonlinear, complex sensor, with specific frequency dependent transmission characteristics, and the physics of human hearing is one of the prime reasons for different subjective quality of sounds of equal sound pressure. In addition, the fact that hearing is binaural (involves two ears) has a considerable influence on sound perception.

The human brain is capable of performing the spatial localization of sound, and suppression of unwanted sounds in the presence of significant background noise. The perception of specific sounds in a complex sound field involving many sound sources at different spatial positions is also dependant on the binaural nature of hearing, the differences between the noise levels and phase occurring between the left and the right ear. This phenomenon is known as the "party" effect. The localization of sound below approximately 1500 Hz is due to the phase difference between the two signals, while above this frequency the interaural level difference and difference in spectrum will be the determining factor in localizing sound.

The binaural technique consists of procedures related to recording, analysis, processing and evaluation of signals from acoustical input to both ears of the listener. Due to the complexity of signal processing in human hearing, the differences in sound level and

Reproduced with permission of the copyright owner. Further reproduction prohibited without permission.

phase can occur between the left and the right ear, especially the case when different sound sources exist at various spatial positions. Consequently, binaural recordings offer an advantage in terms of hearing sound in an aurally equivalent way [12, 14]. The data is collected using two microphones that simulate human ears. They are placed in the physical model of the human head, shoulders and torso, because they simulate the combined effects of the diffraction of the sound waves reaching the eardrums.

A common research topic is a study of the extent to which the subjective evaluation of interior noise is influenced by level and phase differences between the left and right ears [13]. The play back is performed using headphones, such that the recorded sound is reproduced accurately in each ear without the effects of background noise. This provides consistency in evaluations of sound quality by several evaluators. As stated above, the binaural recordings include many benefits, however, there are some limitations as well. The evaluations are typically based on sound recordings only thus excluding the effects of vibration and visual stimuli.

2.4.1.1.2 Monaural Recordings

The sound pressure field is usually measured using a large array of microphones distributed throughout the vehicle passenger space [32]. Mukai et al [26] used a three-dimensional sound intensity probe ("tetraphone"), constructed from four microphones in order to capture sound pressure at about a thousand receiving points for sound evaluation. Psychoacoustic metrics such as loudness, sharpness, fluctuation strength, roughness and pitch are calculated on the basis of conventional microphone recordings. However, these recordings are not suitable for hearing sessions and replaying of sound, as the hearing

Reproduced with permission of the copyright owner. Further reproduction prohibited without permission.

perception is very different from that in the actual sound field, due to the effects of the human head and torso.

2.4.1.1.3 Equalization

The equalization is a technique used to transform data from binaural measurements to corresponding microphone measurements in the same sound field. Conversely, the microphone data may be transformed to include the effects of head and torso in order to simulate the binaurally recorded data [22, 23]. The sound quality metrics are based on free field microphone readings, as they include the physical and the psychological effects of human hearing. Thus, unless an accurate reproduction of sound is required, free field microphone data is adequate for obtaining sound pressure levels.

2.4.1.2 Sound Quality Metrics

A full explanation of sound perception is a function of psychological factors, interpretation of sounds affected by attitude, environment and context, in addition to physics of sound perception. The science of sound perception from both physical and psychological point of view is called psychoacoustics. Due to the complexity of sound processing by the human brain, the sound perception is not easily correlated with the physical characteristics of sound. Various experiments are required to collect data necessary to develop sound quality metrics to objectively quantify sound properties. These metrics consider time as well as spectral properties of the signals. Terazawa and Wakita [39] used psychoacoustic index "powerfulness" based on subjective tests to characterize interior sound resulting from intake noise. Other commonly used metrics are loudness, speech interference level, and articulation index.

Reproduced with permission of the copyright owner. Further reproduction prohibited without permission.

2.4.2 Interior Sound and Vibration Subjective Evaluation

The physical characterization of sound and vibration, in terms of sound pressure and body acceleration measurements, respectively, are usually inadequate as single indicators of sound quality or ride comfort. Ultimately, the customer's opinion is the deciding factor in defining product quality; thus, the vehicle interior sound and vibration are often evaluated subjectively.

The interior noise may be described subjectively by assessing its "pleasantness" [1], "powerfulness", "sportiness" and "luxury" [3], or an evaluation scale based on perceived annoyance ranging from 1 to 10. Feng et al [10] used "roughness" as a subjective criterion to describe annoying properties of powertrain sounds and correlated it to psychoacoustic, objective unit of roughness. In terms of subjective evaluations of vibrations, acceptable comfort levels may be described as "little uncomfortable" or "not uncomfortable" as used by Hemingray [18].

A common test method used for vibroacoustic sound quality evaluation, particularly interior noise, is jury testing. Jury testing is a process involving a team of specialists or customers that judge the sound quality by evaluating various sound characteristics. In a typical jury evaluation test, the participants are exposed to samples of powertrain noise either by driving the vehicle or by listening to various sound recordings over headphones. The evaluation methods may include numerical ratings based on previously mentioned assessment criteria. Other methods include ranking and paired comparisons. The effectiveness of subjective evaluation tests is dependent on the consistency of parameters such as testing procedure, the listening environment and level of training and experience of participants. In general, the subjective evaluation process is costly, time consuming

Reproduced with permission of the copyright owner. Further reproduction prohibited without permission.

and inconsistent due to the strong dependency of results on experience of drivers or participants. There are currently no standard subjective measurement procedures. In fact, since user defined metrics are often used to describe the vehicle sound quality and ride comfort, the required consistency, reliability and repeatability of results are difficult to achieve. Brandl and Biermayer [6] discovered that even with a common subjective evaluation test procedure and operating conditions there are additional factors that affect the outcome. An example of this is brand bias related to the impact of marketing activities of individual vehicle manufacturers on the driver that influence driver's perception of vibroacoustic quality. In addition, there are intercultural differences related to interior noise or vibration quality ratings. For example, Japanese drivers prefer higher frequency content and dislike high amplitude of low frequency interior noise content compared to European drivers under the same test conditions.

2.5 Conclusions

The interior sound and vibration estimation method used in this study was based on techniques known in literature as transfer path analysis. The literature survey conducted was subdivided into the stages of testing and data processing required for this analysis. The advantages and disadvantages of parameters chosen in past research were listed in order to justify those chosen for the study. Specific examples include the indirect, mount-stiffness method used to quantify operating forces versus the direct measurement method, and the use of impact hammers as opposed to mechanical shakers to measure structure-borne frequency response functions. In addition, the advantages of using the binaural instead of monaural recordings to quantify interior sound were presented.

Reproduced with permission of the copyright owner. Further reproduction prohibited without permission.

CHAPTER 3: THEORY

The quantification and interpretation of sound and vibration characteristics of a system requires the selection of appropriate signal acquisition, processing and analysis equipment and software. The following sections introduce fundamental concepts related to the appropriate equipment and software needs, including sound and vibration transducers, analog to digital conversion and digital signal processing techniques considered in this study.

3.1 Sound and Vibration Transducers

In order to acquire acceptable characteristics of sound and vibration, it is necessary to define and minimize the effects of parameters that cause undesirable sound and vibration. This is most frequently accomplished by first quantifying the physical characteristics of interest, such sound pressure level and acceleration. The collected data is then stored digitally and analyzed using a computer. The digital data is obtained by a transducer, for instance a microphone or an accelerometer that converts the physical quantity, such as sound pressure or acceleration into an electrical signal, which may be a voltage or a current. The selection of appropriate sensors for sound and vibration measurements is an integral step in any type of sound and vibration testing. The basic knowledge of the sensing mechanism, the sensor capabilities and its limitations, and the type of desired output signal is necessary to select a suitable sensor and the necessary hardware and software for that particular application. These characteristics are described in the following sections for most common types of sensors for sound and vibration measurements.

Reproduced with permission of the copyright owner. Further reproduction prohibited without permission.

3.1.1 Microphones

A microphone is a sensor that transforms an acoustic signal into an electrical signal. The most common acoustic transducer is a condenser microphone. Its main component is a capacitor, consisting of a pair of metal plates separated by an insulating material. The change in sound pressure causes a movement in one of the plates, resulting in the change in charge. A condenser microphone requires an external power supply provided by a preamplifier. The size of a microphone is an important consideration when selecting sensors for a particular application. The effects of larger diameters include an increase in directional and amplitude sensitivity (i.e. a decrease the measurable pressure amplitudes). The optimum size and most commonly used is a ½ inch microphone. The response difference of microphones described in the next sections is most prominent at higher frequencies where the diameter of the microphone is significantly larger than the wavelength of sound.

3.1.1.1 Free Field Microphones

A free propagation of sound waves from one direction, in a continuous medium with no reflections, typically at zero degrees of incidence is a free field environment. In a free field environment, sound decreases by 6 dB for every doubling of the distance from the source. This type of environment is found in anechoic rooms, and other spaces away from reflecting surfaces and presence of background noise. Thus, the perceived sound is related to the source only. A free field microphone is designed to be most sensitive in the axial direction, measuring the noise level from the direction of the source. Free field condition measurements are most commonly used to calculate sound quality parameters.

Reproduced with permission of the copyright owner. Further reproduction prohibited without permission.

The high frequency response of free field microphones is electronically attenuated in order to compensate for amplification of pressure at zero degrees of incidence resulting from the physical design characteristics.

3.1.1.2 Diffuse Field Microphones

In a diffuse field environment such as reflective or reverberant rooms, sound from the sound sources arrives at the microphone from all directions. There is an equal probability of sound arriving from all angles. Thus, diffuse field microphones are designed to respond uniformly to sounds arriving at the sensing element from all angles. They are typically used for recording background or ambient sound. The sound from the same source is perceived differently in free field and diffuse field conditions.

3.1.1.3 Binaural Head

The perceived sound is a function of the shape of human body, particularly the torso, shoulders and head, or the upper body. The binaural head is a model of the upper body with free field microphones simulating human ears. The main advantage of binaural head is that it captures information pertaining to the sound direction and allows for binaural replay of recorded signals for the purposes of sound design for improved sound quality.

3.1.2 Accelerometers

The piezoelectric accelerometer is a commonly used sensor in vibration testing. It has a linear output over a wide range of amplitudes and a high stiffness allowing for high output without significant strain. The operating principle is based on the Newton's second law of motion stating that a relationship between a force applied on the mass and

Reproduced with permission of the copyright owner. Further reproduction prohibited without permission.

resulting acceleration is linear. The main components of an accelerometer are a housing, seismic mass and a piezoelectric sensing element. As the housing accelerates, the mass exerts a force on the piezoelectric crystals that generate charge proportional to the force created by the acceleration of the mass. This charge is then converted to voltage by one of two possible modes of operation as described in the next sections. Depending on the operating conditions, acceleration can vary at each point on the surface of the structure. Thus, modal analysis is often used to obtain possible mode shapes in order to select the appropriate measurement location and avoid areas close to the nodes, or regions of low displacement. The accelerometer mounting technique is also an important measurement consideration. The optimum mounting techniques include stud and adhesive mounting. Magnetic mounting may also be used on a flat mounting surface for surface vibration content above approximately 1000 Hz.

3.1.2.1 Integrated Circuit Piezoelectric Accelerometers

An integrated circuit piezoelectric (ICP) sensor system consists of microelectronics built into the transducer and constant current signal conditioner. The system produces a low impedance voltage signal that can provide excellent signal quality even through long cables and harsh environments. The complication of integrated circuitry is that the operating temperature must not exceed the specified maximum.

3.1.2.2 Charge Amplified Accelerometers

A charge mode accelerometer produces a high impedance output signal and requires external charge amplifier for signal conditioning. The output charge is susceptible to

Reproduced with permission of the copyright owner. Further reproduction prohibited without permission.

signal contamination from cable movement and electro-magnetic effects, thus low-noise cabling must be used to preserve signal quality. The charge amplifier converts the charge signal to a low impedance voltage signal. The charge mode accelerometers are typically used in high temperature environments, as the electronics are not built into the sensor.

3.2 Structural Excitation Signal Sources

The behaviour of structures is often investigated by exerting impact or acoustic force on the structure and measuring its response. The structural excitation is typically performed using impact hammers and loudspeakers. Their characteristics are described in the next sections.

3.2.1 Impact Hammers

Impact hammers are used to excite the test structure in order to measure a response to impact. They consist of an ICP quartz force sensor that converts impact force into an electrical signal that is then transferred through a cable connected to the end of the handle for analysis. The test structure is excited with a uniform force at all resonant frequencies located within the manufacturer specified operating range of frequencies. The impact signal is applied to the structure for only a fraction of the sample period. Its shape significantly influences the frequency content of the measured response, which may be modified by the use of mass extenders and hammer tips of varying hardness. For example, hard tips and low mass hammers result in short duration impacts, typically used to measure response at high frequencies.

Reproduced with permission of the copyright owner. Further reproduction prohibited without permission.

3.2.2 Loudspeakers

Loudspeakers are devices used to convert electrical energy into acoustic energy. Its transducer consists of the motor, diaphragm and suspension. The motor converts electrical energy into mechanical energy, and the diaphragm converts mechanical energy into acoustic energy. The suspension serves as a constraint to the diaphragm by controlling its motion through its elastic and damping forces.

3.3 Analog to Digital Conversion

The signal sampling and quantization are essential steps in transforming an analog signal to digital output. Sampling is a technique used to convert a continuous time signal to a discrete time signal with continuous amplitude. Quantization is a process of converting a continuous amplitude signal to a discrete amplitude signal. These concepts are described in more detail in the next sections.

3.3.1 Fixed Sampling

Most real-world signals are continuous in nature. The collected, sampled data is an approximation of these signals, in the form of a series of discrete values. Thus, sampling is a product of a continuous signal and a discrete valued sampling function of unit amplitude. The time interval between samples may be either constant or variable, depending on the sampling technique used. The first case is known as the fixed sampling frequency technique, and the second case as the variable sampling frequency or signature analysis technique, where the samples are taken at constant intervals with respect to a specific phenomenon in the process, for instance, a position of a crankshaft in an engine.

Reproduced with permission of the copyright owner. Further reproduction prohibited without permission.

The choice of the sampling technique used depends on the nature of the physical signal. The signature analysis technique is suitable if the frequency of occurrence of signal of the phenomenon we are trying to capture is proportional to the rotational speed. Otherwise, the fixed sampling method is appropriate, as long as the sampling frequency is large enough compared to the maximum frequency of the measured signal. In addition, total sample period of measurement needs to be considered, regardless of the technique used. The fixed sampling technique is illustrated in Figure 3.1. In this example the analog signal is a sinusoidal function for which the maximum frequency is the inverse of its period:

$$f_m = \frac{1}{T} \tag{3.1}$$

This frequency is preserved only if a sufficient number of samples are used to reconstruct the analog signal, i.e. the time interval between samples is small enough.

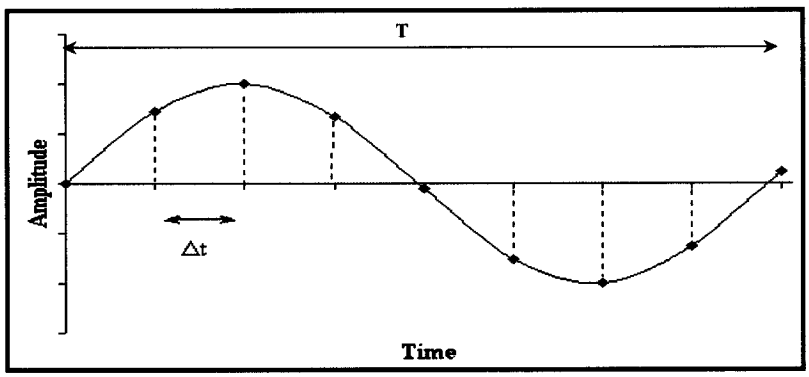

Figure 3.1: Fixed Sampling Frequency (uniform sample spacing).

The fixed sampling frequency is defined as:

$$f_s = \frac{1}{\Delta t} \tag{3.2}$$

Reproduced with permission of the copyright owner. Further reproduction prohibited without permission.

The relationship between the highest required frequency of the analog signal and the sampling frequency is a determining factor in data analysis.

3.3.1.1 Sampling Frequency Considerations

Most real-world signals are a combination of several frequencies as opposed to a single frequency, as shown in Figure 3.1. The sampling frequency must be high enough to capture the highest frequency of interest contained in the signal. Figure 3.2 illustrates the effectiveness of discrete time series representation of the analog signal, considering different sampling frequencies. The higher sampling frequency (i.e. 50 Hz) increases the likelihood of capturing the highest frequency of interest, while a lower sampling frequency (i.e. 15 Hz) generates a false frequency that is lower than the actual frequency contained in the analog signal. Thus, it is important to understand the condition used to select the appropriate sampling frequency, while knowing the highest frequency of interest.

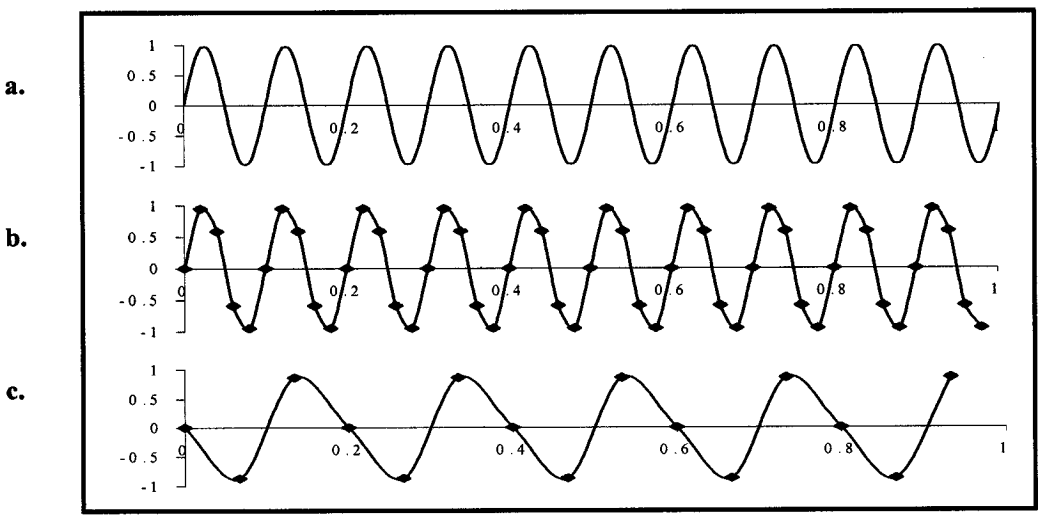

Figure 3.2: The Effect Aliasing in the Time Domain - a. Analog Signal, fm = 10 Hz, b. Sampled Signal, fs = 50 Hz, c. Sampled Signal, fs = 15 Hz.

Reproduced with permission of the copyright owner. Further reproduction prohibited without permission.

The criterion most commonly used to determine the adequate sampling frequency is called the Nyquist Criterion. The theorem states that the sampling frequency must be at least twice as high as the highest frequency of the analog, measured signal.

$$f_s > 2f_m \tag{3.3}$$

In order to correctly reconstruct the sampled signal in the time domain it is recommended that the sampling frequency be at least ten times the value of the highest frequency of interest.

3.3.1.1.1 Aliasing

Aliasing errors occur when the sampling frequency is not high enough, and the analog signal is not reproduced accurately after sampling. These errors are reduced by selecting the appropriate sampling frequency in order to capture the frequency content of the analog signal. The effect of aliasing is visible in both time and frequency domains. Its effect in time domain is illustrated in Figure 3.2. The frequency content of the analog signal that is greater than half of the sampling frequency, also called the Nyquist frequency (f_n), is shown at lower frequencies after sampling. Figure 3.3 illustrates this phenomenon. Frequency components labelled as f_a, f_b, f_c, and f_d, are all viewed as signals at f_a, as they are mapped back over folding lines (multiples of Nyquist frequency) to the lower frequencies.

Reproduced with permission of the copyright owner. Further reproduction prohibited without permission.

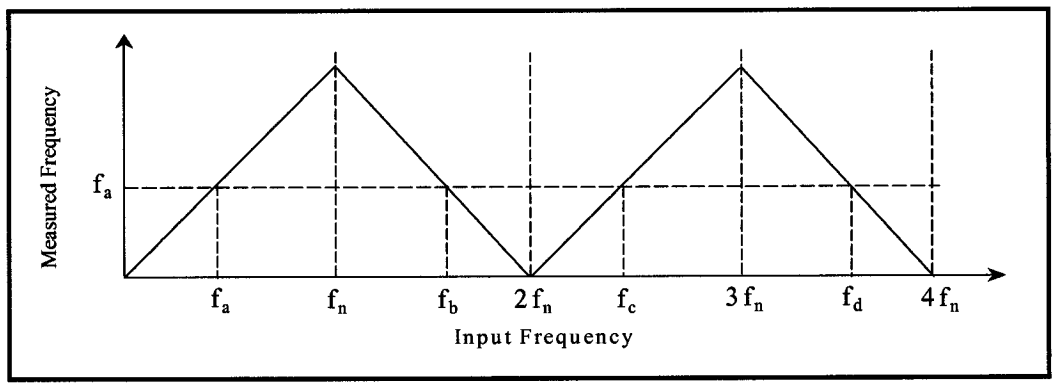

Figure 3.3: The Effect Aliasing in the Frequency Domain.

Therefore, the lowest frequency at which aliasing can occur is half of the sampling frequency, and is referred to as Nyquist frequency.

3.3.1.1.2 Filtering

A filter is a device that removes or attenuates undesirable frequencies from dynamic signals. Low pass filters remove high frequencies, above the specified cutoff frequency, high pass filters remove low frequencies and bandpass filters remove frequencies above and below a selected frequency band. Most analog to digital converters contain a low-pass filter that is applied to the analog signal before sampling in order to eliminate frequencies above the Nyquist frequency. If the maximum frequency of interest is significantly lower than the highest frequency contained in the signal, the sampling rate can be reduced, thus increasing efficiency, and the low pass filter is applied to avoid aliasing. In addition, it is important to take into account the roll off characteristics of a real filter, as the high frequency portion of data may not be filtered out properly. The roll off point typically occurs at eighty percent of bandwidth, so the last twenty percent of bandwidth may contain unreliable data.

Reproduced with permission of the copyright owner. Further reproduction prohibited without permission.

3.3.1.2 Sampling Period Considerations

It is expected that a Discrete Fourier Transform performed on a sinusoidal signal results in a single spectral line. The assumption associated with this expectation is that a sampled signal is periodic in the time domain. If the sampling period is not equal to the period of the analog signal, a leakage of energy with respect to the line spectrum occurs in the frequency domain.

3.3.1.2.1 Leakage

If the sampling period is not equal to the period of the analog signal, a leakage of energy occurs in the frequency domain. It is not possible to completely eliminate these errors, however, they can be reduced by various windowing techniques described below.

3.3.1.2.2 Windowing

The discontinuities at the end of the sampling period, leading to leakage errors, are due to the asynchronous nature of the sampling period with respect to the period of the analog signal. In most instances matching these two periods accurately is impractical or simply not possible. The alternative is to use the technique called windowing. This technique multiplies the sampled value by zero at the beginning and the end of the sampling period, thus making the sampling signal periodic. The window function, however, alters the amplitude and energy content of data. There are different types of windowing functions, and their application is dependent on the nature of the analog signal. There is a possibility of restoring energy or amplitude information of the analog signal by applying different energy or amplitude correction factors characteristic of each windowing function. The most common windowing functions include the uniform window, Hanning

Reproduced with permission of the copyright owner. Further reproduction prohibited without permission.

window, and flattop window. The selection of appropriate time window involves a tradeoff between dynamic range and resolution. Uniform window is applied when function is actually periodic at the beginning and an end of the sampling period, or in cases where leakage is not a problem. Generally, for random signal analysis, Hanning window is most commonly applied. The flattop window is typically used for calibration, or amplitude measurements at a specific frequency.

3.3.2 Variable Sampling Frequency

An alternative sampling technique is associated with variable time interval between samples. The time interval typically varies as a function of angular speed of the rotating element, for instance, an engine crankshaft. The samples are taken at specified, constant crank angle increments. This method is also known as the order analysis, since orders are defined as multiples of rotational speed. For instance, a third order implies that an event occurs three times per engine crankshaft revolution. The maximum possible order captured remains unchanged with rotational speed using the variable sampling frequency method. However, the fixed sampling frequency method results in leakage errors and decreased order resolution at high rotational speeds, and is ineffective in capturing order information at this condition. The data acquisition is triggered by a specific number of times during each revolution of a rotating component, such as a camshaft or a flywheel.

3.3.2.1 Tracking Trace Acquisition and Resampling Techniques

An engine speed is obtained from a tachometer signal or a tracking trace. The tracking sensor output is a voltage signal. An example is a magnetic pickup type of sensor located

Reproduced with permission of the copyright owner. Further reproduction prohibited without permission.

near a flywheel, perpendicularly to its teeth. As a flywheel gear tooth passes through a magnetic pickup pole it generates voltage pulses at a frequency proportional to the speed of the engine. This type of sensor provides high accuracy in terms of resolution, generating several pulses per revolution, which is especially important at high engine speeds. Other common types of tachometer sensors include the Cylinder Identification Sensor (CID) and the Crankshaft Position Sensor (CPS). Both are typically a variable reluctance, non-contact electro-magnetic sensors that generate voltage sine wave pulses. The number of pulses per revolution is equivalent to the number of teeth on the gear in the sensor assembly attached to the camshaft or crankshaft. Based on the tachometer signal characteristics, such as the number of pulses per cycle, engine speed versus time traces and crank angle versus time traces may be calculated. In fact, this is the first step in the resampling process. The resampled tracking signal obtained from CID sensor is typically used to offset the resampled data from other channels with respect to the angular position of cylinder one in a cycle. The number of voltage pulses generated by the CID sensor is proportional to the rotational speed of the camshaft. The camshaft rotates once per cycle in a four-stroke engine, thus, based on the shape of the CID signal, the position of cylinder one is located, and the data is offset accordingly. Consequently, other cyclic events, such as combustion and valve positions in a cycle may now be referenced to a particular crank angle. In a similar manner, defects associated with particular locations in a cycle may be identified. The technique known as adaptive resampling is used to convert the time domain data to an angle domain, as opposed to a fixed resampling technique that converts a signal sampled at a certain sampling rate to a signal with a different sampling rate. The adaptive resampling consists of integrating the rpm versus

Reproduced with permission of the copyright owner. Further reproduction prohibited without permission.

time trace generated from the tracking signal (CID) to obtain the angle versus time trace. This trace is then used to obtain the angular position of time domain samples (see Figure 3.4). Depending on the original sampling rate and the required angular resolution after resampling, it may be necessary to interpolate or upsample the original time signal in order to preserve its spectral properties in the resampling process.

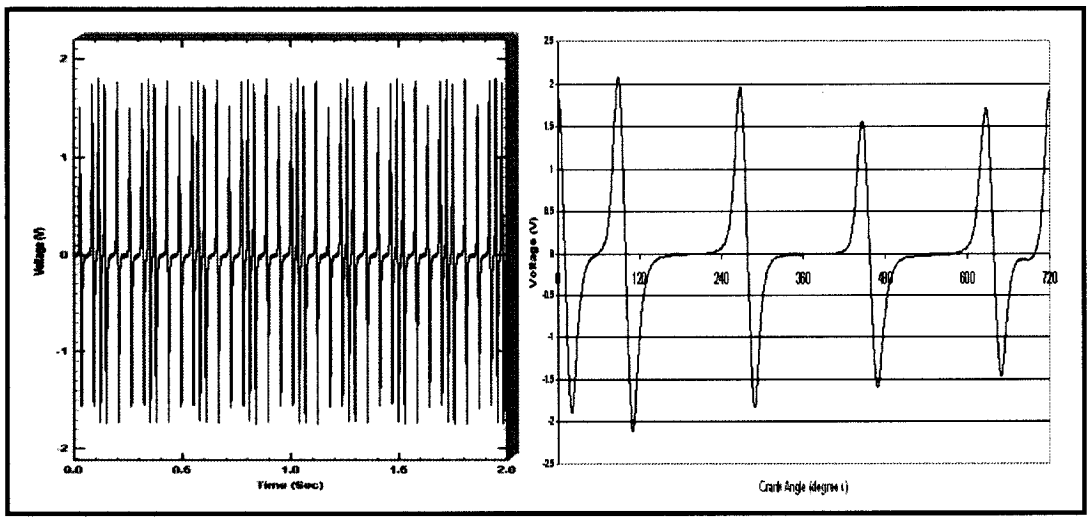

a. b.

Figure 3.4: Raw, time domain CID signal (a) and corresponding resampled, averaged CID signal (b).

3.3.3 Quantization Concepts

A continuous amplitude signal is converted to the digital amplitude signal through the process of quantization. The accuracy of digital output is associated with the number of available bits and the input range that characterize an analog to digital (A/D) converter. For a specified number of bits N, there are 2^N possible output values. For example, an 8-bit A/D converter has 2^8 possible outputs, while the corresponding binary output ranges from 00000000 to 11111111. Thus, a greater number of bits allows for a greater resolution.

Reproduced with permission of the copyright owner. Further reproduction prohibited without permission.

CHAPTER 4: EXPERIMENTAL DETAILS

The following chapter describes the experimental setup, transducers and operating conditions related to the vibroacoustic source, path and receiver measurements required to estimate and verify the vehicle interior sound and vibration characteristics for operating conditions and crankshaft types considered. The methodology used is based on experimental techniques of transfer path analysis (TPA) and an indirect, mount-stiffness method for calculating structure-borne operating forces. In order to investigate the effect of crankshaft material on interior sound and vibration, both steel and cast crankshafts' baseline data were obtained. An attempt was made to minimize extraneous sources of noise unrelated to engine operation, to maintain consistent operating conditions, sampling parameters and the resulting frequency resolution at all stages of testing. These objective data were then compared to subjective evaluations of interior sound and vibration at corresponding operating conditions.

4.1 Interior Sound and Vibration Numerical Estimation Method

The vehicle interior sound and vibration is produced by interacting sources, paths and receivers of sound and vibration. The total engine contribution to interior sound and vibration is a summation of individual contributions from transfer paths associated with engine inputs considered in this study. The transfer path analysis requires separate source and transfer path testing in order to estimate interior sound and vibration and receiver testing to verify the estimated results. The vibroacoustic source testing, the engine radiated sound and mount vibration testing, was performed in a semi-anechoic

Reproduced with permission of the copyright owner. Further reproduction prohibited without permission.

dynamometer test cell. The sound was measured in directions of main noise-emitting surfaces, and vibration was measured in all three directions at the engine and body (frame) side mount locations. The transfer paths between combinations of vibroacoustic sources and receivers were characterized as ratios or transfer functions relating the vibroacoustic sources to receivers. These transfer functions were obtained by modal testing using single input/multiple output testing configurations. The responses considered included binaural sound pressure and triaxial acceleration perceived in the driver's seat. The sign and naming convention for path directions (front, left, right, with respect to the reference axes, driver and passenger) used to organize data during acquisition and processing are shown in Figure 4.1.

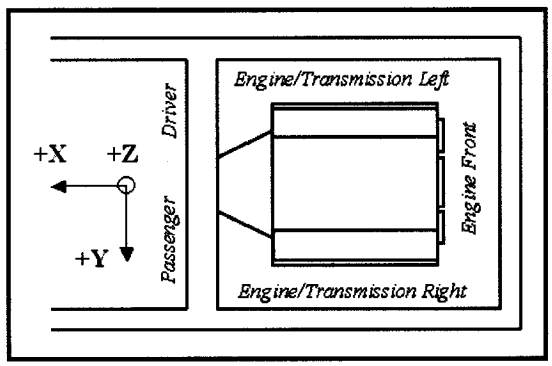

Figure 4.1: Transfer Path Sign and Naming Convention.

The powertrain radiated sound and mount vibration testing consisted of measurements of both, engine and transmission, as described in sections 4.2.1.1 and 4.2.1.2. At the neutral condition considered in this study, the effect of the engine on interior sound and vibration was predominant and only the transfer paths associated with the engine inputs were considered. Table 4.1 is a list of air-borne and structure-borne sources included in the interior vehicle sound and vibration model.

Reproduced with permission of the copyright owner. Further reproduction prohibited without permission.

Table 4.1: Air-borne and Structure-borne Sources Considered.

Air-borne Sources	Structure-borne Sources
1. Front, X-dir	1. Right Mount, X-dir
2. Right, Y-dir	2. Right Mount, Y-dir
3. Top, Z-dir	3. Right Mount, Z-dir
4. Left, Y-dir	4. Left Mount, X-dir
5. Bottom, Z-dir	5. Left Mount, Y-dir
	6. Left Mount, Z-dir

Source measurements (sound pressures and accelerations for air-borne and structure-borne sources, respectively, as indicated in Table 4.1) and frequency response function measurements with respect to the receivers were required for each transfer path considered in this study. A total of fifty-five frequency response functions were required due to the number of sources and the five receiver locations considered - binaural sound pressure (left and right driver's ear) and triaxial driver's outboard seat track acceleration.

4.2 Powertrain Sources of Vehicle Interior Sound and Vibration

The tests conducted in the semi-anechoic engine dynamometer involved a powertrain system consisting of the engine, clutch and transmission assembly, Front End Accessory Drive (FEAD) subsystem, powertrain mounts and mount brackets used in-vehicle and the complete engine induction and exhaust systems. The powertrain contributions to total interior vehicle sound and vibration were associated with measured powertrain radiated sound expressed in terms of sound pressure and mount vibration expressed in terms of acceleration. The engine speed was measured by the VRS 3010 speed sensor which was thread mounted on the transmission bell housing and actuated by flywheel teeth (to vary the strength of its magnetic field and generate AC voltage waveform). This procedure was impractical for in-vehicle testing, so the CID sensor signal was used instead to

Reproduced with permission of the copyright owner. Further reproduction prohibited without permission.

extract engine speed. The CID sensor connector was located on the top portion of the front cover so it was easily accessible in the vehicle. The LMS data acquisition system and Cada-X software (throughput acquisition mode) were used for data collection with the procedures and operating conditions described in the next sections.

4.2.1 Semi-Anechoic Engine Dynamometer Test Cell

In order to ensure accurate engine sound measurements with minimal background noise it was necessary to test in a free-field environment such as a semi-anechoic test cell; a room with sound absorbing wedges on walls with reflective floor. The background noise in the test cell was less than 50 dB mainly due to its structural characteristics, low noise ventilating and air conditioning system. The sound absorbing wedges in the test cell were constructed with perforated metal and filled with fibreglass. The double walls were constructed on an isolated foundation and the space between them was filled with fiberglass. The reflective floor, also built on an isolated foundation, provided a stable base for powertrain, its supporting components and test equipment. The AC dynamometer provided control of speed and load settings to simulate in-vehicle operating conditions. It was controlled by Automated Data Acquisition and Control System (ADACS) software from a Hewlett Packard UNIX based computer workstation.

4.2.1.1 Powertrain Radiated Sound

The powertrain radiated sound test was based on the SAE J1074 standard. The purpose of the test was to quantify acoustical radiation from exterior surfaces of the engine. The transducers used to measure engine radiated sound were GRAS 40AF ½-inch free field

Reproduced with permission of the copyright owner. Further reproduction prohibited without permission.

(side, front and top locations) and diffuse field microphones (bottom locations), in conjunction with a GRAS 26AJ preamplifier and a GRAS 12AG power module. The microphone windscreens were used to protect the diaphragm and reduce extraneous noises. Also, all microphones, except for the bottom microphones, were mounted on slender stands using slender extension rods of adequate length to reduce sound pressure field disturbances. There were nine microphones placed around the engine and transmission, in directions perpendicular to the main sound radiating reference surfaces, at a distance of one meter from these surfaces, as shown in Figure 4.2.

After the engine was installed on engine stands its bottom reference surface was not necessarily located at a one meter distance from the bottom microphone as required. Although the stands could be adjusted for vertical placement of the engine, the engine had to be installed at a specific angle with respect to the fixed drive shaft mounting flange of the dynamometer, consequently the bottom microphone distance was usually less than one meter from the engine as the microphone was placed on the floor during data collection. Therefore, in order to obtain equivalent free field spectra at a one metre distance the correction spectra consisting of approximately 10 dB corrections at each 1/3 octave band had to be subtracted from the test cell spectra.

Reproduced with permission of the copyright owner. Further reproduction prohibited without permission.

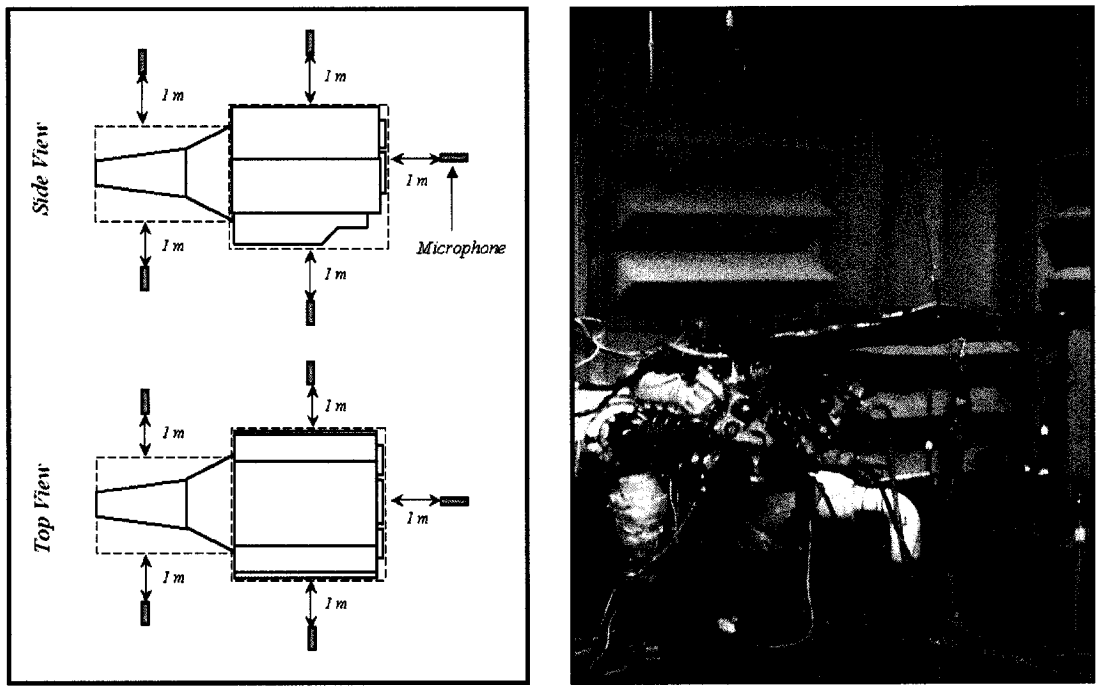

a. b.

Figure 4.2: Air-borne Source Measurements - Location of Transducers (a) and Experimental Setup (b).

The reference surfaces enclosed the intake and exhaust manifolds, crankshaft pulley and any other component that was at least 10 cm^3 in volume. The intake and exhaust components outside of the reference enclosure were wrapped to reduce their contribution to measured sound. Prior to testing, the test cell was visually inspected for leaks, the bedplate was drained and cleaned of any spills, and equipment and tools not part of the experimental set-up were removed. Prior to data acquisition, all microphones were calibrated using a Bruel & Kjaer 4321 sound level calibrator. The sampling frequency used for acquisition was 32768 Hz. The test cell acoustic cut-off frequency is 100 Hz.

Reproduced with permission of the copyright owner. Further reproduction prohibited without permission.

4.2.1.2 Mount Vibration

The structure-borne transfer path measurements were considered at all three mount locations in all three directions, as illustrated in Figure 4.3. The triaxial acceleration measurements were obtained from both the body and active (engine/transmission) sides of the mounts using a total of eighteen channels. The transducers used were ICP-type, Dytran 3053B2 triaxial accelerometers and the sampling frequency was 4096 Hz. The accelerometer axes were mounted to be aligned within 5° of the reference axes' directions. The active mount side accelerometer was placed on the powerplant side of the mount attachment bracket. The passive mount side accelerometer was placed on the body side of the mount attachment bolt. The stud and screw mounting techniques were impractical despite the possibility of providing the widest usable frequency range; thus, an alternative adhesive mounting technique was chosen to mount the accelerometers. This was accomplished by using adhesive mounting bases connected to the accelerometers with mounting studs to prevent damage to the accelerometers from the adhesive. Occasionally, the active accelerometer had to be mounted using a mounting cube to ensure that its axes were perpendicular with respect to the reference axes (see Figure 4.3b). The hanger brackets used to place the engine on the pallet were removed before the start of testing to eliminate their influence on the results. The accelerometer locations, directions and sensitivities were verified for accuracy for each channel, using a Bruel & Kjaer 4294 calibration exciter. In addition, the pallet qualification measurements, consisting of impact testing on the mounts, were completed to investigate the effect of pallet resonant frequencies on engine side vibration.

Reproduced with permission of the copyright owner. Further reproduction prohibited without permission.

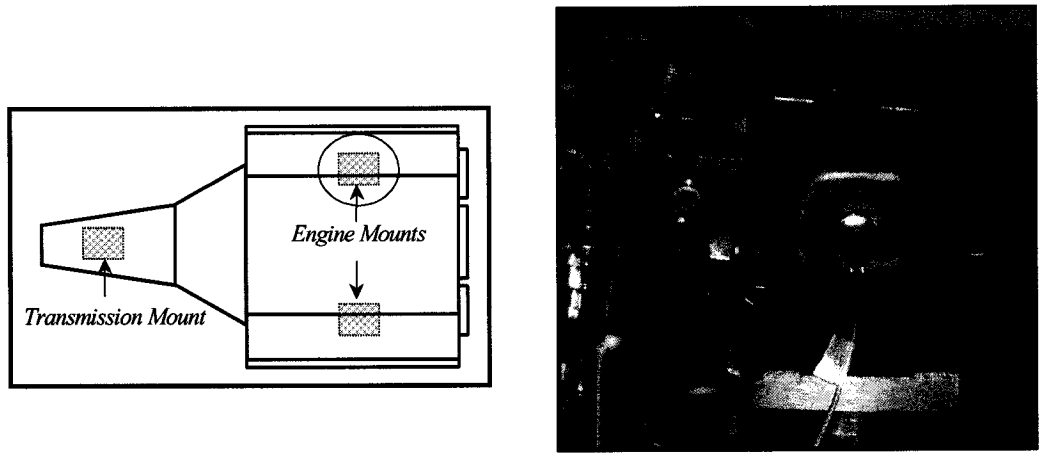

a. b.

Figure 4.3: Structure-borne Sources Measurements - Location of Engine and Transmission Mounts (a) and Left Engine Mount Transducers (b).

The resulting frequency responses of the engine side and the pallet side were observed to ensure that the difference was adequate. This difference was typically around 20 dB. The cut-off frequency for obtaining mount data was 100 Hz.

4.2.2 Operating Conditions

The powertrain system (engine and transmission) was tested in the vehicle and in a dynamometer semi-anechoic room with the variable speed (run-up or speed sweep) operating conditions. The rate of sweep was approximately 50 rpm per second, ranging from approximately 1000 to 4000 rpm. A performance test was completed prior to all sound and vibration testing, to ensure that the magnitudes of engine output torque and power coincided with the specifications over the range of operating speeds. Also, operating conditions during both vehicle and dynamometer tests were monitored to ensure consistency and a valid basis of comparison of data.

Reproduced with permission of the copyright owner. Further reproduction prohibited without permission.

4.3 Frequency Response Function Measurements

The frequency response function testing involved applying a known excitation signal as an input to a system while measuring its response. The frequency response function measurements were performed using single input/multiple output approach in order to quantify attenuation characteristics of the vibroacoustic paths considered, in terms of ratios of outputs (human receivers) to engine air-borne (radiated sound) and structure-borne (force) inputs. The acoustic and mechanical impact excitations were used to simulate the radiated sound and force inputs from within the engine compartment, respectively. The measured receivers were binaural sound pressure in the driver's seat and outboard driver's seat track triaxial acceleration.

The frequency response function testing was performed on the vehicle frame and body assembly with the engine removed. Since disassembling the engine from its compartment directly was not feasible due to insufficient space, an alternate procedure was required involving vehicle body disassembly. The engine mounts and body support mounts connect the engine and body to the frame consisting of two steel channel rails, front and rear cross member and transmission support cross member. The engine was removed by first disassembling the body from this frame, lifting and supporting the body on a hoist while the engine assembly was removed using an engine lift bracket and floor crane. The air-conditioning system, radiator, intake manifold, powertrain control module, starter electrical connectors and wiring harnesses were also removed in the process. The body was then assembled onto the frame in order to perform modal analysis on this assembly. The effect of loose components remaining on the frame and body (such as linkages and cables) on the modal results was minimized by suspending these

Reproduced with permission of the copyright owner. Further reproduction prohibited without permission.

components and preventing their impact with the body/frame or other components during modal excitation. These components included various support brackets on the body and frame that were impractical to remove. The influence of the support for the structure used during data acquisition had to be reduced. It was assumed that the tires provide soft enough support to reduce the effect of rigid modes, due to supports, at low frequencies.

RT Pro Photon 5.06 4-channel data acquisition system (Real Time Dynamic Signal Analysis - Modal Data Acquisition module) was used to obtain all frequency response function data. This system was also used as a waveform generator - a voltage source driving the loudspeaker through its output channel. The signal to noise ratio for all measurements was improved by averaging data from multiple tests thus eliminating signal components that were uncorrelated to the actual structural response to the input. These data were collected, in multiple frames, until the number of specified (linear, frequency-domain) averages was reached. Each acquisition was associated with specific combinations of excitation and response signal locations and coordinates. The acquired FRF data was exported and stored in comma separated values (csv) format for post processing.

4.3.1 Acoustic Excitation

The engine acoustic inputs were simulated using white noise input through Harman/Kardon HK395 loudspeakers. The RT Pro Photon system was used to drive the loudspeakers by controlling the voltage input to the loudspeakers. The loudspeaker sensitivity to voltage input is a measure of its ability to produce acoustical output. The loudspeaker sensitivity was measured in a semi-anechoic test cell at a one-meter distance

Reproduced with permission of the copyright owner. Further reproduction prohibited without permission.

from the loudspeaker using a reference voltage of 1.8 V rms and generating a white noise[1] output signal in order to observe the response over the required frequency range. This signal was sensed with an ICP microphone and sampled at 16 kHz. The sound pressure amplitude at each frequency was the same and the power distribution was independent of the frequency so the loudspeaker response to the input voltage was observed using the same energy input at all frequencies. The loudspeaker emits acoustical energy in all directions and its sensitivity may be described by an infinite number of frequency response functions. The engine in this study was modeled as a source that emanates sound perpendicularly to the surfaces of the smallest rectangle that encloses the engine (Figure 4.2). Thus, the loudspeaker sensitivity was measured perpendicular to the emitting face of the loudspeaker used to simulate these sound producing surfaces. During the FRF measurements, the loudspeakers were placed inside the engine compartment on a padding on the front cross member for front, right, top and left excitation, and affixed to the hood and facing downwards for bottom excitation. Figure 4.4 illustrates acoustic excitation in the front direction.

The vehicle was tested at the ride height and the hood, doors and windows were closed during acquisition to eliminate noise leaks. The height and angle of the seats and sensor locations in vehicle corresponded to those of the interior sound and vibration measurements. The bandwidth and frequency resolution used for calculating frequency response functions was 8000 Hz and 5 Hz, respectively, for a total of 100 linear, frequency-domain averages using a white noise input.

[1] White noise is a random, time domain signal, composed of all audible frequencies heard simultaneously.

Reproduced with permission of the copyright owner. Further reproduction prohibited without permission.

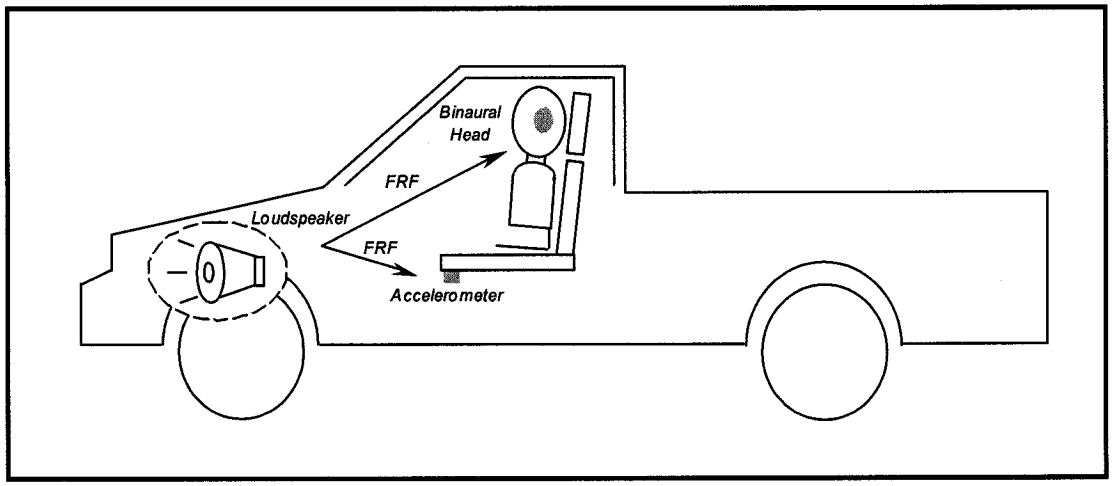

Figure 4.4: Acoustic Excitation in the Engine Compartment - Front Direction.

4.3.2 Impact Excitation

The engine force input through the frame was simulated by impact hammer excitation of the frame, with the engine removed, using PCB 086D20 impact hammer. The impact locations were selected based on their proximity to points of contact between the engine and the mount, and accessibility - the impact directions had to coincide with transfer path directions and adequate space to exert impact in those directions was required. The frame was impacted on interfacing surfaces with the engine mounts or as close as possible to those surfaces. Figure 4.5 is an example impact location on the right mount, in the X-direction. The data collection was initiated by the trigger signal - the rising edge of the analog input force signal at a level of, typically, 5% of the available range. The impact force level was consistent in terms of magnitude, location and orientation normal to the surface under impact. The data quality was maintained by avoiding overloads and double hits during acquisition.

Reproduced with permission of the copyright owner. Further reproduction prohibited without permission.

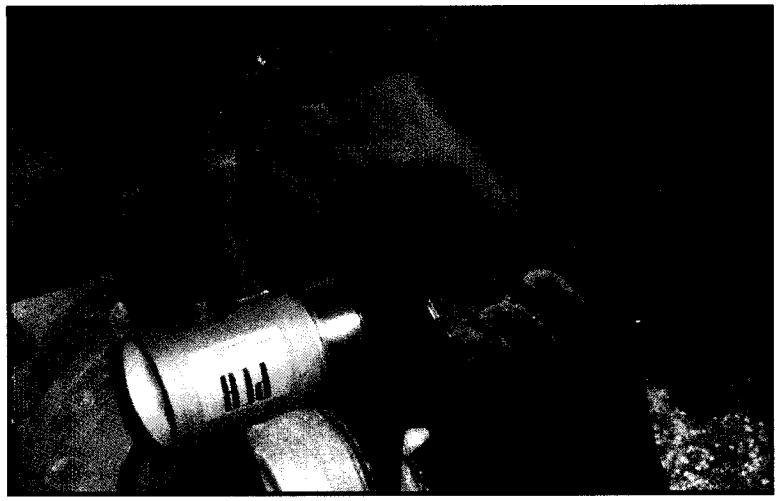

Figure 4.5: Hammer Impact Excitation, Right Mount, X-direction.

All frames with voltage overloads were automatically rejected (and not averaged) while the time window illustrating impact force was monitored to detect frames with double hits to manually reject those frames. Due to the transient nature of the hammer impact excitation signal, the windowing function used was Force/Exponential[2] applied in the time domain.

The frequency content of structure-borne vibration was typically less than 1000 Hz. Thus, a hard plastic impact hammer tip was used to obtain frequency content up to 1000 Hz. The bandwidth and frequency resolution used for calculating frequency response functions was 4000 Hz and 5 Hz, respectively, for a total of 20 linear, frequency-domain averages.

[2] Force/Exponential function applies damping to the time traces of each frame to ensure that the response signal fully decays during that time thus preventing leakage, suppressing noise and improving quality of FRF measurements.

Reproduced with permission of the copyright owner. Further reproduction prohibited without permission.

4.4 Interior Sound and Vibration Measurements

The interior sound and vibration were measured using binaural head (HEAD Acoustics HSU III Head and Shoulder Unit) and triaxial accelerometer (Dytran 3053B2), respectively at the same five receiver locations used in the frequency response function measurements (see Figure 4.6). The sensor cables from the vehicle interior were routed carefully through the door seal to the data acquisition system. The windows and doors were closed and any potential acoustic leaks were eliminated.

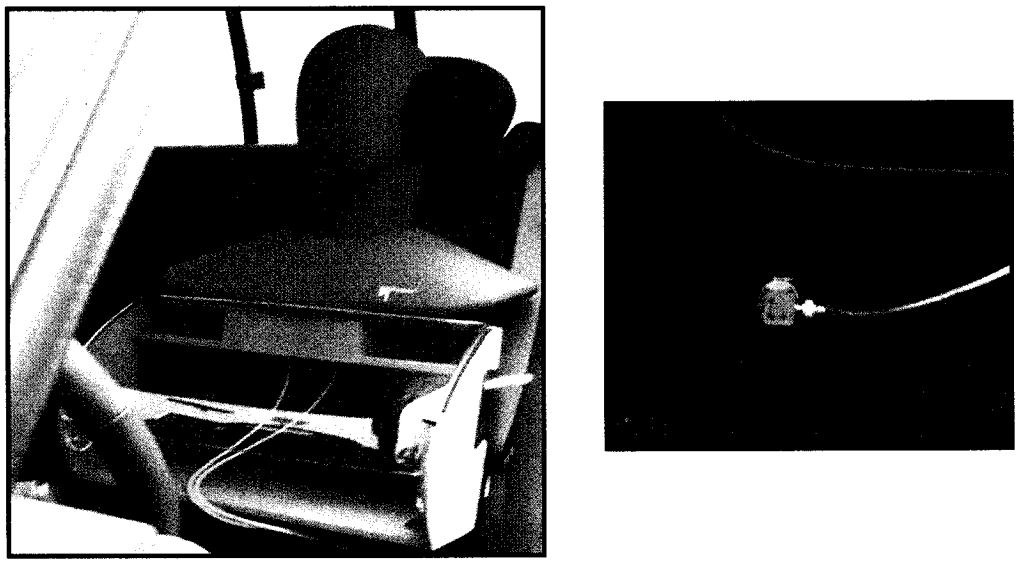

a. b.

Figure 4.6: Interior Noise (a) and Vibration (b) Measurement Sensors and Locations.

The rate and range of speed sweep and acquisition duration used was as described in section 4.2.2. The CID signal was obtained for engine speed calculation synchronously with the five receiver channels measuring interior sound and vibration. The speed was varied from the front passenger location so the influence of the passenger on the sound field was also included in the interior sound reading. The data were collected using

Reproduced with permission of the copyright owner. Further reproduction prohibited without permission.

Prosig P5600 Acquisition system with a sampling frequency of 24,000 Hz. These data were exported in SDF (Standard Data Format) files for post processing.

4.5 Subjective Evaluation of Interior Sound and Vibration

The interior sound and vibration was also evaluated subjectively by jury testing using an evaluation scale ranging from 1 (very bad) to 10 (excellent). The individually evaluated operating conditions included 500 rpm increments from 1000 rpm to 4000 rpm. The sweeps were completed while the vehicle transmission selector was set at the neutral position. The evaluation categories included noise emanating from right and left side panels, and seat vibration in all three directions. The evaluation was completed by 10 randomly selected adjudicators, the same adjudicators were used for all jury testing. In addition, the binaural replay techniques were used to verify the jury evaluation results.

Reproduced with permission of the copyright owner. Further reproduction prohibited without permission.

CHAPTER 5: DATA ANALYSIS METHODS

The interior sound and vibration was expressed in terms of sound pressure and acceleration, respectively, as functions of engine speed and frequency. The time domain source data was converted into the frequency domain and combined with appropriate frequency response functions to estimate the interior sound and vibration. The actual interior sound and vibration measurements in the time domain were converted into the frequency domain and the results compared to the estimated results. This chapter describes the time data processing techniques such as mount acceleration signal integration, frequency response function calculations and spectral processing required to estimate the vehicle interior sound and vibration and obtain a comparison of the estimated results to the measured results.

5.1 Analysis Overview for Estimated Interior Sound and Vibration

The time domain data collected at all stages of testing had to be converted into the frequency domain. In addition, it must be remembered that the source and receiver sound and vibration amplitudes were functions of operating conditions, or engine speed. These amplitudes were attenuated as the vibroacoustic inputs from the engine compartment were transferred to the vehicle interior. The attenuation was quantified in terms of frequency response functions in order to eventually estimate the engine contribution to vehicle interior sound and vibration. Figure 5.1 provides an overview of the sequence of data collection and processing for the vehicle interior sound and vibration numerical

Reproduced with permission of the copyright owner. Further reproduction prohibited without permission.

estimation method based on engine radiated sound and mount vibration utilized at all operating conditions and engine sources considered (see Table 4.1).

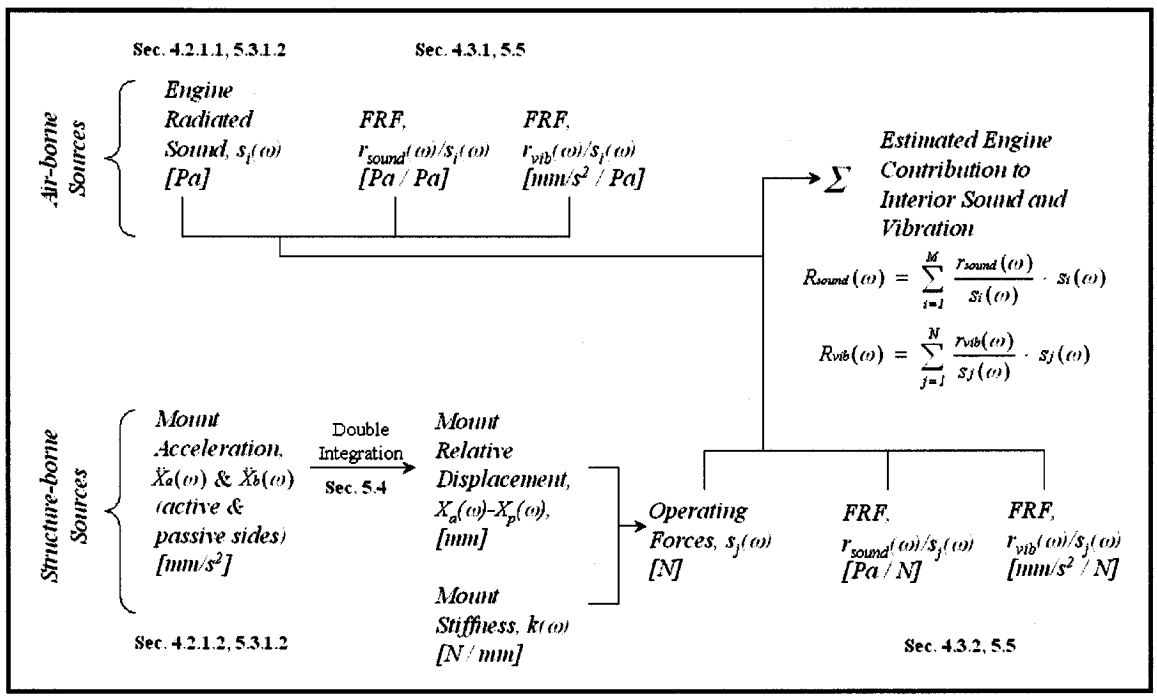

Figure 5.1: Vehicle Interior Sound and Vibration Numerical Estimation Method Overview.

The engine radiated sound is a source of air-borne contributions to interior sound and vibration. In order to calculate these contributions it was necessary to first convert the time domain sound data into the frequency domain for each collected channel of data (source) and operating condition (rpm) using the techniques of tracked spectral processing, as described in section 5.3.1.2.

The forces transmitted through engine mounts resulting from engine operation are structure-borne sources of interior sound and vibration. These forces are functions of relative displacements across the mounts, the frequency-dependant mount stiffness and operating conditions. In this study the forces were determined indirectly using the indirect, mount-stiffness method (see section 2.2.3.2.1) because their direct

Reproduced with permission of the copyright owner. Further reproduction prohibited without permission.

measurements were impractical. The acceleration time signal obtained from mount vibration test was converted into the frequency domain also using tracked spectral processing, and the resulting signal integrated twice to eventually obtain relative displacements across mounts using numerical integration in the frequency domain, as described in section 5.4. The relative displacements are proportional to the forces transmitted through the mounts and into the vehicle body at each operating condition and frequency. The proportionality constant is the frequency-dependent, manufacturer-specified mount stiffness.

All source data was collected in time history files, referred to as TDF (Test Data Files), using Cada-X throughput acquisition module. The receiver SDF data was imported to TDF database and both, source and receiver data were processed using Cada-X time data processing module. The source data was processed into the frequency domain and then combined with appropriate frequency response functions to ultimately estimate the vehicle interior sound and vibration in the form of spectral maps. Similarly, the receiver data (actual vehicle interior sound and vibration) was captured in the time domain and converted into the frequency domain using the same processing parameters. These also resulted in a series of spectral maps. The following sections describe the parameters used to process and analyze the data at the sources, paths, and receiver locations of vehicle interior sound and vibration.

5.2 Time Domain Analysis

The system characteristics such as sound pressure and acceleration are often sampled in the time domain. Depending on the nature of the signal, sampling duration and

Reproduced with permission of the copyright owner. Further reproduction prohibited without permission.

frequency, it may be possible to deduce a general trend, in terms of signal amplitude and fluctuation in amplitude with respect to time. The time domain data is also used as a quick visual indicator of signal quality, prior to data post processing and analysis. However, for a thorough understanding of complex processes associated with vehicle or engine operation, a sole time domain data analysis is generally not adequate.

5.2.1 Root Mean Square

The root mean square (rms) of sound pressure and acceleration is often used to quantify the severity of sound and vibration, or establish benchmarks of acceptable levels of sound and vibration. It is a convenient way of quantifying variables such as sound pressure and acceleration at different operating conditions and locations. All source and receiver sound and vibration data in this study were processed in terms of rms amplitudes as functions of frequency and engine speed. The sound pressure level, L, expressed in dB, is defined based on rms sound pressure, such that:

$$L = 20 \log \frac{P}{P_0} \tag{5-1}$$

Where P is rms sound pressure and P_0 is the reference rms sound pressure of $2 \cdot 10^{-5}$ Pa.

5.3 Frequency Domain Analysis

The frequency domain analysis is based on the application of Fourier analysis. The Fourier analysis is derived assuming periodicity of a signal; however, due to the non-periodic nature of most real life signals, certain approximations are required for correct

Reproduced with permission of the copyright owner. Further reproduction prohibited without permission.

application to obtain the frequency content of these signals. These approximations are outlined in the following sections.

5.3.1 Fourier Analysis

A periodic function with a finite number of discontinuities, maxima and minima in a cycle may be represented by a Fourier series. Real world periodic signals meet these conditions and may be defined by a Fourier series as follows:

$$x(t) = A_0 + \sum_{n=1}^{\infty} (A_n \cos \frac{2\pi n}{T} t + B_n \sin \frac{2\pi n}{T} t) \tag{5-2}$$

Rewriting the above expression and simplifying yields:

$$x(t) = A_0 + \sum_{n=1}^{\infty} C_n \sin(\frac{2\pi n}{T} t + \phi_n^*) \tag{5-3}$$

Where T is the period of the function and A_0, A_n, B_n, C_n and ϕ_n^* are constant coefficients defined as:

$$A_0 = \frac{1}{T} \int_{-T/2}^{T/2} x(t)dt \tag{5-4}$$

$$A_n = \frac{2}{T} \int_{-T/2}^{T/2} x(t) \cos \frac{2\pi n}{T} tdt; \quad n = 1,2,3... \tag{5-5}$$

$$B_n = \frac{2}{T} \int_{-T/2}^{T/2} x(t) \sin \frac{2\pi n}{T} tdt; \quad n = 1,2,3... \tag{5-6}$$

Reproduced with permission of the copyright owner. Further reproduction prohibited without permission.

$$C_n = \sqrt{A_n^2 + B_n^2} \tag{5-7}$$

$$\phi_n^* = \tan^{-1} \frac{A_n}{B_n} \tag{5-8}$$

The limits of integration from equations 5-4 through 5-6 indicate that all coefficients are evaluated over one cycle. Thus, the main requirement for evaluating the Fourier series is function periodicity. It is not always possible to meet this requirement, especially if the frequency content of a transient or non-periodic signal is needed. In order to calculate the frequency content of a transient signal, the Fourier series is rewritten in exponential form:

$$x(t) = \sum_{n=-\infty}^{\infty} X(f) e^{j\frac{2\pi n}{T}t} \tag{5-9}$$

Where:

$$X(f) = \frac{1}{T} \int_{-T/2}^{T/2} x(t) e^{-j\frac{2\pi n}{T}t} dt \tag{5-10}$$

The frequency resolution, Δf, or the distance between each component of a series is a function of the period, T, which assumes a value of infinity for a non-periodic function. The resulting numerical version of inverse Fourier Transform, also known as Discrete Fourier Transform is defined as:

$$x(t) = \lim_{\Delta f \to 0} \sum_{n=-\infty}^{\infty} X(f) e^{j\frac{2\pi n}{T}t} \Delta f \tag{5-11}$$

Integral forms of Fourier transform and its inverse, shown in the next section, are obtained by evaluating this limit.

Reproduced with permission of the copyright owner. Further reproduction prohibited without permission.

5.3.1.1 Fourier Transform

The transformation from the time to the frequency domain and back is based on the Fourier Transform and its inverse:

$$X(f) = \int_{-\infty}^{\infty} x(t)e^{-j2\pi ft}dt \tag{5-12}$$

$$x(t) = \int_{-\infty}^{\infty} X(f)e^{j2\pi ft}df \tag{5-13}$$

The Fourier Transform of sampled data in digital form is evaluated using numerical integration, or Discrete Fourier Transform (DFT). Generally, numerical integration techniques are used to approximate the Fourier Transform because data is composed of discrete values and collected over a finite time interval. The DFT method is computationally intensive, especially for a large number of samples. The algorithm used to compute the DFT more efficiently is the Fast Fourier Transform (FFT). The FFT requires that the number of samples be a power of 2. A number of samples, N, in time data series T to be converted into frequency domain is referred to as a blocksize. The number of spectral lines in the frequency domain is one-half the blocksize, so that:

$$\frac{1}{T} = \frac{Bandwidth}{Spectral\ Lines} = \frac{Sampling\ Frequency}{Blocksize} = \Delta f \tag{5-14}$$

5.3.1.2 Tracked Spectral Processing

In this study, the tracked spectral processing technique based on Discrete Fourier Transform was used to convert time domain data into the frequency domain using the engine speed as a tracking variable. The end results were displayed in spectral maps.

Reproduced with permission of the copyright owner. Further reproduction prohibited without permission.

The flywheel was used as an actuator for the speed sensor for source testing in the dynamometer test cell. The resulting voltage signal contained 164 pulses per revolution (corresponding to the number of flywheel teeth). Tracking trace based on the CID signal contained five pulses per cycle, four of which were evenly spaced. The fifth odd pulse was used for variable cam timing (see Figure 3.4a) - its zero crossing was referenced to 10 degrees after top dead centre of cylinder 1 firing (see Figure 3.4b). The speed was extracted based on the four evenly spaced pulses per cycle, or two pulses per revolution. Since the flywheel speed sensor output generated a significantly higher number of pulses per revolution compared to the CID sensor output, it provided better resolution of the speed in rpm. The parameters specified in extracting speed included the cross level - the sensed voltage level used to calculate time between pulses, upper and lower tolerances - levels that had to be reached before evaluating the next crossing to avoid false detections due to noise, and the hold off percentage - the parameter specifying the time period after the cross level point during which the cross overs were ignored (this parameter was used to eliminate the odd CID pulse in rpm calculations). The target sample rate of the rpm vs. time trace was kept consistent with that of the original tracking trace.

The tracked spectral processing results consisted of a series of frequency spectrum maps. Initially each time trace was divided into sections based on the range of tracking values. For this study the division occurred after each 50 rpm speed increment from 1000 rpm to 4000 rpm. A number of samples corresponding to the specified blocksize was extracted around the data point located at the end of each section - at every 50 rpm increment location, and transformed into the frequency domain. The rpm range and rpm increments considered yielded 72 sections of data referred to as blocks which were measurement

Reproduced with permission of the copyright owner. Further reproduction prohibited without permission.

data records loaded into memory. The frequency resolution required for both, source and receiver data was 5 Hz. Other processing parameters included amplitude format, amplitude scaling and windowing.

The spectrum can be viewed in either power or linear format. For the purposes of this study linear, rms amplitude of spectral processing results was used. The power contained in frequency band is dependant on the spectral resolution. For this reason the power spectrum is often normalized with respect to frequency resolution for outputting power spectral density plots. The total power is then found by integrating the power spectral density over the frequency range of interest. The linear spectrum is the square root of the power spectrum.

The leakage errors associated with the Discrete Fourier Transform were reduced by windowing. The Hanning window, with energy correction, was used for all vibroacoustic source and receiver data processing.

5.4 Integration of Acceleration Signal to Obtain Displacement

The relative displacement across the engine mounts was required to calculate structure-borne engine operating forces transmitted through the mounts. The acceleration spectra on active and body sides of the mounts had to be integrated twice to obtain these displacements. The frequency domain integration was performed by dividing each spectral line by the square of the frequency (measured in radians/second). For example, if we consider a time domain double integration of sinusoidal acceleration signal of the following form to obtain displacement, we get:

$$\ddot{x}(t) = -\omega^2 A \sin \omega \cdot t \qquad (5\text{-}15)$$

Reproduced with permission of the copyright owner. Further reproduction prohibited without permission.

$$x(t) = A \sin \omega \cdot t \qquad (5\text{-}16)$$

Where A and ω are sine wave amplitude and frequency, respectively. Correspondingly, the acceleration spectra amplitude is divided by the square of the frequency of each spectral line to obtain the displacement spectra. At very low frequencies the resulting calculated displacement amplitudes are unreasonably high due to a numerical error resulting from integration. Since these values are not true representations of actual signals, the first few spectral lines must be set to a value of zero. In fact, for this study, all sound and vibration data below 100 Hz was filtered out due to the semi-anechoic dynamometer test cell acoustic and structural cut-off frequencies.

5.5 Frequency Response Functions

The effect of the engine on vehicle interior sound and vibration was estimated by using engine sound and vibration data in combination with data related to sound and vibration transmission characteristics from the engine compartment to vehicle interior. The sole results of tests on an individual system component such as an engine do not always reflect the effect of those components on the overall (vehicle) system performance. This certainly applies to engine radiated sound and mount vibration test results as they relate to vehicle interior sound and vibration aspects of performance, due to the effect of the vehicle body on transmission of sound and vibration from the engine compartment to vehicle interior. However, if the effects of vibroacoustic transfer paths are taken into account then combining the properties of both, sources and transfer paths allows for a better estimate of the response at the receivers in vehicle interior.

Reproduced with permission of the copyright owner. Further reproduction prohibited without permission.

The frequency response function (FRF) may be described as a ratio between the output and the input signal, in the frequency domain - a Fourier transform of the response, divided by the Fourier transform of the input. This definition can be applied only in situations where there is no noise contamination of signals and there is a direct relationship between the input and the output. In reality, the FRF formulation is estimated based on measured input and output signals and their linear spectra, autopower, and crosspower spectra. The estimated frequency response functions are known as H_1 and H_2 estimators. The Fourier Transform of the time spectrum is a complex valued function known as linear spectrum or frequency spectrum. The real and imaginary parts of this function correspond to frequency content cosinusoidal and sinusoidal with respect to start of sampling, respectively. The autopower spectrum is a real valued function equivalent to the square of the magnitude of linear spectrum. The phase information is lost in the process. The autopower spectrum is defined as:

$$S_{xx}(\omega) = X(\omega) \cdot X^*(\omega) \tag{5-17}$$

Where $X(\omega)$ and $X^*(\omega)$ are real and imaginary components of linear spectrum. The crosspower spectrum is defined as the linear spectrum of one signal multiplied by the complex conjugate of the linear spectrum of another. It is a measure of mutual power between two signals at specific frequencies, $X(\omega)$ and $Y(\omega)$. The phase information is included in the crosspower, and it is a relative phase between two signals. The crosspower spectrum is defined as:

$$S_{xy}(\omega) = X(\omega) \cdot Y^*(\omega) \tag{5-18}$$

Reproduced with permission of the copyright owner. Further reproduction prohibited without permission.

In general, the crosspower spectrum is used internally by dynamic signal analyzers to compute coherence and frequency response functions, and not as often in measurement situations. The excitation and the response in random vibration is presented in the following relationships:

$$S_{xy}(\omega) = H(\omega) \cdot S_{xx}(\omega) \tag{5-19}$$

$$S_{yy}(\omega) = H(\omega) \cdot S_{yx}(\omega) \tag{5-20}$$

Rearranging equations 5-19 and 5-20, one can obtain estimates for frequency response functions H_1 and H_2, respectively:

$$H_1(\omega) = \frac{S_{xy}(\omega)}{S_{xx}(\omega)} \tag{5-21}$$

$$H_2(\omega) = \frac{S_{yy}(\omega)}{S_{yx}(\omega)} \tag{5-22}$$

If a signal noise is not related to the input side of measurements H_1 is the preferred estimator, while H_2 assumes that there is no noise on the receiver side of measurements and is the preferred estimator in that situation. In this study, the H_1 estimator was used in order to minimize the influence of noise on interior sound (binaural sound pressure) and vibration (triaxial seat track acceleration) measurements by the method of least squares. The FRF testing is an application of experimental modal analysis. The FRF measurements assume a linear system, that is, only the frequencies used to excite the structure are contained in the output signal, with changed amplitude and phase. For a typical FRF, the high amplitude components occur at resonant frequencies, where a low

Reproduced with permission of the copyright owner. Further reproduction prohibited without permission.

input level generates a high response, and low response levels caused by high inputs correspond to antiresonant frequencies of the structure (see Figure 5.2a).

5.5.1 Coherence

Coherence is a fraction of the energy of the output signal caused by the input signal. It is a function of frequency, and its value ranges from zero to one. A coherence of less than one may be caused by unmeasured inputs or multiple energy sources, the presence of noise, or a nonlinear system relating the input to the output. The coherence function is typically used to ensure the quality of the frequency response function measurements. For a high value of coherence in a particular frequency range, the output is caused by the input and the frequency response function estimate is valid for that range of frequencies. For example, the FRF in Figure 5.2a is valid for the frequency range shown due to a high value of coherence in the same range (see Figure 5.2b).

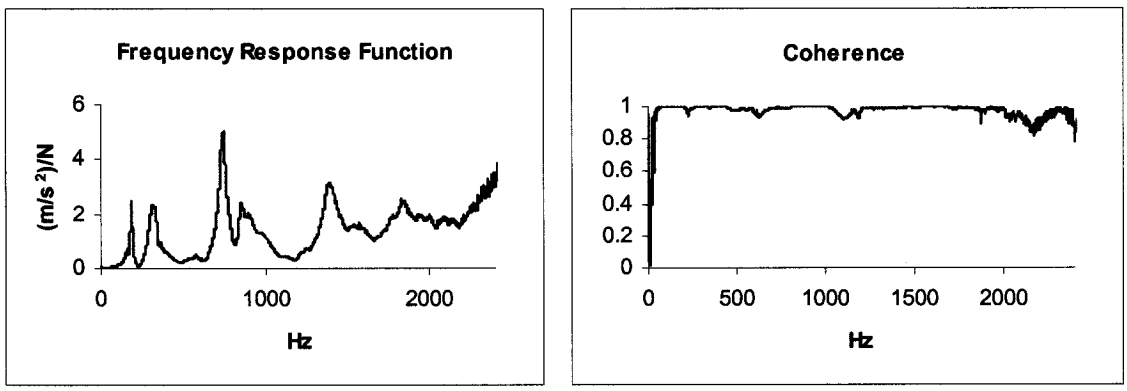

a. b.

Figure 5.2: Example of Inertance FRF (a) and Corresponding Coherence Function (b).

The coherence function, γ^2, is defined as:

$$\gamma^2 = \frac{S_{yx}{}^2}{S_{xx} \cdot S_{yy}} \tag{5-23}$$

Reproduced with permission of the copyright owner. Further reproduction prohibited without permission.

The frequency response function estimates H_1 and H_2, are not identical when they are derived from actual measurements. The ratio between these two types of frequency response function estimates is the coherence function.

Reproduced with permission of the copyright owner. Further reproduction prohibited without permission.

CHAPTER 6: RESULTS AND DISCUSSION

The following chapter provides a summary of the results that includes the source, the frequency response function and the receiver results, estimated and actual, and subjective evaluations of vehicle interior sound and vibration. These results are for both steel and cast iron crankshaft engines and include binaural replay of actual measurements carried out to verify subjective results. In addition, the perceived quality of interior sound and vibration of different engines and operating conditions obtained from subjective evaluations was used to assess the significance of differences in corresponding objective measurement results, both in terms of overall levels and transfer path contribution.

6.1 Engine Radiated Sound and Mount Vibration

The spectral maps of engine radiated sound and mount vibration are often used to establish engine NVH performance baselines and to study quality issues or design changes on engine components. Figures 6.1 and 6.2 illustrate example spectral maps resulting from tracked spectral processing of the collected time data of air-borne (right engine radiated sound) and structure-borne (Z-direction force) sources of sound and vibration, respectively, using the steel crank engine. They illustrate the changes in frequency content with operating conditions. Unfortunately, the effect of each source on the level and quality of interior sound and vibration can not be determined without further vehicle testing.

Reproduced with permission of the copyright owner. Further reproduction prohibited without permission.

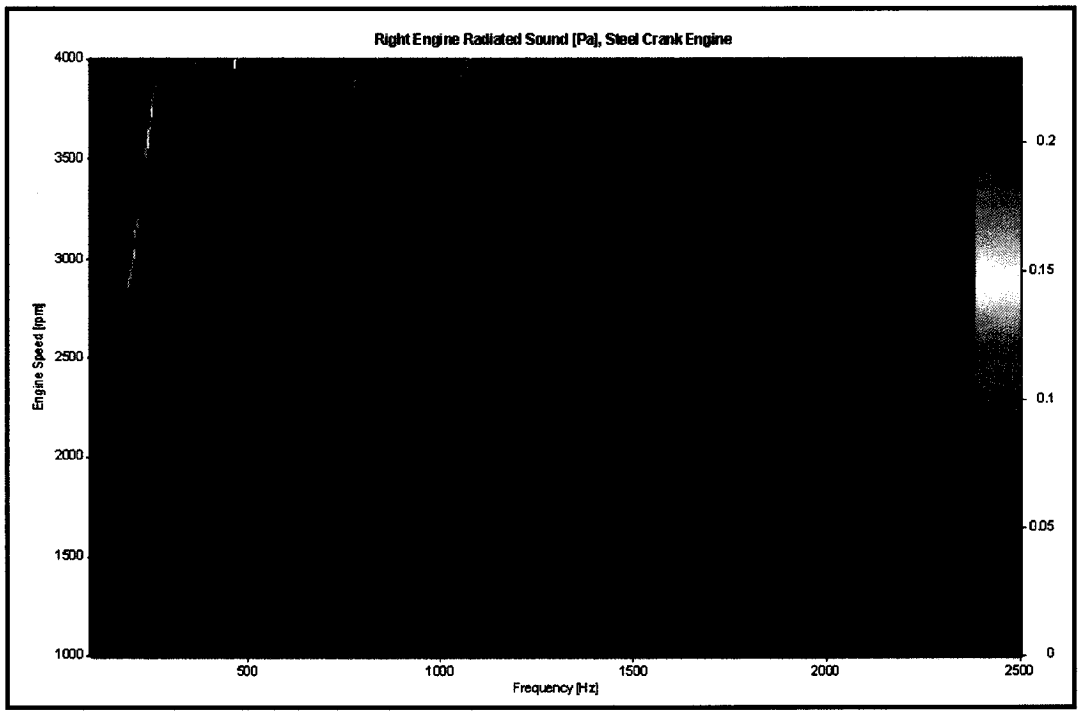

Figure 6.1: Right Engine Radiated Sound [Pa], Steel Crank Engine.

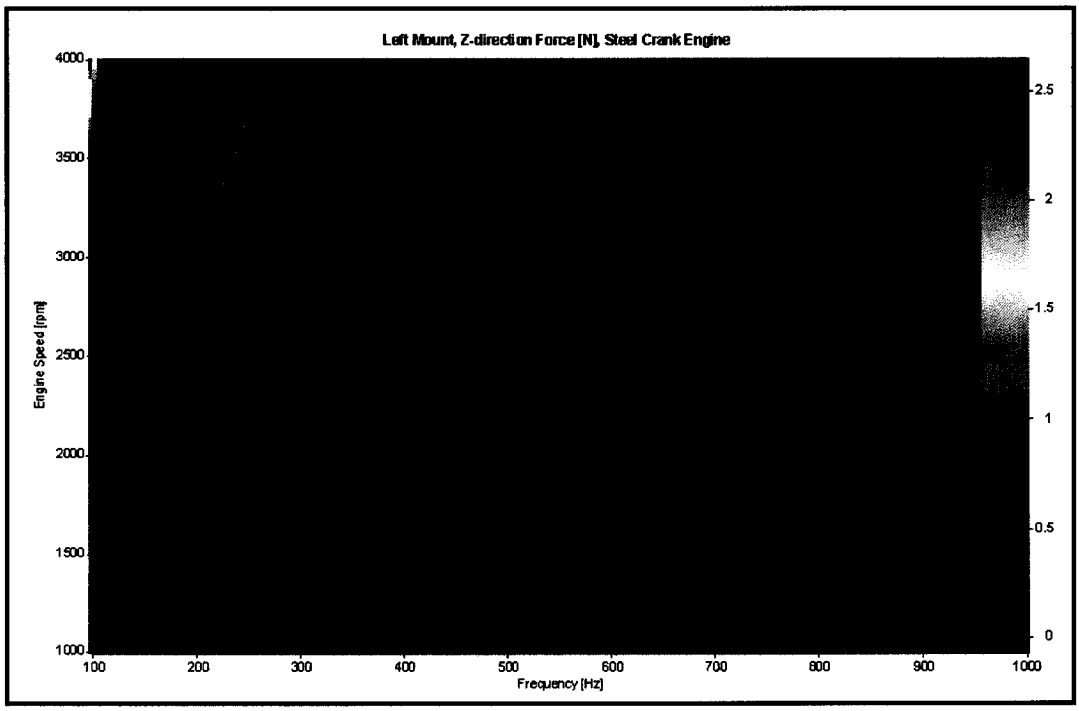

Figure 6.2: Left Mount, Z-direction Force [N], Steel Crank Engine.

Reproduced with permission of the copyright owner. Further reproduction prohibited without permission.

The high amplitude engine radiated sound and vibration occurred at each half-order increment and generally increased with engine speed. The fourth order which corresponds to the V8 engine firing order was most dominant in terms of amplitudes of both engine sound and vibration. The cast iron crankshaft source data was processed in the same manner; however, it was uncertain at that point whether any differences in the results were indicative of the differences in customer's perception of vehicle interior sound and vibration. Consequently, the frequency response functions had to be obtained to estimate vehicle interior sound and vibration levels. This was accomplished by conducting the transfer path analysis in order to calculate the required frequency response functions. The frequency response function calculation results are presented in the next section.

6.2 Frequency Response Functions

The frequency response functions of the system were calculated in order to quantitatively describe the relationships between the inputs and outputs of sound and vibration using modal testing results. They were expressed in terms of attenuation factors for each unit of input at different frequencies with respect to an output. Each of the eleven engine sources (inputs) considered in this study (see Table 4.1) contributed to the five receivers (outputs) of interior sound and vibration considered - left and right ear, and tri-axial acceleration resulting in fifty five frequency response functions. Thus, the frequency response function testing required systematic data collection and analysis. The responses in vehicle interior were measured while exciting the structure acoustically by white noise and through mechanical impact, to obtain sensitivities to air-borne and structure-borne

Reproduced with permission of the copyright owner. Further reproduction prohibited without permission.

inputs to the system, respectively. Figures 6.3, 6.5, 6.7 and 6.9 illustrate examples of the four types of frequency response functions considered in this study. The remaining results are shown in Appendix B.

It is observed that vibration response with highest sensitivity, regardless of the type of excitation, occurs in the Z-direction, which is also the most critical direction in terms of sensitivity of human body to vibration. In addition, Z-direction data is generally most coherent, compared to X-direction and Y-direction data. The trends in terms of resonant frequencies are consistent in all three directions.

The engine sound is attenuated more effectively at higher frequencies (up to 40 dB), however, between 100 Hz and 500 Hz there is less attenuation due to higher sensitivity to engine sound input (approximately 10 dB) at those frequencies.

6.2.1 Coherence

The accuracy of transfer path analysis results depends on the accuracy of frequency response function measurements. In this study, the coherence function was used as an accuracy criterion for determining the usable values or ranges of values of frequency response functions to be included in transfer path analysis. The sound and vibration fields in vehicle interior are complex and not always correlated with the sources considered, such as engine sound and vibration. This is due to the complexity of the structure of the vehicle (components of different materials, use of fasteners) and structural nonlinearities, presence of sources unrelated to the engine, and changing test conditions during acquisition resulting in low coherence and poor relationships between vibroacoustic inputs and outputs. For accurate estimations of vehicle interior sound and

Reproduced with permission of the copyright owner. Further reproduction prohibited without permission.

vibration the vibroacoustic transfer path information from the engine compartment to vehicle interior is very significant and it requires accurate frequency response function measurements. Thus, a coherence function was calculated and analyzed for each frequency response function obtained to decide which data to include in the analysis. Figures 6.4, 6.6, 6.8 and 6.10 illustrate the coherence functions corresponding to the frequency response functions from Figures 6.3, 6.5, 6.7 and 6.9, respectively. The remaining coherence functions are shown in Appendix B.

Based on the test cell sound and vibration cut-off frequencies and coherence data obtained during mounting system qualification testing, the usable frequency ranges include frequency response function data between 100 Hz and 8000 Hz for air-borne transfer paths and between 100 Hz and 1000 Hz for structure-borne transfer paths.

Also, the results indicate that, in general, greater number of vibroacoustic modes of transfer result in less coherent frequency response functions. For example, structural impact excitation frequency response functions result in higher coherence compared to the acoustic excitation frequency response functions considering the same receiver and consequently justify more stringent coherence criteria to be applied in that situation. As a guideline, the impact test data having a coherence value greater than approximately seventy percent were accepted while acoustic excitation data with coherence greater than sixty percent were used in estimating interior sound and vibration.

Reproduced with permission of the copyright owner. Further reproduction prohibited without permission.

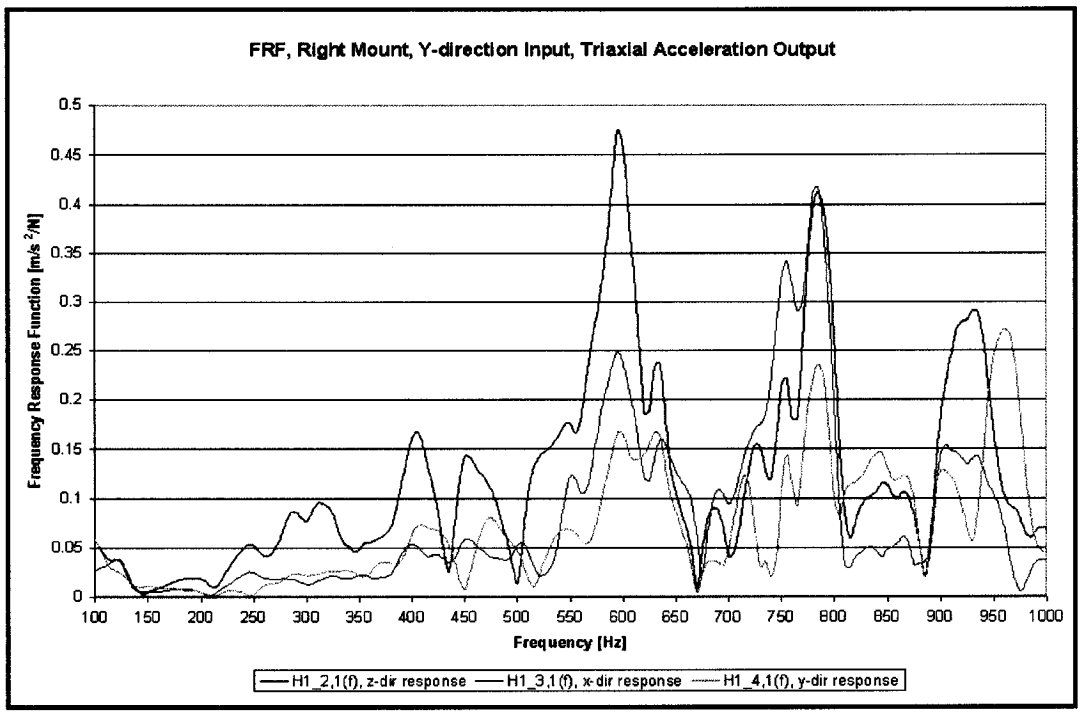

Figure 6.3: Frequency Response Function, Right Mount, Y-direction Input, Triaxial Acceleration Output.

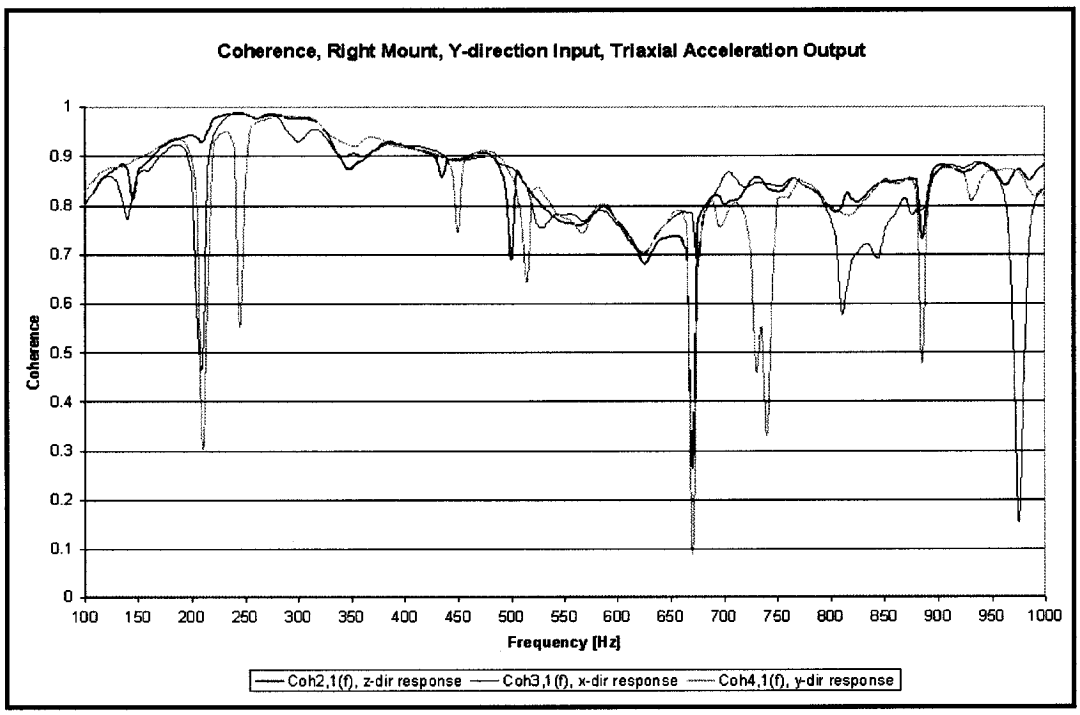

Figure 6.4: Coherence, Right Mount, Y-direction Input, Triaxial Acceleration Output.

Reproduced with permission of the copyright owner. Further reproduction prohibited without permission.

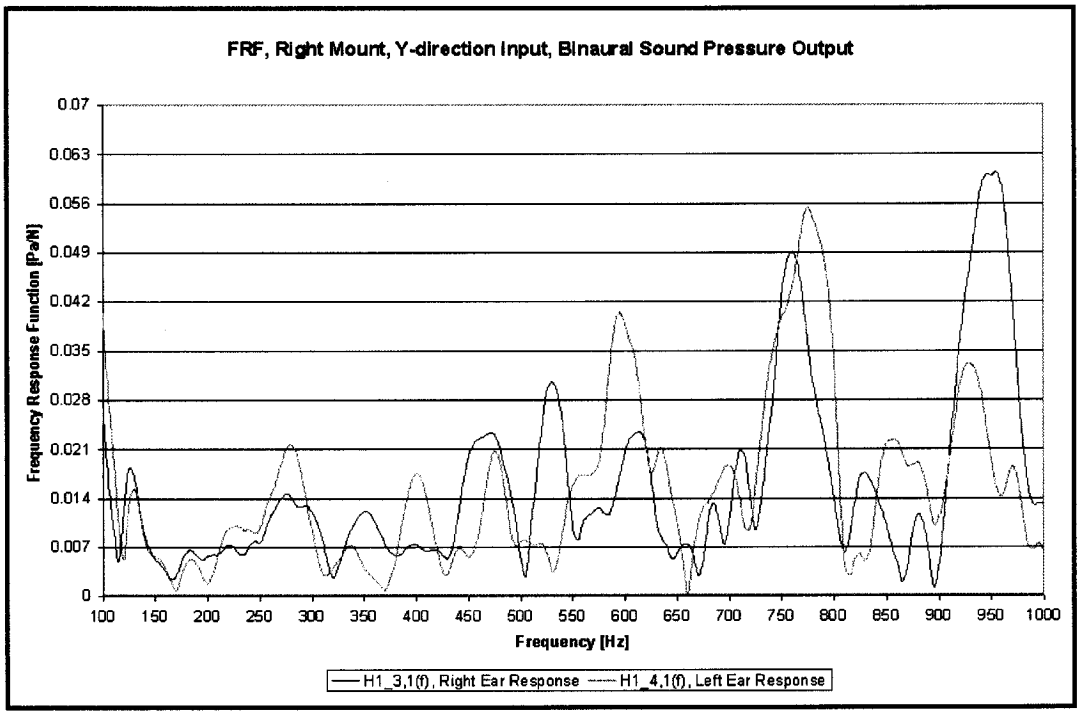

Figure 6.5: Frequency Response Function, Right Mount, Y-direction Input, Binaural Sound Pressure Output.

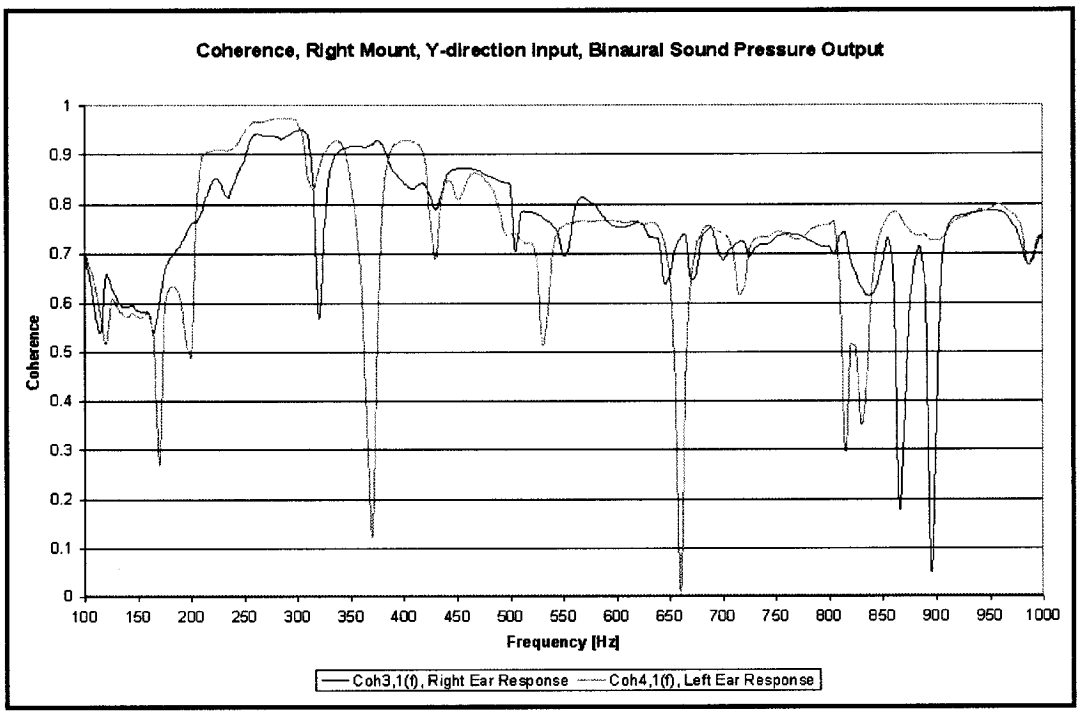

Figure 6.6: Coherence, Right Mount, Y-direction Input, Binaural Sound Pressure Output.

Reproduced with permission of the copyright owner. Further reproduction prohibited without permission.

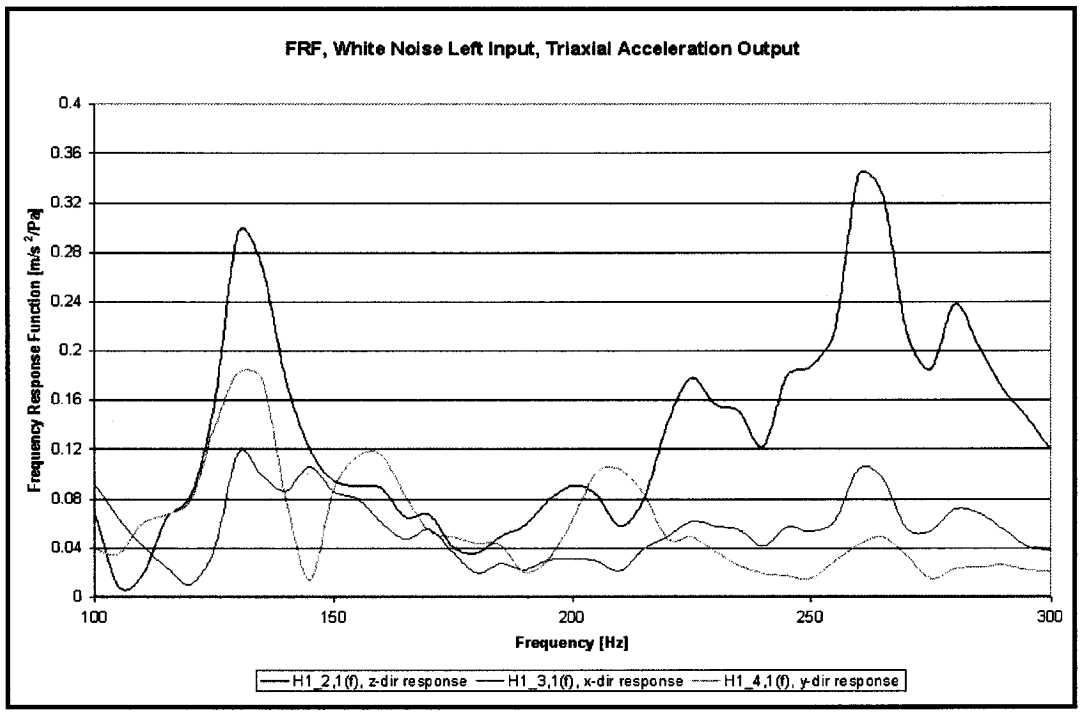

Figure 6.7: Frequency Response Function, White Noise Left Input, Triaxial Acceleration Output.

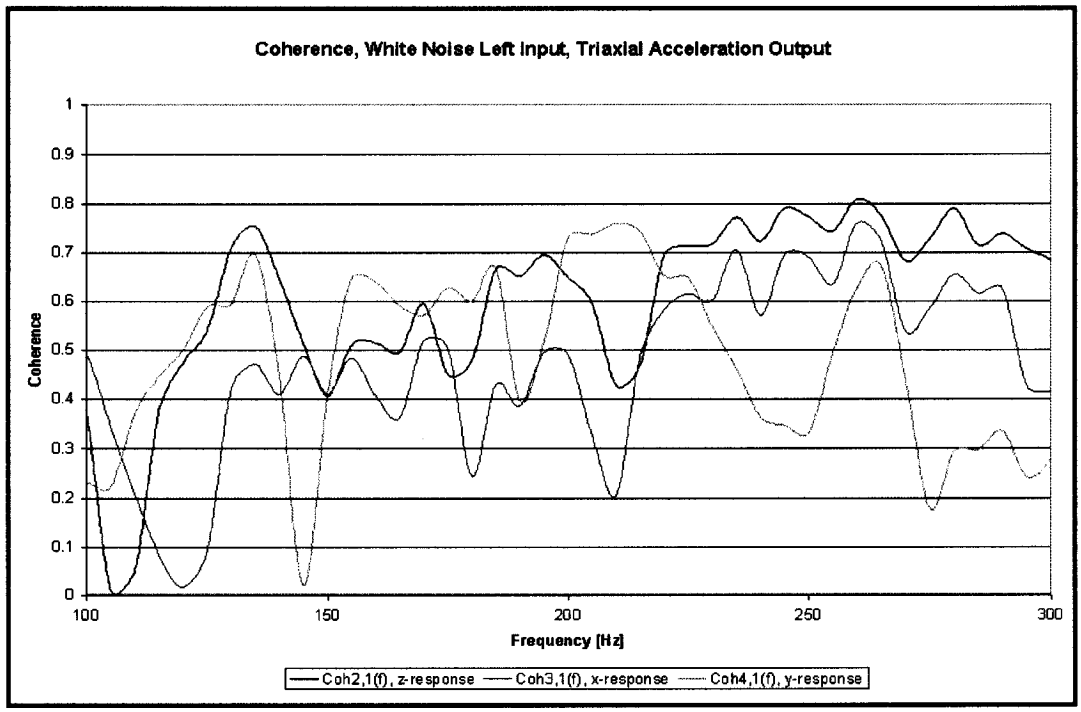

Figure 6.8: Coherence, White Noise Left Input, Triaxial Acceleration Output.

Reproduced with permission of the copyright owner. Further reproduction prohibited without permission.

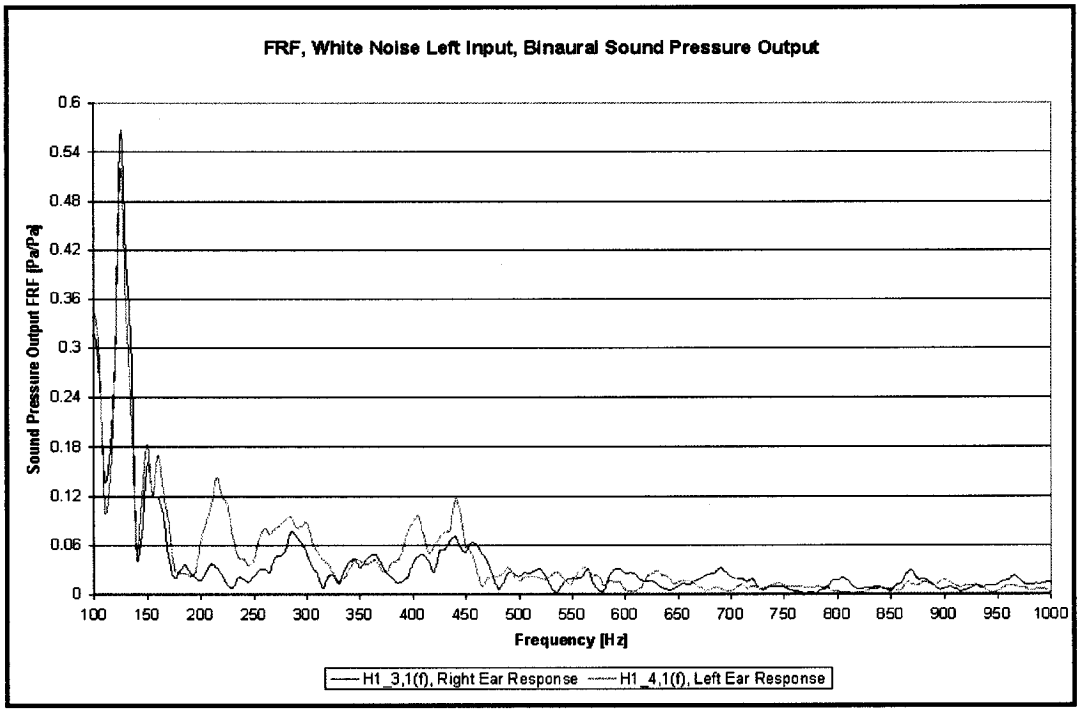

Figure 6.9: Frequency Response Function, White Noise Left Input, Binaural Sound Pressure Output.

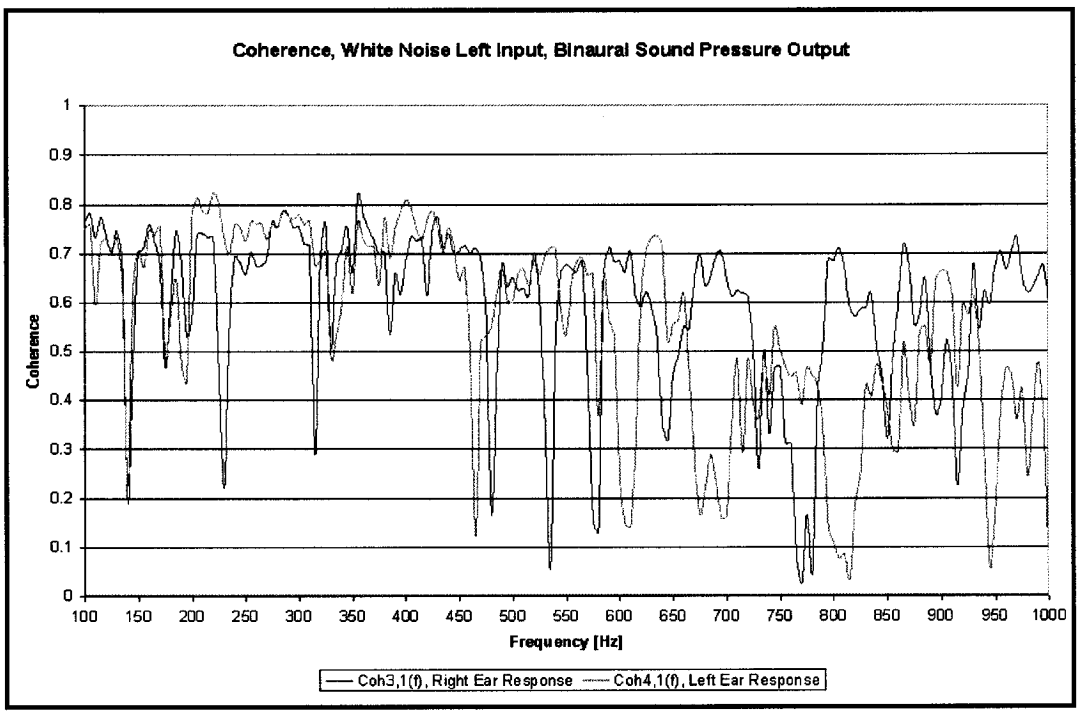

Figure 6.10: Coherence, White Noise Left Input, Binaural Sound Pressure Output.

Reproduced with permission of the copyright owner. Further reproduction prohibited without permission.

6.3 Vehicle Interior Sound and Vibration Evaluation

In order to capture data relevant in depicting customer's perception of vehicle interior sound and vibration the transducers were positioned at representative receiver locations in vehicle interior, namely, the driver's ears and seat track. The binaural head was used to capture the effect of the human head and torso on the sound field and any significant interaural differences that are otherwise impossible to obtain with a simple free field microphone. Other potential locations for vibration measurements included the accelerator pedal, the floor and the steering wheel, but due to unavailability of adequate mounting surfaces their use was likely to result in a limited usable frequency range of collected data, particularly due to the filtering effect at those frequencies. Thus, the data based on the selected receiver measurement locations were both, representative of perceived interior sound and vibration and practical to obtain. The following sections provide examples of objective evaluation results based on these receiver measurements, including estimated and actual vehicle interior sound and vibration.

6.3.1 Objective Evaluation

The total vehicle interior environment results from the sound and vibration combinations of all engine sources and transfer paths of sound and vibration. The transfer path analysis conducted in this study was used to calculate these contributions. In order to ensure accurate calculations it was necessary to verify that the transfer path analysis estimates corresponded as closely as possible to actual measurements of interior sound and vibration. Figures 6.11 and 6.12 show the estimated and actual interior sound at the left ear, respectively, for the frequency range from 100 Hz to 1000 Hz.

Reproduced with permission of the copyright owner. Further reproduction prohibited without permission.

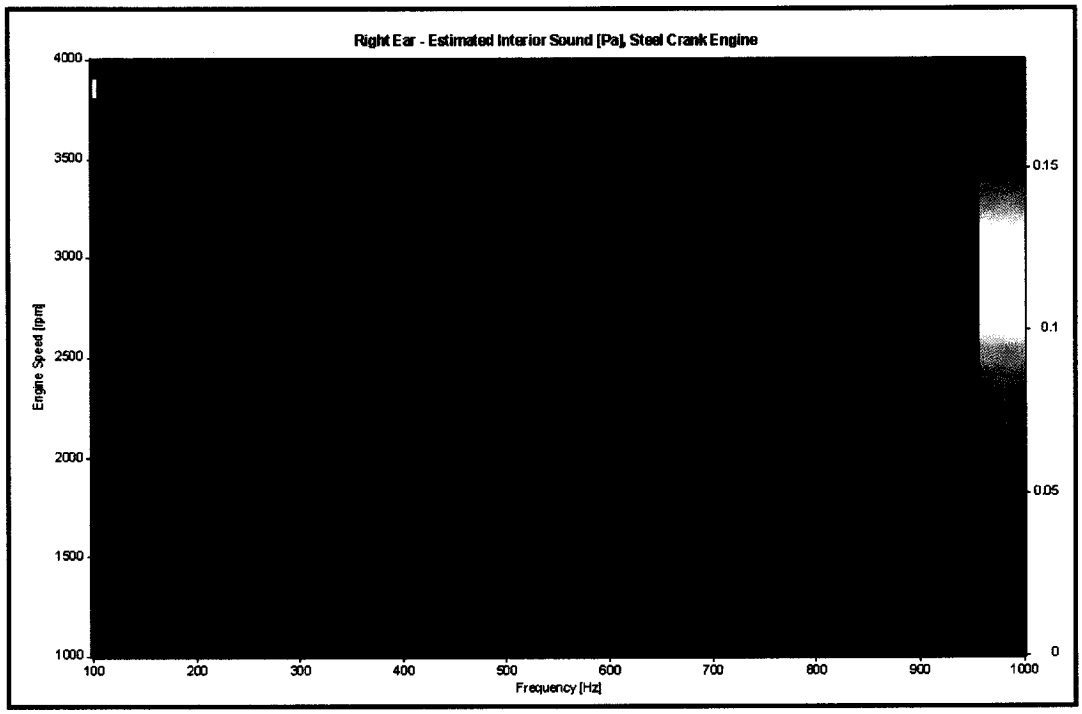

Figure 6.11: Estimated Interior Sound Pressure [Pa], Right Ear, Steel Crank Engine.

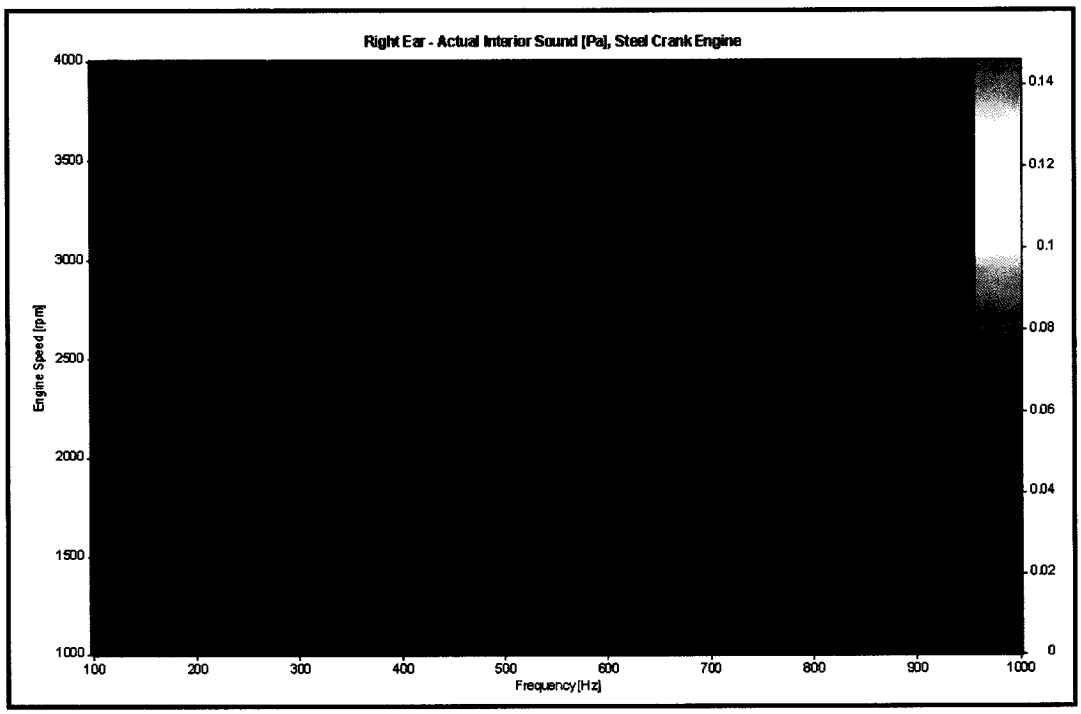

Figure 6.12: Actual Interior Sound Pressure [Pa], Right Ear, Steel Crank Engine.

Reproduced with permission of the copyright owner. Further reproduction prohibited without permission.

The trends in terms of amplitude changes with engine speed and frequency are similar. Although significantly attenuated compared to engine sound and vibration results, fourth order data is still dominant as indicated by both actual and estimated results. In addition, half order amplitudes are also evident and comparable as well. The remaining results, including the cast crank engine results, are shown in Appendix C.

The overall estimated and actual sound levels were calculated at each 50 rpm increment over the considered range of speeds. They were quantified using a logarithmic scale and expressed in terms of decibels (dB). The minimum perceivable sound difference characteristic of human hearing is approximately 3 dB. This information allows a convenient interpretation of overall level data compared to the linear pressure scale. Thus, the difference in sound pressure levels between channels in question and for particular operating conditions must be at least 3 dB, but up to 5 dB, if it is considered to be significant. This criterion is used to compare the estimated and actual levels (as well as steel and cast crank engine results) and establish whether the correlation between them is satisfactory.

In this study, the available interior vibration data includes frequencies above 100 Hz only, and is evaluated in terms of rms acceleration. The lower limit of acceleration amplitude perceptible by the human body may be used as a criterion for correlating estimated and predicted results. However, in this study, a comparison on the basis of general trends, as opposed to amplitudes was utilized due to the necessary filtering of low-frequency components (below 100 Hz) that were significant contributors to interior vibration amplitudes. In addition, the study of human response to vibration (generally concerned with occupational vibration) is associated with low frequency vibration, below

Reproduced with permission of the copyright owner. Further reproduction prohibited without permission.

50 Hz, where the human body is most sensitive to vibration. For example, body vibration resonant frequencies occur between 1 Hz to 10 Hz. Also, the general criteria for whole body vibration includes limits on transmissibility of vibration from the seat to the head and other body parts at low frequencies, and is used to derive standards on occupational vibration. Therefore, the existing data above 100 Hz is insufficient for any general conclusions regarding existing measures of human vibration comfort at those frequencies. It can be observed from the results that the interior vibration levels increase with engine speed. The rate of change of acceleration with respect to time (or speed, since the rate of speed sweep was constant in this study) defined as jerk sometimes influences human vibration comfort, so the criterion may be used in this study to identify operating conditions with potential interior vibration issues. The subjective evaluation results can verify the adequacy of using this criterion to evaluate vibration comfort.

Figures 6.13 through 6.15 illustrate example results of the steel crank/right ear estimated and actual sound pressure levels and Z-direction estimated and actual acceleration, respectively, as functions of engine speed. The remaining results are provided in Appendix C. The satisfactory correlation was established in terms of minimum perceptible sound levels and general vibration amplitude trends, particularly at critical, moderate speeds (between 1500 rpm to 2000 rpm), enabling further analysis of individual path contributions to interior sound and vibration. Also, there were no significant differences in interior sound pressure levels between left and right ear, for both steel and cast crank engines. The differences observed at low and high speeds were due to variability of parameters influencing the interior sound and vibration. These include variability in engine mount stiffness, engine sound and vibration and frequency response

Reproduced with permission of the copyright owner. Further reproduction prohibited without permission.

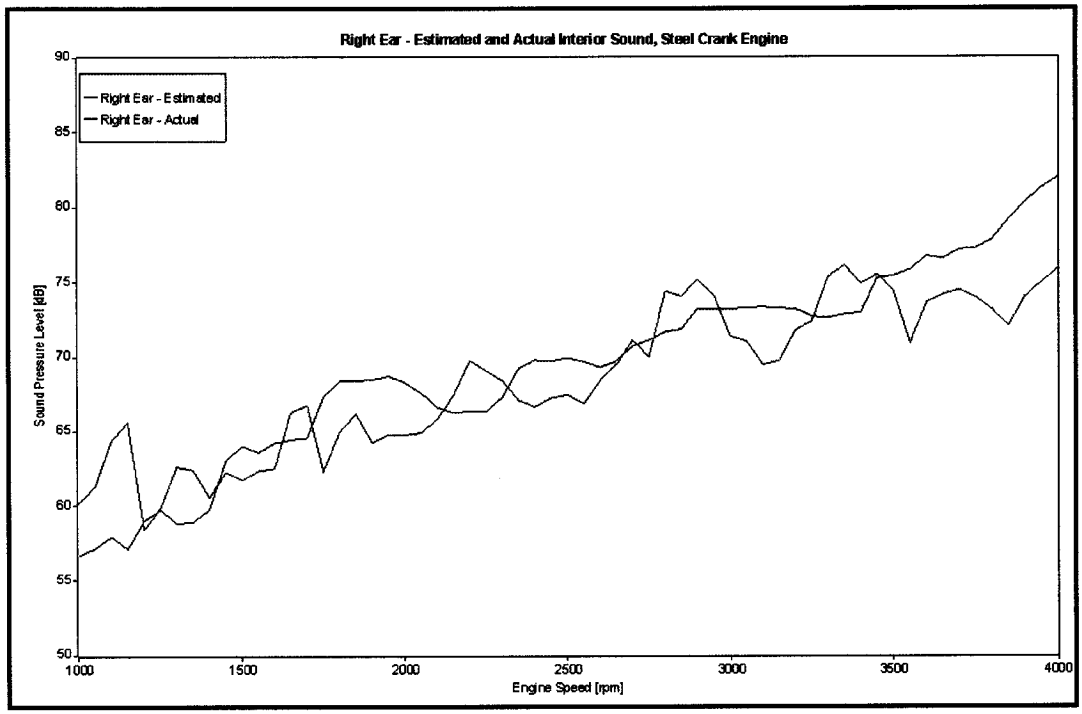

Figure 6.13: Estimated and Actual Interior Sound, Right Ear, Steel Crank Engine.

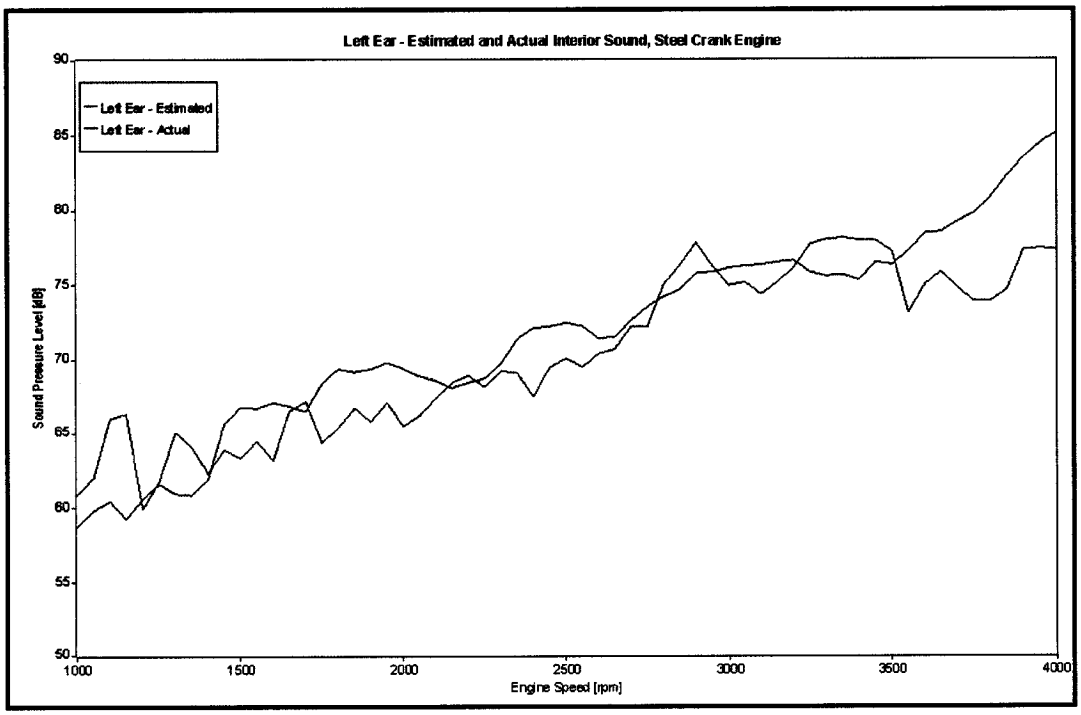

Figure 6.14: Estimated and Actual Interior Sound, Left Ear, Steel Crank Engine.

Reproduced with permission of the copyright owner. Further reproduction prohibited without permission.

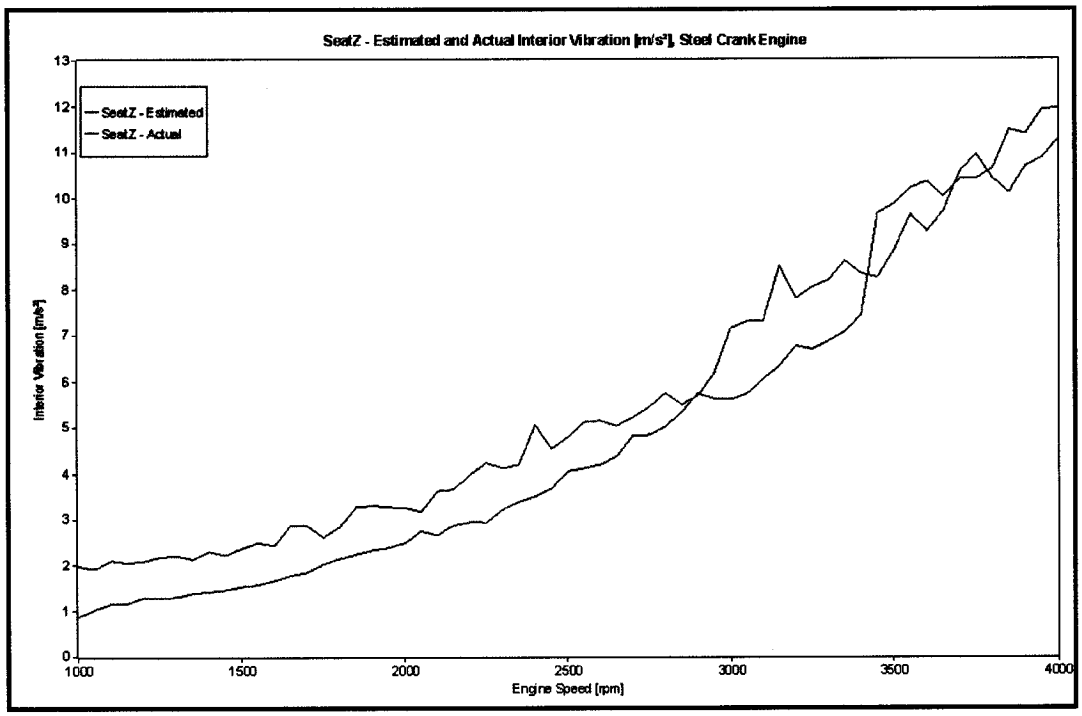

Figure 6.15: Estimated and Actual Interior Vibration, Z-direction, Steel Crank Engine.

functions, and digital signal processing errors (from discrete Fourier transform and frequency domain integration). In addition, a 100 Hz cut-off frequency excluded the effects of low frequency content of engine sound and vibration (such as all first order data caused by out of balance forces), which was especially evident in differences between the estimated and actual vibration levels.

In terms of interior vibration, it is noticeable that both estimated and actual acceleration increases fairly linearly until approximately 2000 rpm, when the rate of change of acceleration starts to increase and continues an increasing trend with notably higher fluctuations in acceleration, particularly at higher speeds, above 3000 rpm. This is the case for all three directions considered for both steel and cast crank engine results. Also, the estimated vibration in the Z-direction most closely follows the actual, measured

Reproduced with permission of the copyright owner. Further reproduction prohibited without permission.

vibration, compared to X-direction and Y-direction estimated and actual vibration (see Appendix C).

The interior sound and vibration are functions of individual contributions of source sound and vibration as well as operating conditions. The transfer path contributions to receivers were calculated for each operating condition and example results shown in Figures 6.16 and 6.17 using the interior sound at the right and left ear, respectively, all for the steel crank engine. The results indicate that, although the overall sound pressure levels closely corresponded to the actual sound pressure levels, there were evident differences in the transfer path contribution to interior sound measured at the left and right ear locations (for both, steel and cast crank engines).

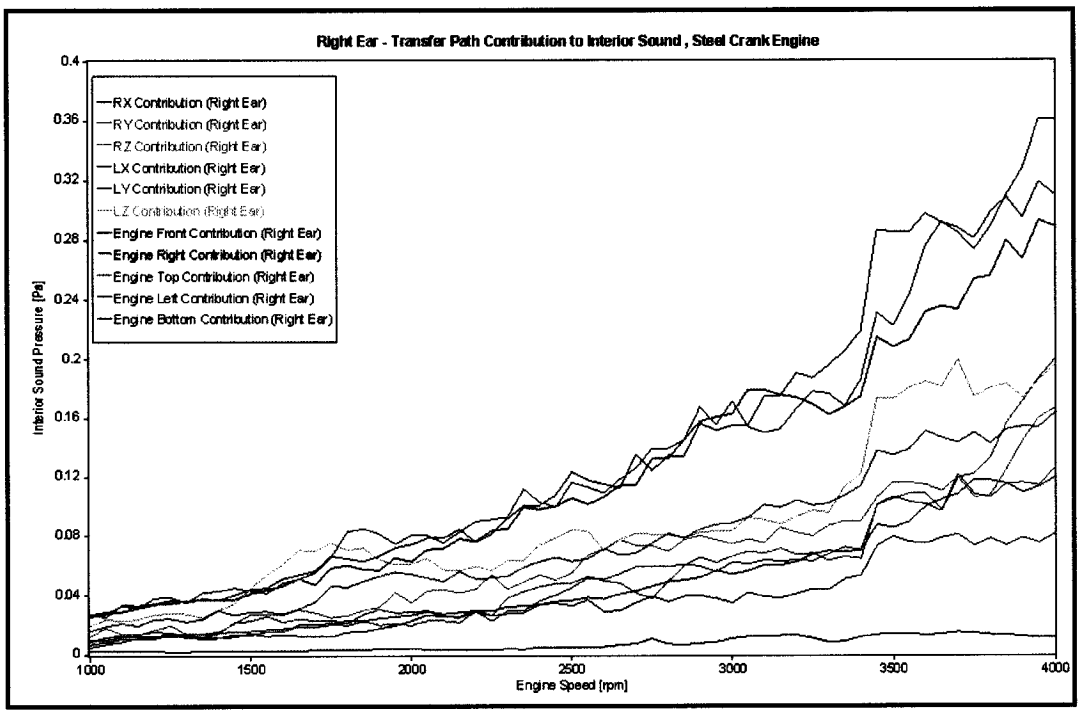

Figure 6.16: Transfer Path Contribution to Interior Sound - Right Ear, Steel Crank Engine.

Reproduced with permission of the copyright owner. Further reproduction prohibited without permission.

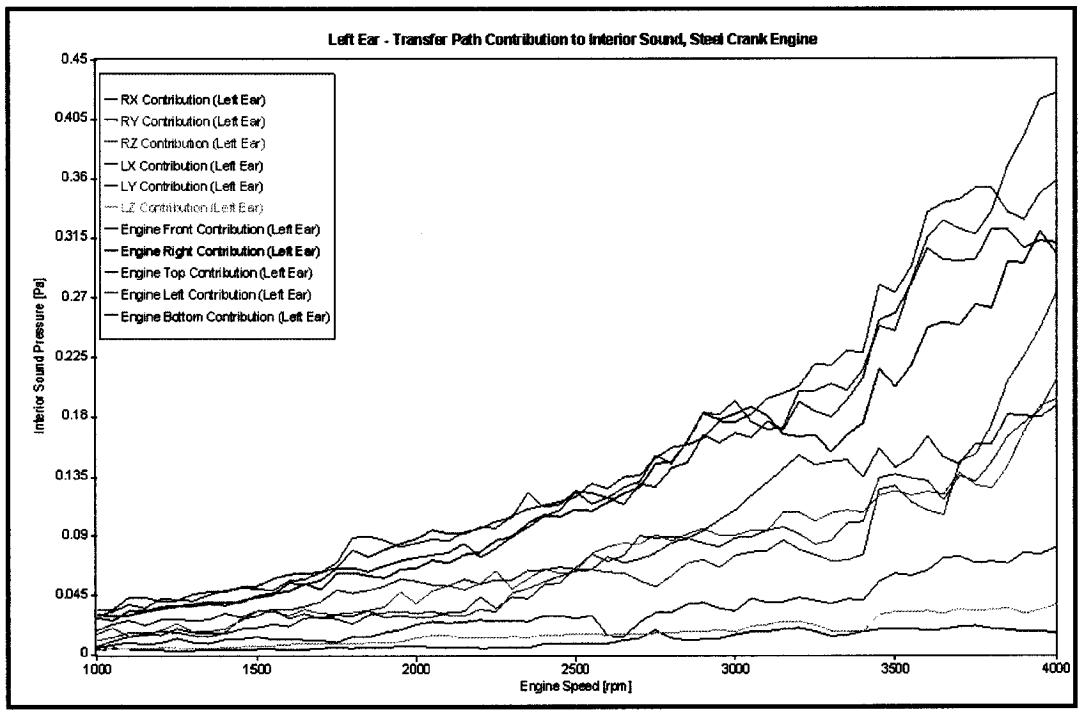

Figure 6.17: Transfer Path Contribution to Interior Sound - Left Ear, Steel Crank Engine.

These differences may be correlated with the differences in perceived and measured sound and as such they may be used as part of a sound quality assessment. The results of subjective evaluations (perceived sound) are expected to verify or challenge this claim.

For a quick summary of results the paths are ranked in terms of their average overall contribution to each receiver. The results are presented in Table 6.1. The ranking of transfer path contributions provides the reader with a graphic indication of contributions when a simple colour scheme is used. For example, the right mount X-direction input is one of the least significant contributors to all receivers of sound and vibration. Also, the front (X-dir) and the left (Y-dir) radiated sound inputs are one of the most significant contributors to vehicle interior sound and vibration. It is noticeable that the left mount, Z-direction input is one of the highest contributors to interior sound at the right ear location, while it is one of the least significant contributors at the left ear location, for

Reproduced with permission of the copyright owner. Further reproduction prohibited without permission.

both steel and cast crank engines. Also, bottom, Z-direction contribution to interior sound at the left ear is significantly higher for a cast crank engine.

Table 6.1: Transfer Path Contribution Ranking.

		Interior Sound				Interior Vibration					
		Right Ear		Left Ear		X-dir		Y-dir		Z-dir	
		Steel Crank	Cast Crank	Steel Crank	Cast Crank	Steel Crank	Cast Crank	Steel Crank	Cast Crank	Steel Crank	Cast Crank
Air-borne Sources	Front, X-dir	2	1	3	3	1	1	1	1	1	1
	Right, Y-dir	3	3	4	4	4	5	4	4	4	5
	Top, Z-dir	5	7	5	8	5	7	5	5	5	6
	Left, Y-dir	1	2	1	2	2	3	2	2	2	2
	Bottom, Z-dir	9	9	2	1	3	2	3	3	3	4
Structure-borne Sources	Right Mount, X-dir	11	11	11	11	11	11	11	11	11	11
	Right Mount, Y-dir	7	6	8	7	6	9	6	8	6	8
	Right Mount, Z-dir	6	5	7	5	7	4	8	7	7	3
	Left Mount, X-dir	10	10	9	9	10	10	10	10	10	10
	Left Mount, Y-dir	8	8	6	6	9	6	7	6	8	7
	Left Mount, Z-dir	4	4	10	10	8	8	9	9	9	9

Significant:	1 - 4
Moderately Significant:	5 - 7
Insignificant:	8 - 11

6.3.2 Subjective Evaluation

The subjective evaluations of interior sound and vibration reflect customer's perception of sound quality. This perception may be based on vastly different criteria for different customers, depending on their personal preferences and expectations in terms of vehicle interior sound and vibration. The subjective evaluations of 10 randomly selected adjudicators provided a fair estimate of typical customer's perception of sound quality. The adjudicators were instructed to evaluate the sound and vibration of the engines at the operating conditions under investigation using a predetermined evaluation scale (scores of 1 to 10). The evaluation was performed over 500 rpm increments from 1000 rpm to

Reproduced with permission of the copyright owner. Further reproduction prohibited without permission.

4000 rpm, so an average evaluation was a reasonable indicator of the overall impression of sound and vibration quality at particular operating conditions (500 rpm increments). The adjudicators were asked to localize sounds by evaluating noise emanating from right and left sides of vehicle interior. Figure 6.18 provides a summary of average interior sound evaluations. Figures 6.19 and 6.20 illustrate average overall interior sound and vibration evaluations, respectively. It is evident that the noise emanating from the right side is slightly worse in quality at all operating conditions, while both steel and cast crank engines exhibit similar results in all sound evaluation categories and operating conditions.

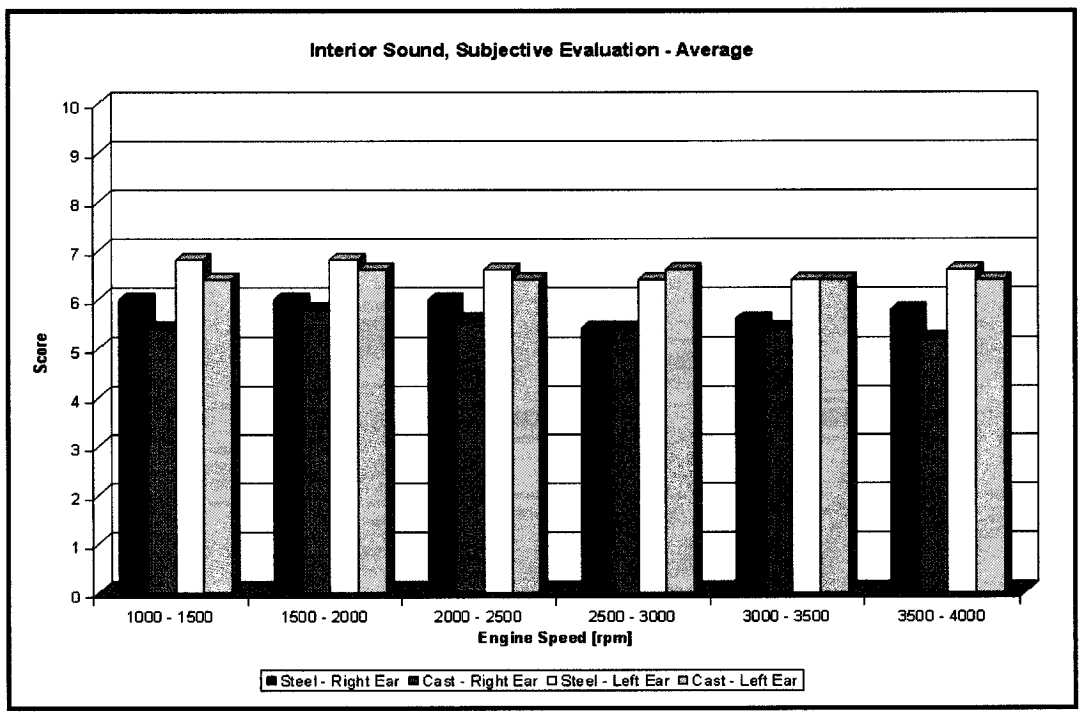

Figure 6.18: Interior Sound, Subjective Evaluation - Average.

Reproduced with permission of the copyright owner. Further reproduction prohibited without permission.

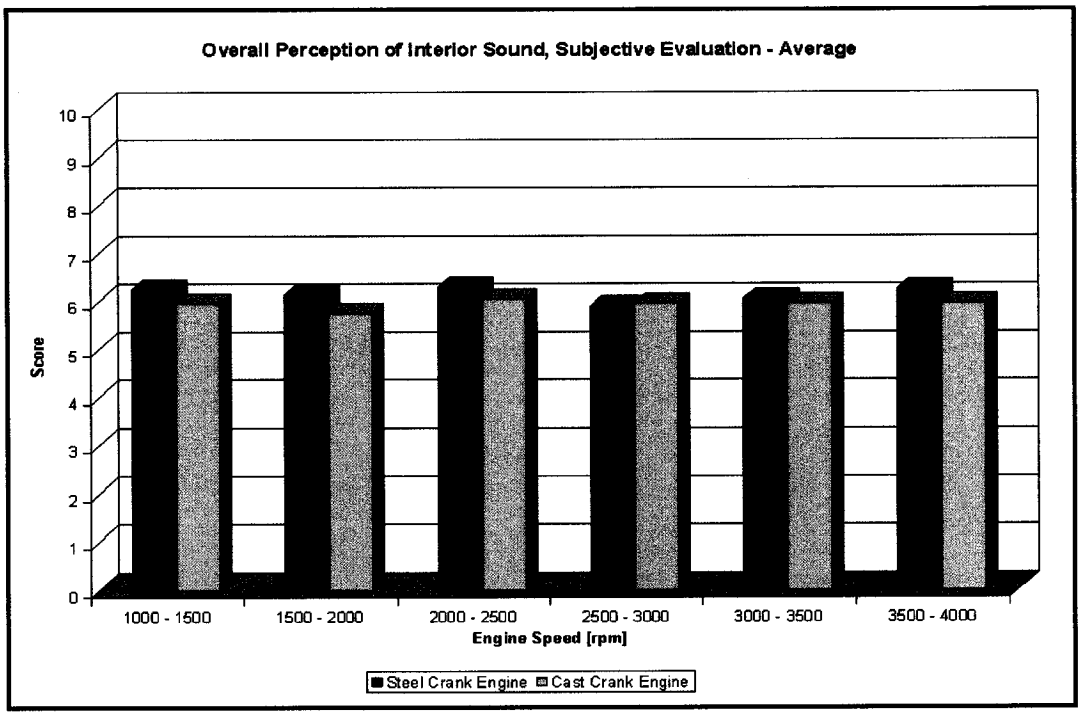

Figure 6.19: Overall Perception of Interior Sound, Subjective Evaluation - Average.

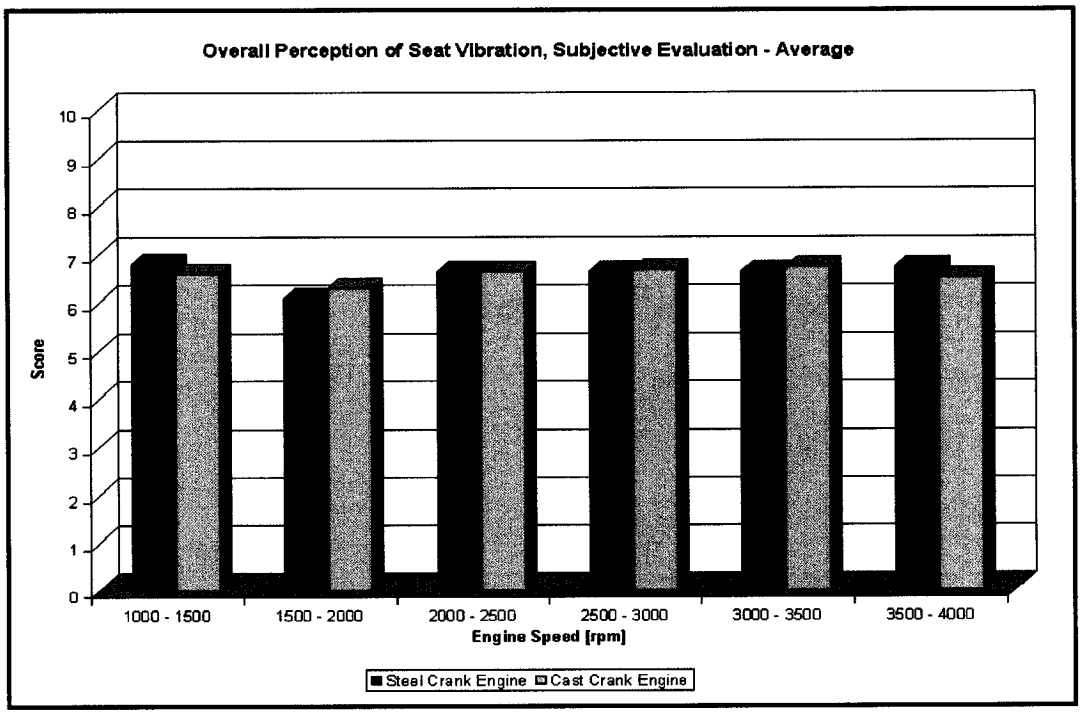

Figure 6.20: Overall Perception of Seat Vibration, Subjective Evaluation - Average.

Reproduced with permission of the copyright owner. Further reproduction prohibited without permission.

The interior vibration objective evaluation included seat track acceleration measurements in all three directions; however, subjective evaluation results indicated that the directional differences in terms of seat vibration were not clearly discernable. The majority of evaluators (70%) evaluated overall vibration only, without individual X, Y, and Z-direction vibration evaluations. Thus, the direction(s) most closely describing customer's response potentially bears most significance and the data collection from the remaining channel(s) may be eliminated in future testing to reduce both testing and processing time. In this study Z-direction data was most valuable as its results exhibited the highest coherence of frequency response functions (see Appendix B) in addition to its accurate estimated results (see Appendix C). Finally, its role in defining human vibration comfort as the axis associated with highest sensitivity in terms of human body vibration is more significant compared to both front to back (X) and side to side (Y) direction vibration. In addition, although the difference was not significant (less than one) in terms of average overall vibration scores, 50% of the evaluators noticed an adverse change in vibration between 1500 rpm to 2000 rpm, while the remaining scores remained unchanged in the same speed range. The objective evaluations indicated that there was a change in the rate of vibration or jerk in that range verifying its adequacy as human comfort criteria in this study.

6.3.2.1 Binaural Replay

The main objective of binaural replay in this study was to confirm the results of subjective evaluations. The data collected from binaural head was converted to stereo WAV files and replayed for evaluation. The sound perception is influenced by physical characteristics of human ear, head and torso, and psychological effects of hearing. The

Reproduced with permission of the copyright owner. Further reproduction prohibited without permission.

physical features actually modify the sound field, thus, accurately recorded sound data must incorporate binaural head recordings. For consistent subjective comparisons of sound samples continuous replay of these samples was performed. Also, the data was replayed using headphones as opposed to loudspeakers to avoid the influence of the surrounding environment on the recordings. The binaural recording and replay allowed for accurate depiction and evaluation of recorded sound in the vehicle interior and confirmed the results of subjective evaluations.

Reproduced with permission of the copyright owner. Further reproduction prohibited without permission.

CHAPTER 7: CONCLUSIONS AND RECOMMENDATIONS

This chapter summarizes the conclusions and recommendations obtained from this study. The conclusions section lists the main results of the study while recommendations provide suggestions for further investigation and improvement of current interior sound and vibration numerical estimation method.

7.1 Conclusions

The following conclusions were reached after thorough analysis of the results of this study:

1. The vehicle interior sound and vibration numerical estimation method based on engine radiated sound and mount vibration was implemented and verified based on close correlation of estimated results and actual measurements. This verified the effectiveness of the acoustic and impact excitation methods employed to simulate the air-borne and structure-borne engine inputs and the transfer paths included in the study for the operating conditions considered.
2. The contributions of individual engine air-borne and structure-borne paths of sound and vibration to total vehicle interior sound and vibration were evaluated and a ranking method was used for rapid identification of significant paths. Common paths of significance included the X-direction of the right mount (consistently the least significant path) and front radiated sound (one of the most significant paths).

Reproduced with permission of the copyright owner. Further reproduction prohibited without permission.

3. The subjective measurements of sound indicated that despite similar overall level objective measurements the differences in perceived sound may still exist and are due to differences in transfer path contribution to interior sound, as illustrated by interaural sound measurements (between left and right ear). The adverse changes in interior vibration comfort were related to the change in rate of change of acceleration known as jerk. The Z-direction acceleration of the seat was sufficient in describing interior vibration; the directions of vibration were indiscernible in subjective evaluations.
4. Although there were slight differences in transfer path contribution the effect of using a more production cost efficient cast crank engine compared to a more durable steel crank engine was negligible in terms of interior sound and vibration as indicated in estimated, objective and subjective results.

7.1.1 Significant Contributions to Research

The following significant contributions have been made to a major powertrain research facility:

1. Developed a comprehensive method to estimate vehicle interior sound and vibration based engine radiated sound and mount vibration tests performed regularly at powertrain research facilities.
2. Utilized a four-channel power source and data acquisition unit to perform the necessary modal testing of vehicle body and frame assembly.
3. Developed a ranking method in order to identify the significance of transfer paths contributing to vehicle interior sound and vibration.

Reproduced with permission of the copyright owner. Further reproduction prohibited without permission.

4. Established that there is a relationship between perceived sound quality and arrangement of transfer path contributions to interior sound.

7.2 Recommendations

The following recommendations may be used for future research of interior vehicle sound and vibration estimation method:

1. Investigate interior sound and vibration at other receiver locations such as passenger seat(s). Also, other sources of interior sound and vibration such as intake and exhaust systems using the developed estimation method should be included to improve the vehicle interior sound and vibration estimations.
2. Utilize currently available sound quality metrics to further characterize interior sound.
3. Improve the engine mounting system set-up for mount vibration testing in order to expand the usable frequency range and allow investigation of structure-borne transfer paths below 100 Hz.
4. Implement engine torsional vibration as a source input for the estimation method used in the study.

Reproduced with permission of the copyright owner. Further reproduction prohibited without permission.

REFERENCES

1. Alt, N.W., Wiehagen, N., Schlitzer, M.W., "Interior Noise Simulation for Improved Vehicle Sound", SAE Paper 2001-01-1539, 8 pages.

2. Amman, S., Pielemeier, W., Meier, R., Bergeron, S., Shiau, N.M., Gorodisher, A., "Subjective and Objective Quantification of Steady-State Idle Vibration Felt Through the Seat", SAE Paper 2003-01-1512, 6 pages.

3. Biermayer, W., Thomann, S., Brandl, F., "A Software Tool for Noise Quality and Brand Sound Development", SAE Paper 2001-01-1573, 11 pages.

4. Boardman, A.J., Paddan, G.S., "Estimation of Occupied Seat Vibration Transfer Functions", SAE Paper 2000-01-0646, 5 pages.

5. Bocksch, R., Schneider, G., Moore, J., Ver, I., "Empirical Noise Model for Power Train Noise in a Passenger Vehicle", SAE Paper 1999-01-1757, 12 pages.

6. Brandl, F.K., Biermayer, W., "A New Tool for the Onboard Objective Assessment of Vehicle Interior Noise Quality", SAE Paper 1999-01-1695, 11 pages.

7. Diemer, P., Hueser, M.G., Govindswamy, K., D'Anna, T., "Aspects of Powerplant Integration With Emphasis on Mount and Bracket Optimization", SAE Paper 2003-01-1468, 11 pages.

8. Dumbacher, S.M., Brown, D.L., Blough, J.R., Bono, R.W., "Practical Aspects of Making NAH Measurements", SAE Paper 99NV-174, 10 pages.

9. Esposito, R.A., Freeman, G.E., "Glazing for Vehicle Interior Noise Reduction", SAE Paper 2002-01-1993, 9 pages.

10. Feng, B., Wakefield, G.H., Good, M.D., Otto, N.C., Rebandt, R., "On the Perceived Roughness of Automotive Powertrain Sounds", SAE Paper 951312, 9 pages.

11. Ferraz, F.G., Cherman, A.L., "Acoustic and Tactile Transfer Functions Measurements on Automotive Development", SAE Paper 2003-01-3569, 3 pages.

12. Genuit, K., "Objective Analyses of Binaural Recordings", SAE Paper 951287, 5 pages.

13. Genuit, K, Bray, W.R., "A Virtual Car: Prediction of Sound and Vibration in an Interactive Simulation Environment", SAE Paper 2001-01-1474, 7 pages.

Reproduced with permission of the copyright owner. Further reproduction prohibited without permission.

14. Genuit, K., Poggenburg, J., "The Design of Vehicle Interior Noise Using Binaural Transfer Path Analysis", SAE Paper 1999-01-1808, 6 pages.

15. Grasso, C., Martonelli, M., Petrella, L., Sbarbati, F., "Powertrain NVH Refinement", SAE Paper 2004-01-0400, 6 pages.

16. Gu, Y, "A Comparison Test of Transmissibility Response from Human Occupant and Anthropodynamic Dummy", SAE Paper 980655, 2 pages.

17. Haste, F., Nachimuthu, A., "Calculating Partial Contribution Using Component Sensitivity Values: A Different Approach to Transfer Path Analysis", SAE Paper 1999-01-1693, 10 pages.

18. Hemingray, P., "The Relationship of Automotive Balance Limits to Human Perception", SAE Paper 2004-01-0401, 5 pages.

19. Hoffman, D.M.W., Dowling, D.R., "Modeling Fully-Coupled Rigid Engine Dynamics and Vibrations", SAE Paper 1999-01-1749, 11 pages.

20. Lee, J.H., Oh, K., Park, Y.S., Gwon, D.H., Park, S.K., "Transfer Path Analysis of Structure-Borne Shock Absorber Noise in a Passenger Car", SAE Paper 2001-01-1441, 7 pages.

21. Liu, J., Franz, E., "An Examination of the Effect of Seat Free-play on Modal Analysis Results", SAE Paper 2003-01-1598, 6 pages.

22. LMS International, "Sound Quality Engineering: The fundamentals to get the sound right", 1997.

23. LMS International, "Transfer Path Analysis: The Qualification and Quantification of Vibro-Acoustic Transfer Paths", 1997.

24. Madjlesi, R., Khajepour, A., Ismail, F., Mihalic, J., Rice, B., "Advance Noise Path Analysis, a Robust Engine Mount Optimization Tool", SAE Paper 2003-01-3117, 10 pages.

25. Maruyama, S., Hasegawa, A., Hyoudou, Y., "Interior Noise Analysis Based on Acoustic Excitation Tests at Low-Frequency Range", SAE Paper 1999-01-1806, 7 pages.

26. Mukai, H., Sawatari, K., Naruse, K., Fukumori, H., "Visualization of Sound Field in Automobile Cabin using Sound Intensity Technique", SAE Paper 2003-01-2017, 3 pages.

Reproduced with permission of the copyright owner. Further reproduction prohibited without permission.

27. Muller, M., Weltin, U., Law, D., Roberts, M.M., Siebler, T.W., "The Effect on Engine Mounts on the Noise and Vibration Behavior of Vehicles", SAE Paper 940607, 8 pages.

28. Patil, A., Crocker, J., "Prediction and Optimization of Radiated Sound Power and Radiation Efficiency of Vibrating Structures Using FEM", SAE Paper 2000-01-0726, 8 pages.

29. Paul, D., "Estimation of Engine NVH Variability", SAE Paper 2001-01-1522, 5 pages.

30. Pinto, F.C., De Jesus, G.F., Martinez, R.B., Morinaga, R., "Powertrain Vibrations vs. Internal Noise, Eternal Challenge", SAE Paper 2001-01-3945, 5 pages.

31. Renzo, B., Paola, B., Celibreti, L., Vanni, F., "Objective Evaluation of Vibroacoustical Quality", SAE Paper 2004-01-0405, 12 pages.

32. Rust, A., Edlinger, I., "Active Path Tracking - A Rapid Method for the Identification of Structure Borne Noise Paths in Vehicle Chasis", SAE Paper 2001-01-1470, 7 pages.

33. Schroeder, L.E., "Feasibility of Using Acoustic Room Models and Measured Sound Power to Estimate Vehicle Interior Noise", SAE Paper 2001-01-1533, 4 pages.

34. Selmane, A., Felice, M., Li, Y., "Engine Cylinder Block and Heads NVH Improvements: Bolt Accelerations Computation Methodology", SAE Paper 2004-01-0990, 7 pages.

35. Silveira de Abreu, D., Yoneda, R., Cherman, A.L., Sczibor, V., "Vibroacoustic Study in Automobile Vehicles", SAE Paper 2003-01-3606, 8 pages.

36. Singh, V.K., Wani, N., Monkaba, V.D., Bloughand, J.R., Gwaltney, G., "Powertrain Transfer Path Analysis of a Truck", SAE Paper 2001-01-2817, 5 pages.

37. Suh, I.S., "Application of Time-Frequency Representation Techniques to the Impact-Induced Noise and Vibration from Engines", SAE Paper 2002-01-0453, 9 pages.

38. Tjong, J., "Engine Dynamic Signal Monitoring and Diagnostics", Ph.D. Dissertation, University of Windsor, 1992.

39. Terazawa, N., Wakita, T., "A New Method of Engine Sound Design for Car Interior Noise Using a Psychoacoustic Index" SAE Paper 2004-01-0406, 8 pages.

Reproduced with permission of the copyright owner. Further reproduction prohibited without permission.

40. Unruh, J.F., Till, P.D., "Interior Noise Source/Path Identification Technology", SAE Paper 2000-01-1709, 9 pages.

41. Van Der Linden, P.J.G., Keppens, T., Raff, J., Schnur, J., "Determination of the Noise Contributions of Engine Surfaces", SAE Paper 2001-01-1482, 7 pages.

42. Verver, M.M., Van Hoof, J., "Determination of Human-Seat-Interaction in Vertical Vibrations in MADYMO", SAE Paper 2002-01-3083, 6 pages.

43. Wang, D., Goetchius, G.M., Onsay, T., "Validation of a SEA Model for a Minivan: Use of Ideal Air- and Structure- Borne Sources", SAE Paper 1999-01-1697, 8 pages.

44. Wang, T., Sturia, F., Salazar, V.C., "Mount Rate Robust Optimization for Idle Shake Performance", SAE Paper 2004-01-1536, 5 pages.

Reproduced with permission of the copyright owner. Further reproduction prohibited without permission.

BIBLIOGRAPHY

1. Beidl, C.V., Rust, A., Rasser, M., "Key Steps and Methods in the Design and Development of Low Noise Engines", SAE Paper 1999-01-1745, 9 pages.

2. Bell, D.H., Bell L.H., "Industrial Noise Control - Fundamentals and Applications: Second Edition, Revised and Expanded", Marcel Dekker, 1994, pages 37-63.

3. Bruel and Kjaer Company, Technical and Lecture Notes.

4. Clapper, M., Blommer, M., "Masking Perception Analysis Software (MPAS) for Tonal Level Setting in Powertrain NVH", SAE Paper 2003-01-1500, 9 pages.

5. Ewins, D.J., "Modal Testing: Theory and Practice", Bruel and Kjaer, 1986, pages 87-152.

6. Kaatz, S., Abe, T., Vanhaaften, W., Wilson, B.K., Schwalm, B., Obourn, L., Newberger, N., "The Ford Motor Company Transmission NVH Test Cell", SAE Paper 2003-01-1681, 7 pages.

7. LMS International, Transfer Path Analysis Technical and Lecture Notes.

8. Qatu, M., Sirafi, M., "Accurate Modeling for the Powertrain and Subframe Modes", SAE Paper 2003-01-1469, 4 pages.

9. Wang, S., Baron, E., "Study of Influences of Flywheel Bending Stiffness on Powertrain Acceleration Noises", SAE Paper 2003-01-1445, 7 pages.

10. Yamashita, K., Okamura, H., Shimizu, S., Sakamoto, H., Ishida, M., "NVH Experimental Analyses for an Engine Structure Model Assembled with Ordinary Tap Bolts and with Through Bolts", SAE Paper 2003-01-1732, 9 pages.

Reproduced with permission of the copyright owner. Further reproduction prohibited without permission.

APPENDICES

Reproduced with permission of the copyright owner. Further reproduction prohibited without permission.

A. SUMMARY CHART OF THE REFERENCES

Reproduced with permission of the copyright owner. Further reproduction prohibited without permission.

Table A.1: Summary Chart of the References

	Year	Ref. No.	Transfer Path Analysis / Principal Component Analysis	Structure-borne Operating Force Input	Structure-borne Transfer Function Measurements	Air-borne Sound Pressure Inputs	Air-borne Transfer Function Measurements	Finite Element Analysis	Interior Sound and Vibration Subjective Evaluation	Interior Sound and Vibration Objective Evaluation	Sound and Vibration Analysis Techniques
Alt, N.W.	2001	1			x		x		x		
Amman, S.	2003	2								x	
Biermayer, W.	2001	3							x		
Boardman., A.J.	2000	4			x						
Bocksch, R.	1999	5				x	x				
Brandl, F.K.	1999	6							x		
Diemer, P.	2003	7		x							
Dumbacher, S.M.	1999	8								x	
Esposito, R.A.	2002	9								x	
Feng, B.	1995	10							x		
Ferraz, F.G.	2003	11		x	x						
Genuit, K.	1995	12								x	
Genuit, K.	2001	13								x	
Genuit, K.	1999	14			x		x			x	
Grasso, C.	2004	15								x	
Gu, Y.	1998	16								x	
Haste, F.	1999	17	x								
Hemingray, P.	2004	18							x	x	
Hoffman, D.M.W.	1999	19		x							
Lee, J.H.	2001	20	x								
Liu, J.	2003	21			x						
LMS International	1997	22								x	
LMS International	1997	23								x	
Madjlesi, R.	2003	24			x						
Maruyama, S.	1999	25		x				x			
Mukai, H.	2003	26								x	
Muller, M.	1994	27		x							
Patil, A.	2000	28						x			
Paul, D.	2001	29									x
Pinto, F.C.	2001	30		x						x	
Renzo, B.	2004	31							x	x	
Rust, A.	2001	32	x	x	x					x	
Schroeder, L.E.	2001	33								x	
Selmane, A.	2004	34									x
Silvera de Abreu, D.	2003	35								x	
Singh, V.K.	2001	36		x							
Suh, I.S.	2002	37								x	
Tjong, J.	1992	38									x
Terazawa, N.	2004	39							x	x	
Unruh, J.F.	2000	40	x								
Van Der Linden, P.J.G.	2001	41				x					
Verver, M.M.	2002	42								x	
Wang, D.	1999	43								x	
Wang, T.	2004	44						x			

Reproduced with permission of the copyright owner. Further reproduction prohibited without permission.

B. FREQUENCY RESPONSE FUNCTIONS

Reproduced with permission of the copyright owner. Further reproduction prohibited without permission.

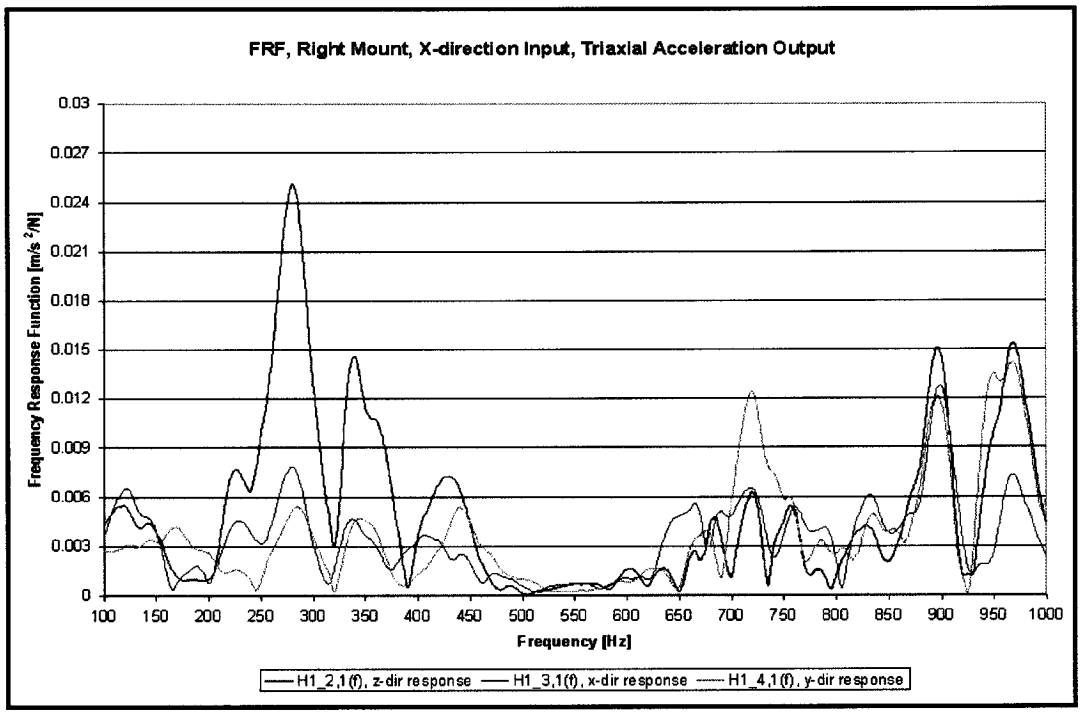

Figure B.1: Frequency Response Function, Right Mount, X-direction Input, Triaxial Acceleration Output.

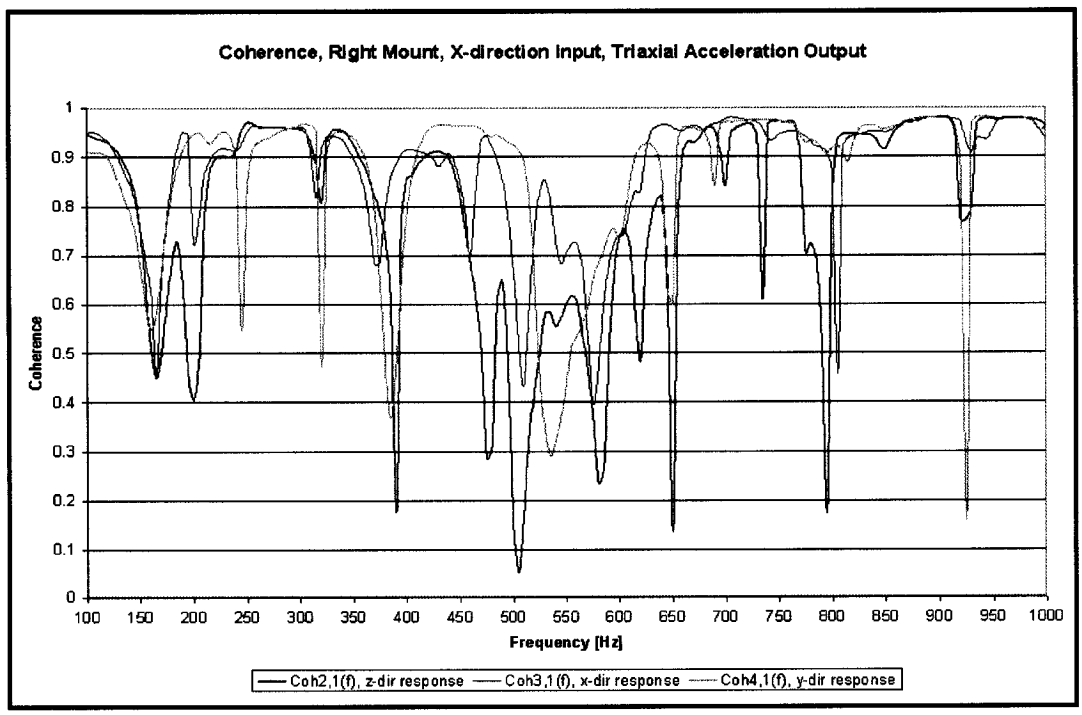

Figure B.2: Coherence, Right Mount, X-direction Input, Triaxial Acceleration Output.

Reproduced with permission of the copyright owner. Further reproduction prohibited without permission.

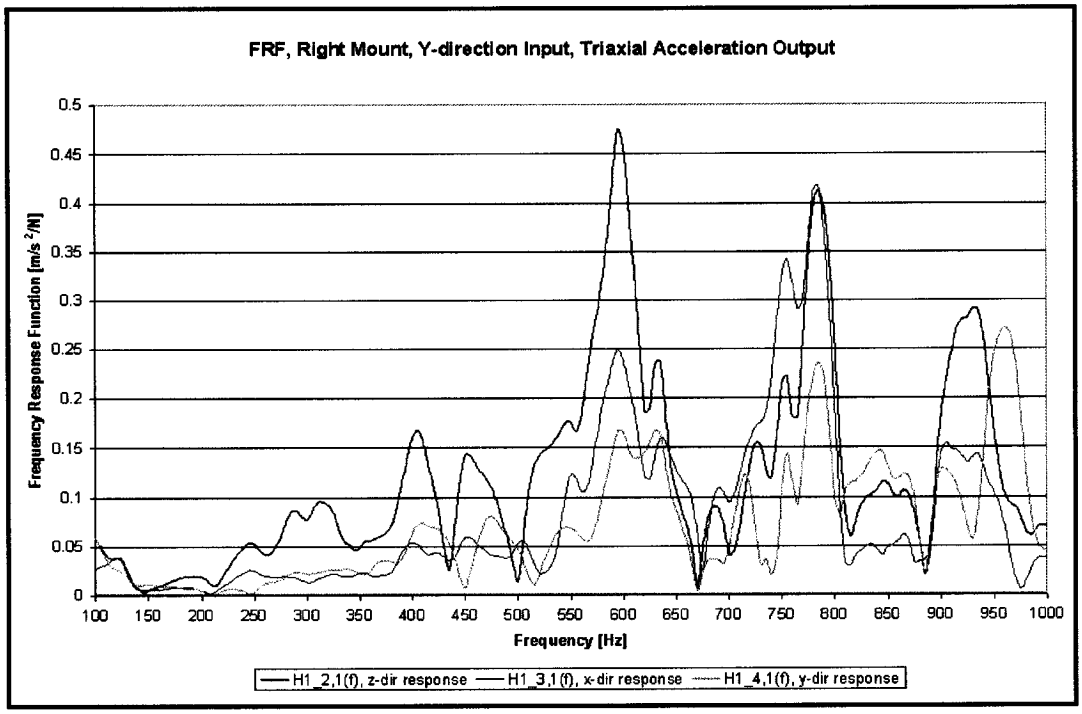

Figure B.3: Frequency Response Function, Right Mount, Y-direction Input, Triaxial Acceleration Output.

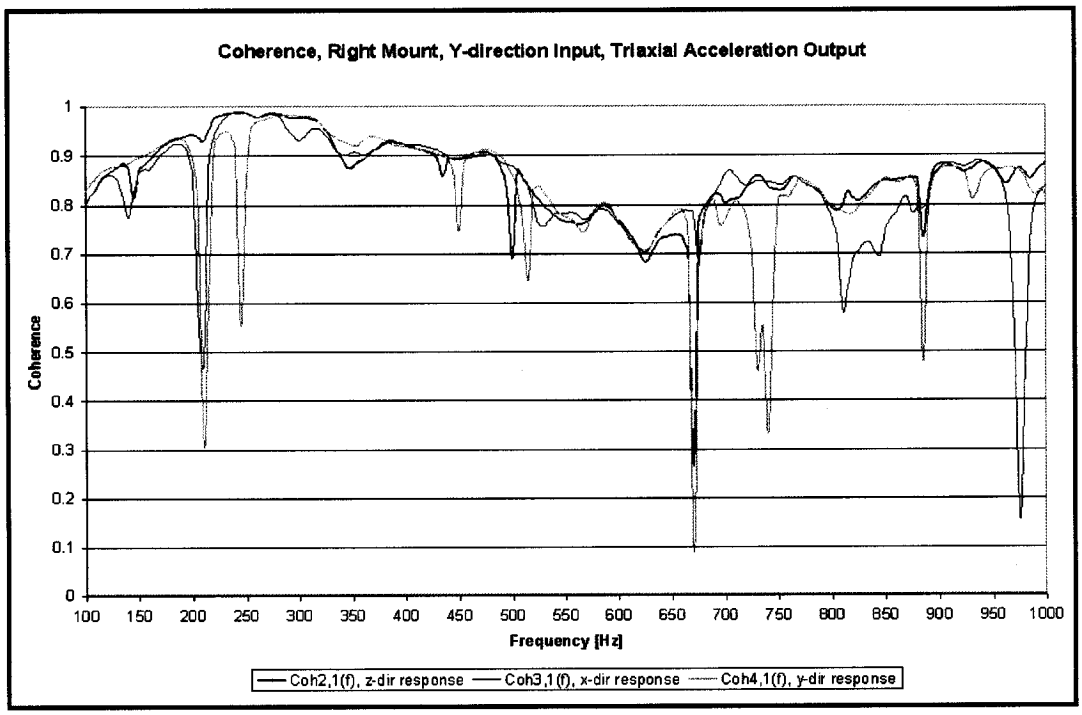

Figure B.4: Coherence, Right Mount, Y-direction Input, Triaxial Acceleration Output.

Reproduced with permission of the copyright owner. Further reproduction prohibited without permission.

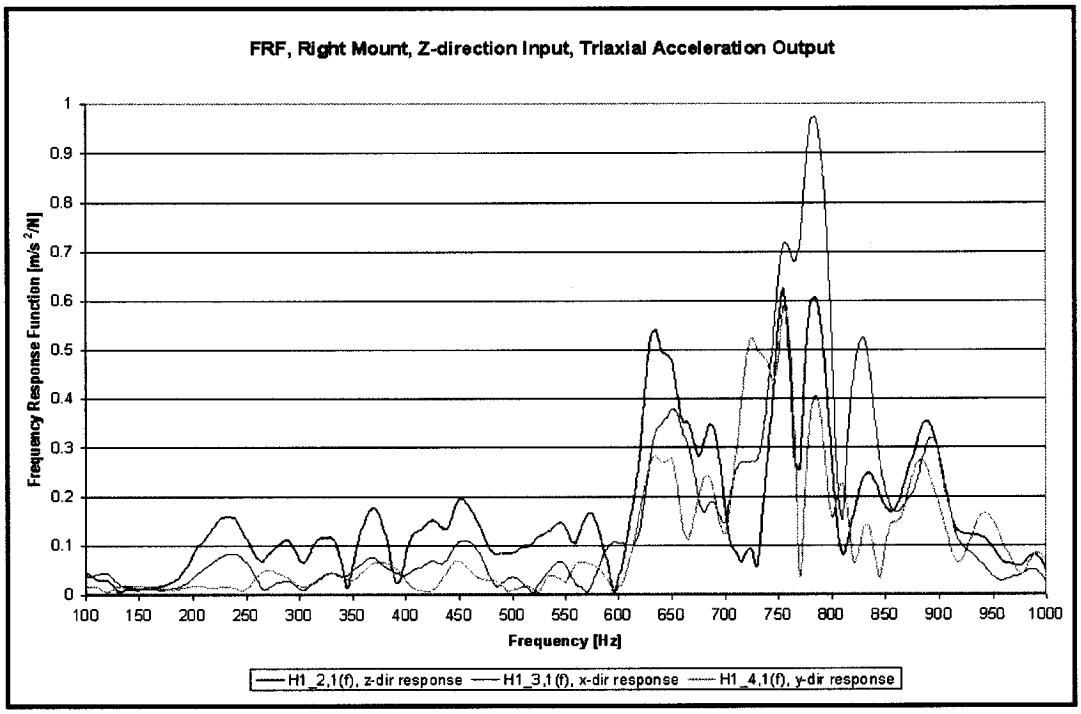

Figure B.5: Frequency Response Function, Right Mount, Z-direction Input, Triaxial Acceleration Output.

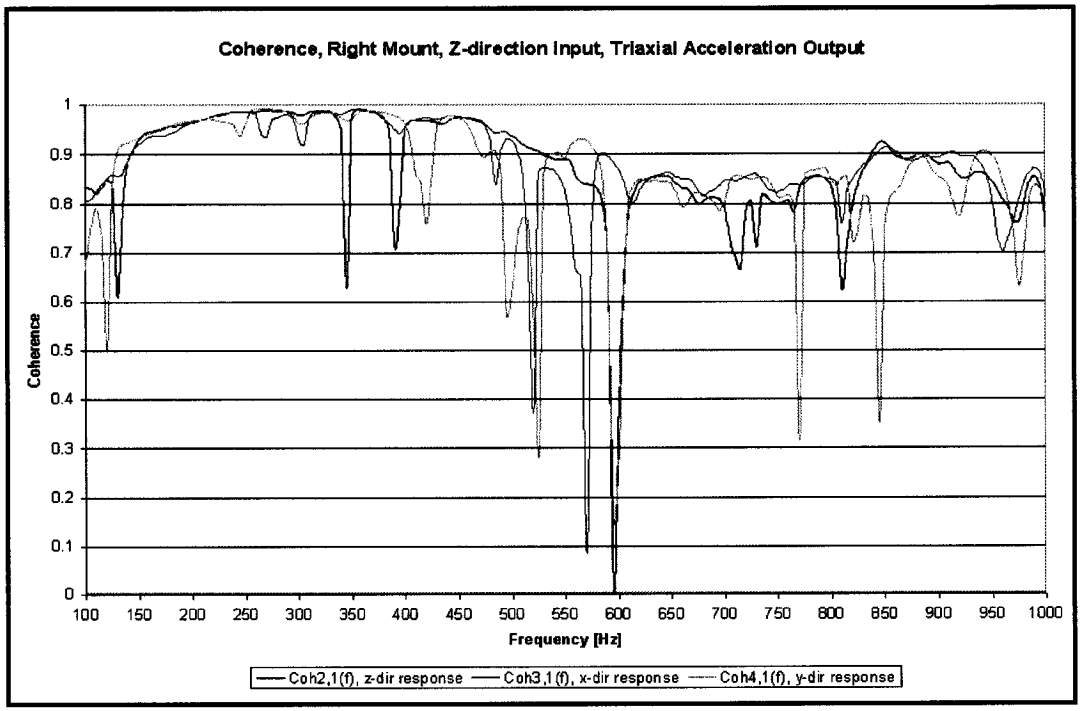

Figure B.6: Coherence, Right Mount, Z-direction Input, Triaxial Acceleration Output.

Reproduced with permission of the copyright owner. Further reproduction prohibited without permission.

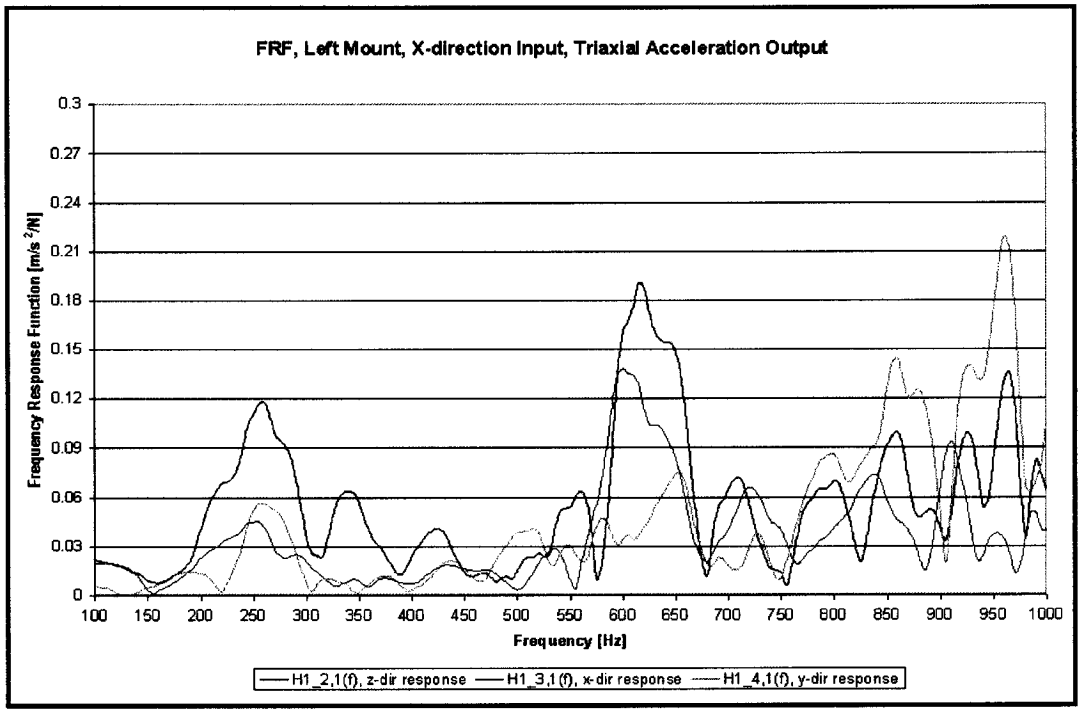

Figure B.7: Frequency Response Function, Left Mount, X-direction Input, Triaxial Acceleration Output.

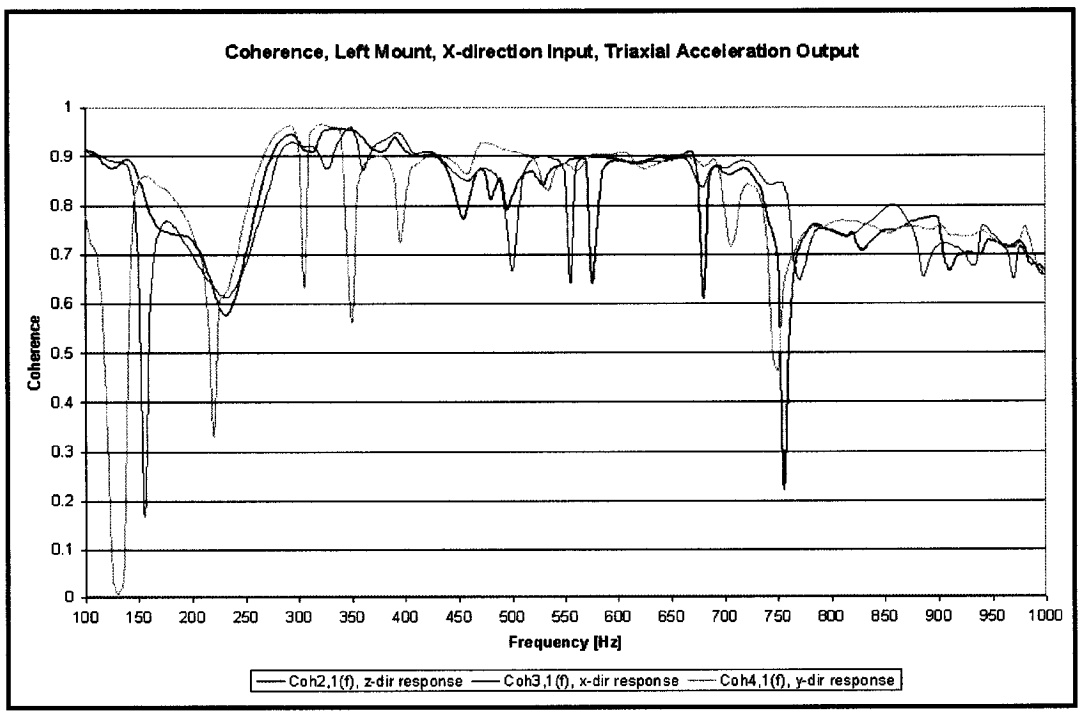

Figure B.8: Coherence, Left Mount, X-direction Input, Triaxial Acceleration Output.

Reproduced with permission of the copyright owner. Further reproduction prohibited without permission.

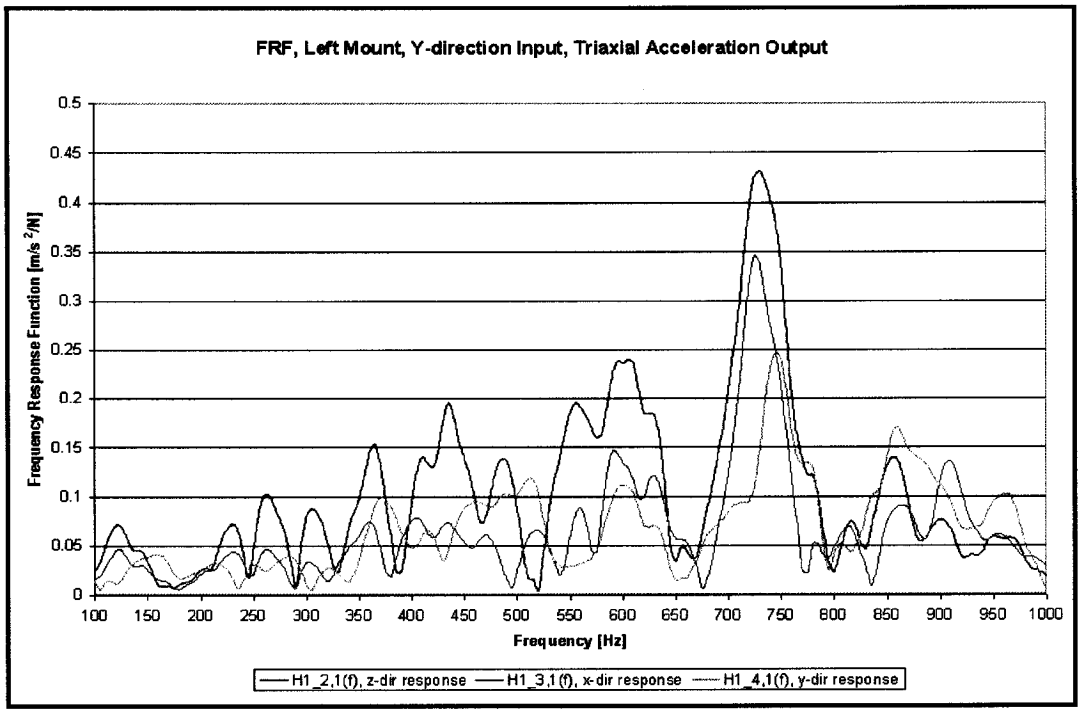

Figure B.9: Frequency Response Function, Left Mount, Y-direction Input, Triaxial Acceleration Output.

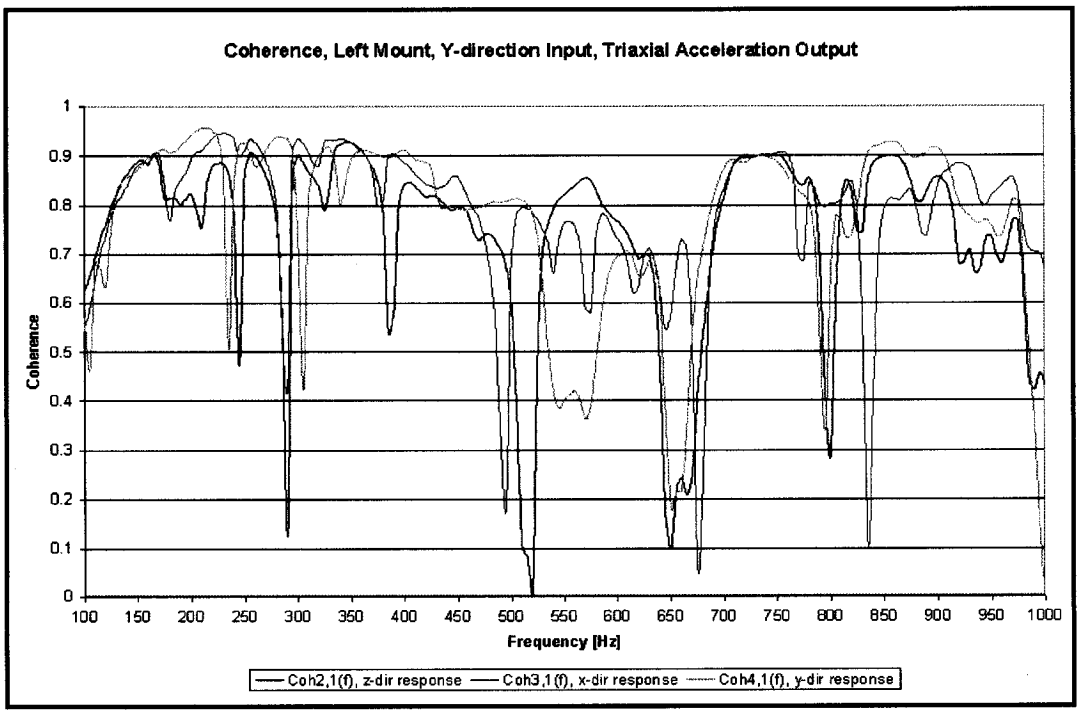

Figure B.10: Coherence, Left Mount, Y-direction Input, Triaxial Acceleration Output.

Reproduced with permission of the copyright owner. Further reproduction prohibited without permission.

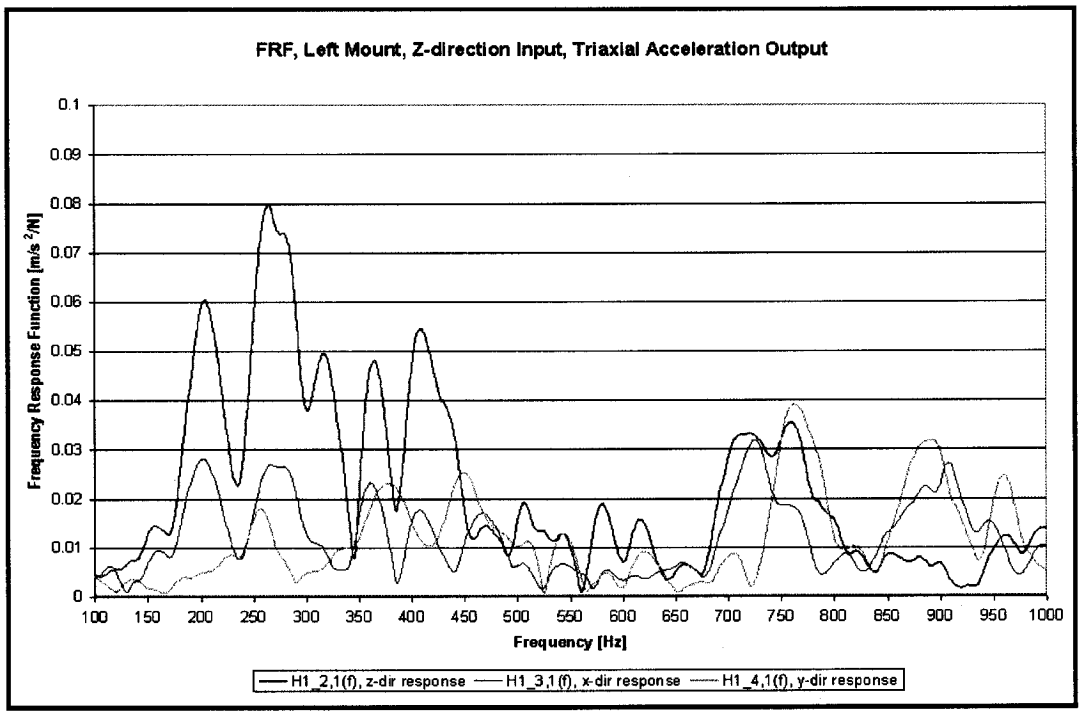

Figure B.11: Frequency Response Function, Left Mount, Z-direction Input, Triaxial Acceleration Output.

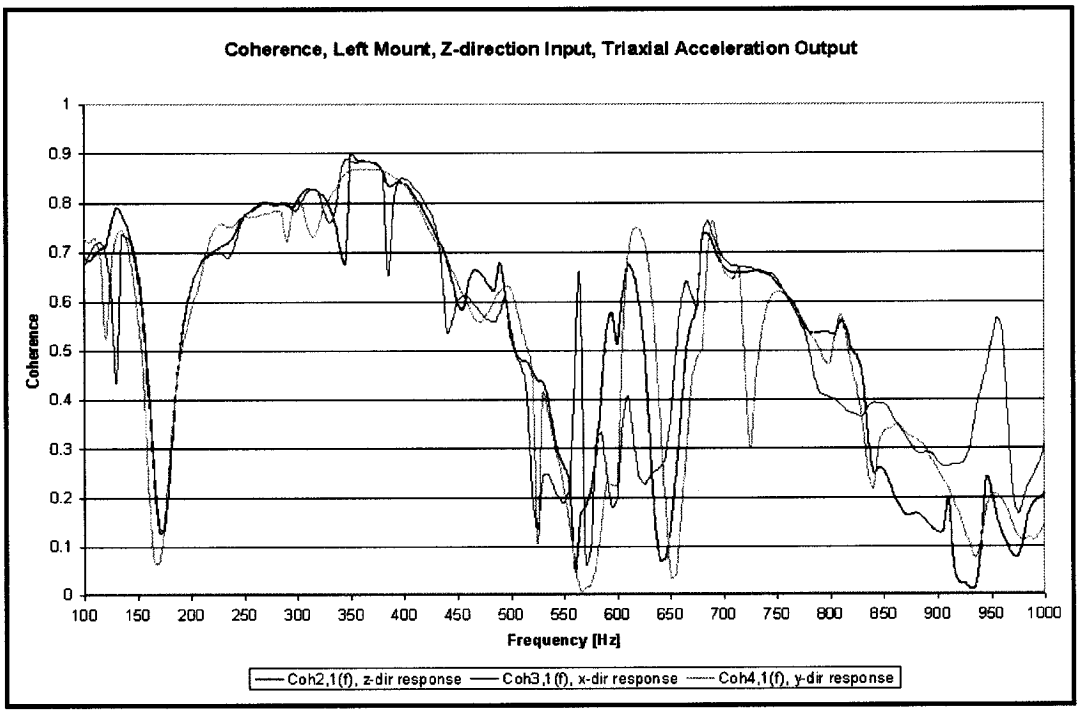

Figure B.12: Coherence, Left Mount, Z-direction Input, Triaxial Acceleration Output.

Reproduced with permission of the copyright owner. Further reproduction prohibited without permission.

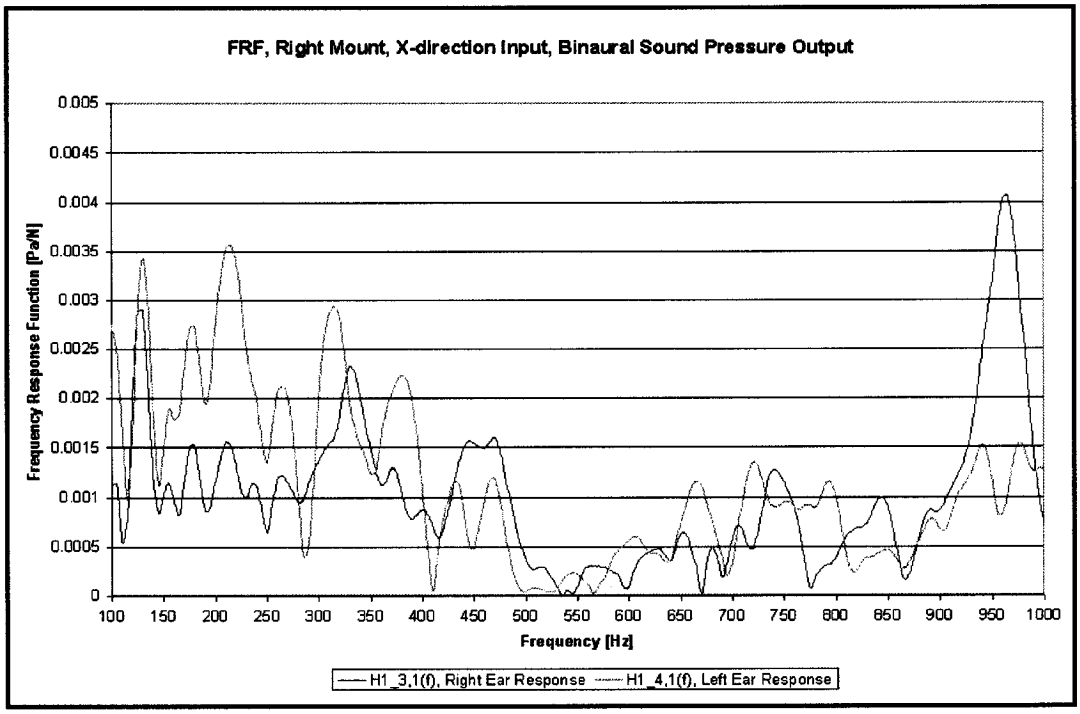

Figure B.13: Frequency Response Function, Right Mount, X-direction Input, Binaural Sound Pressure Output.

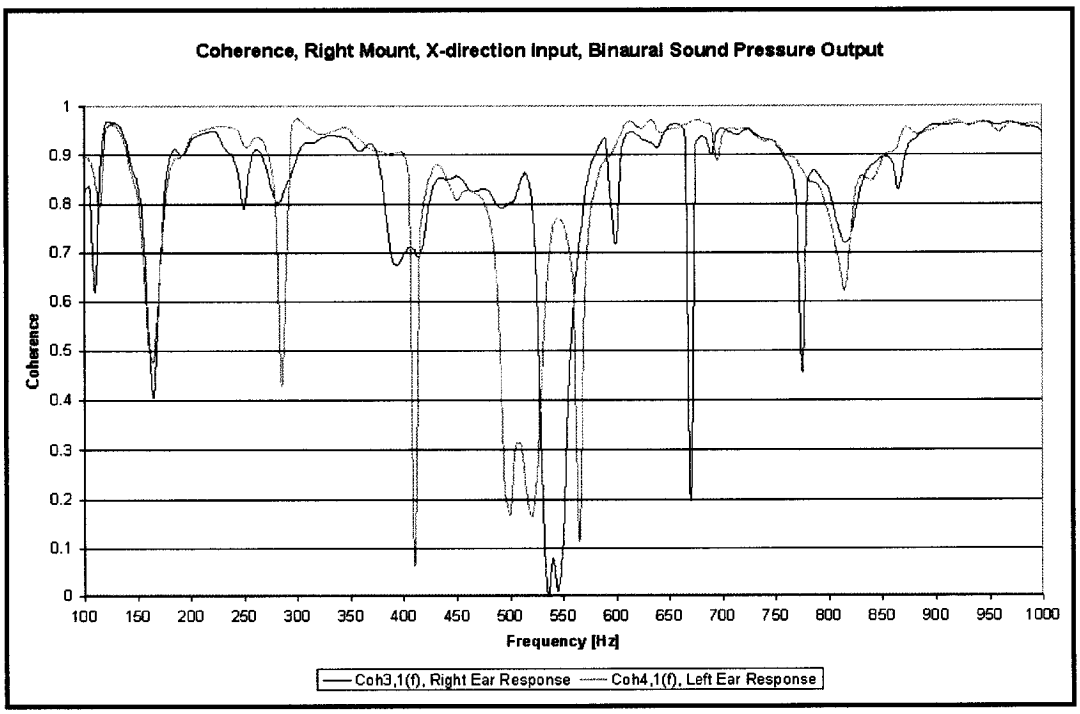

Figure B.14: Coherence, Right Mount, X-direction Input, Binaural Sound Pressure Output.

Reproduced with permission of the copyright owner. Further reproduction prohibited without permission.

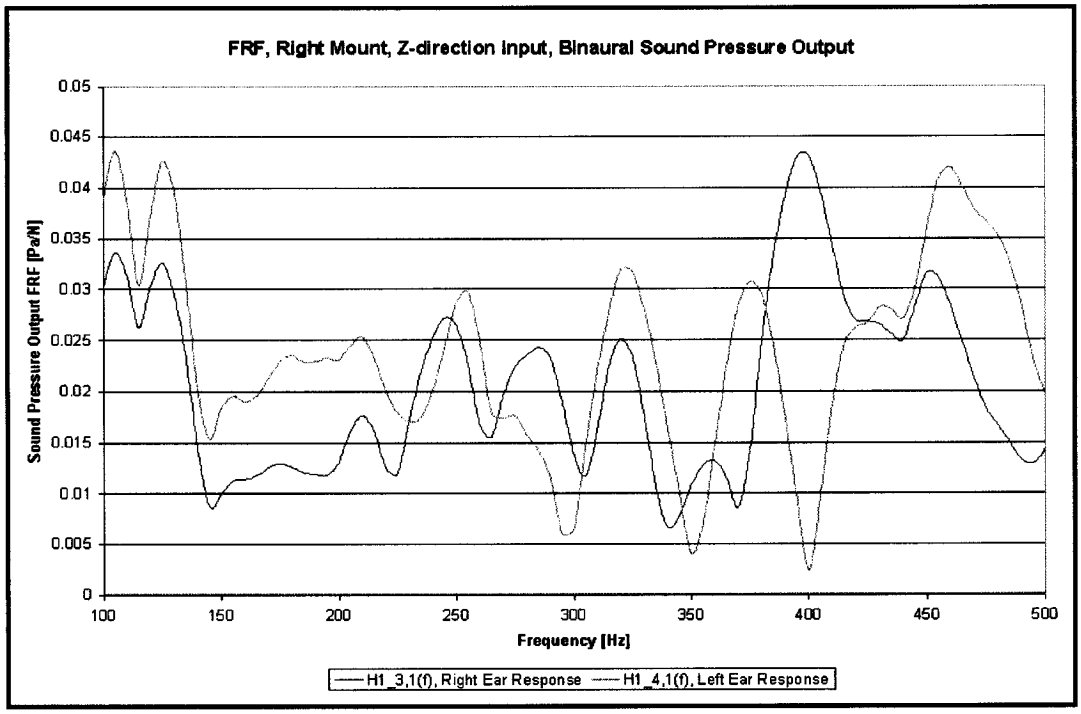

Figure B.15: Frequency Response Function, Right Mount, Z-direction Input, Binaural Sound Pressure Output.

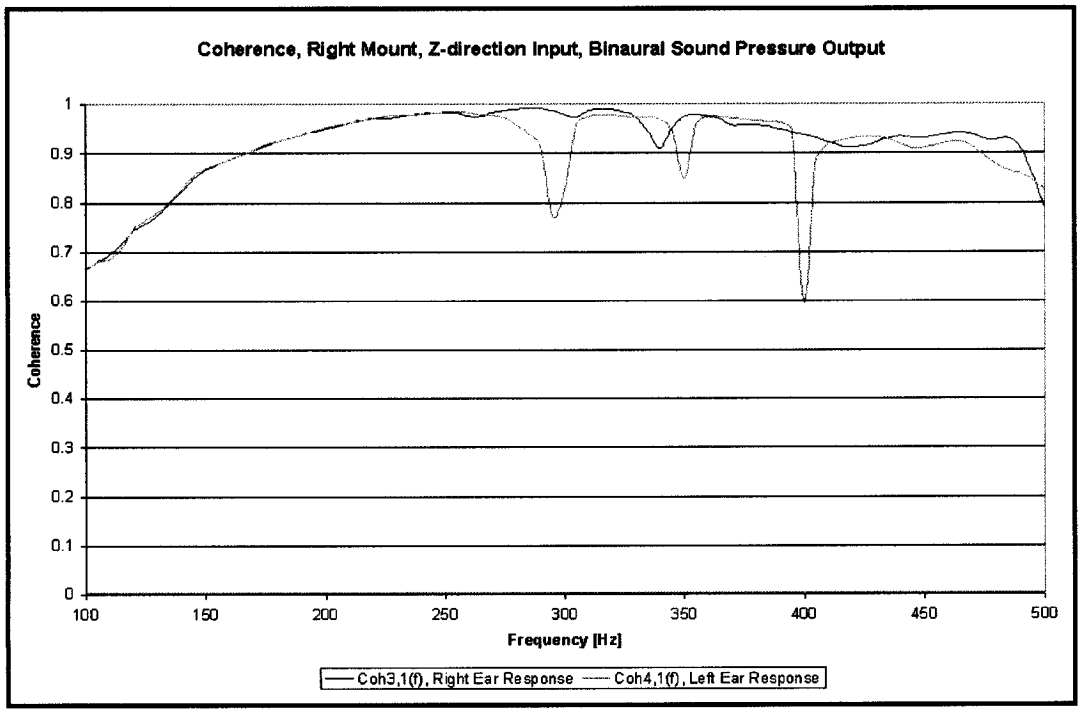

Figure B.16: Coherence, Right Mount, Z-direction Input, Binaural Sound Pressure Output.

Reproduced with permission of the copyright owner. Further reproduction prohibited without permission.

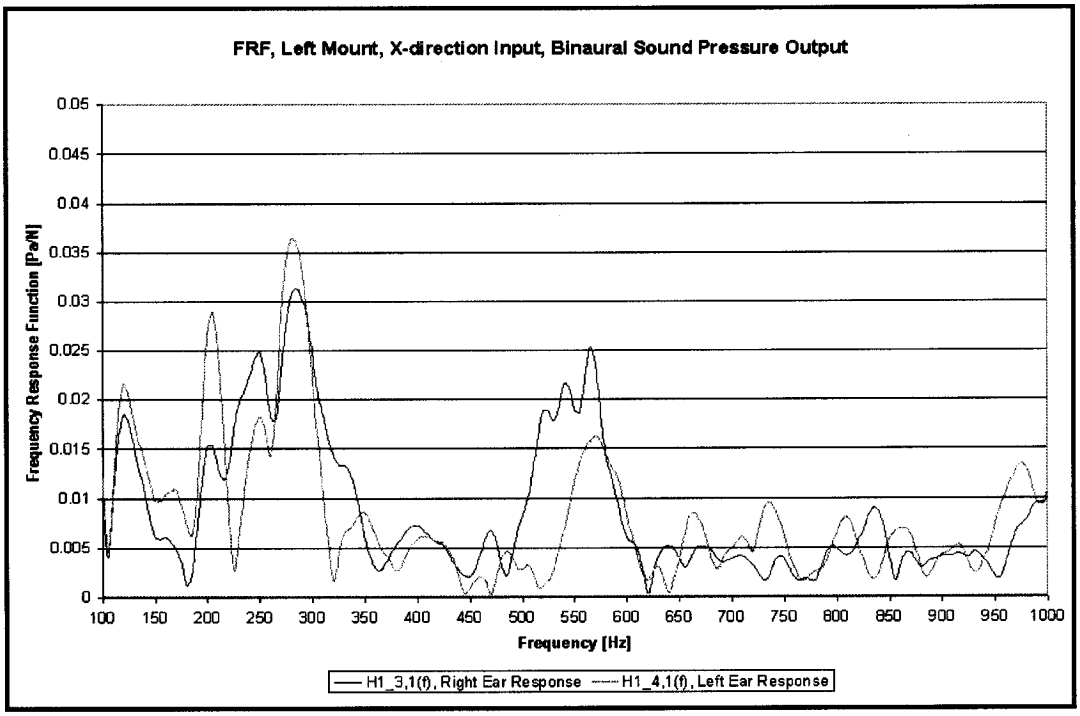

Figure B.17: Frequency Response Function, Left Mount, X-direction Input, Binaural Sound Pressure Output.

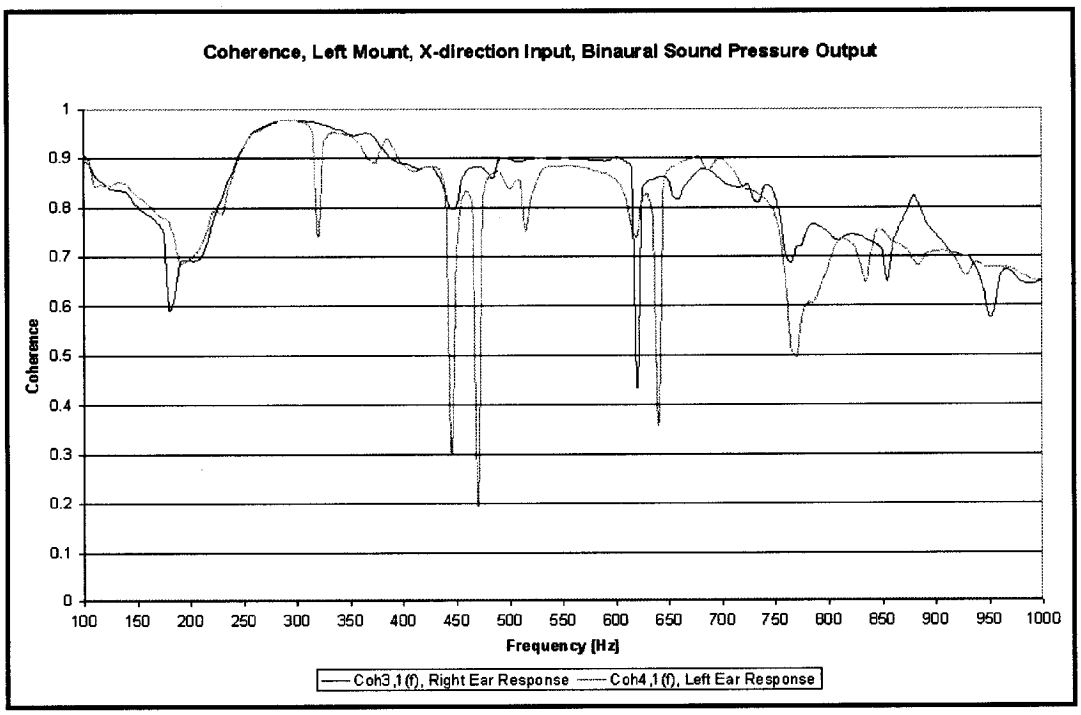

Figure B.18: Coherence, Left Mount, X-direction Input, Binaural Sound Pressure Output.

Reproduced with permission of the copyright owner. Further reproduction prohibited without permission.

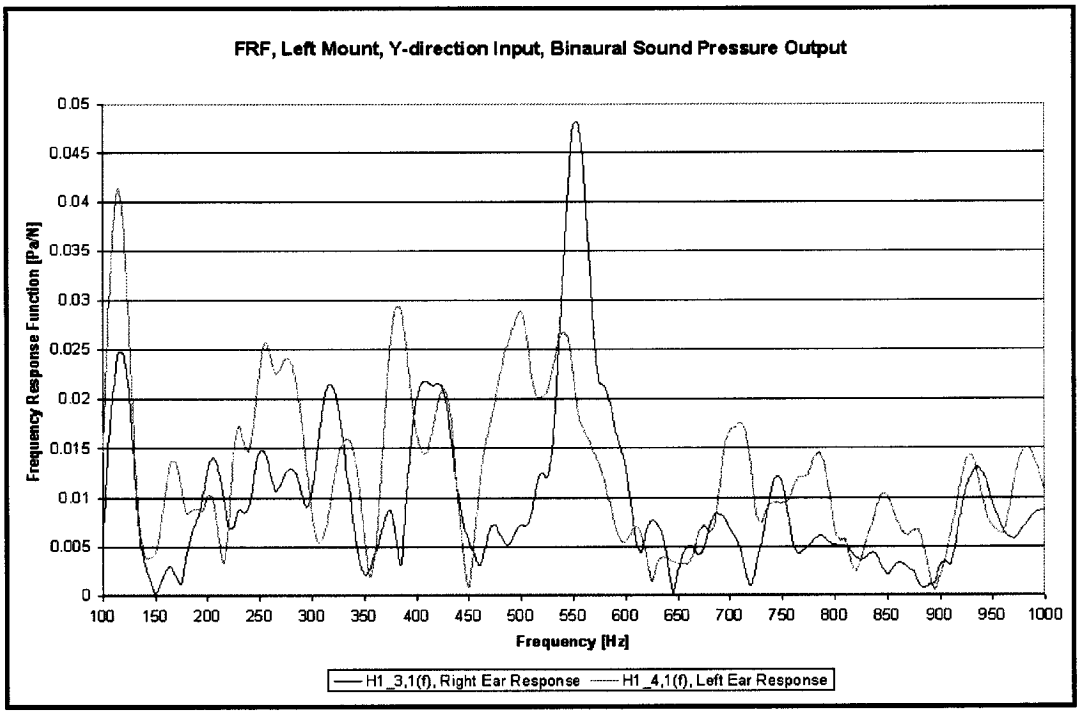

Figure B.19: Frequency Response Function, Left Mount, Y-direction Input, Binaural Sound Pressure Output.

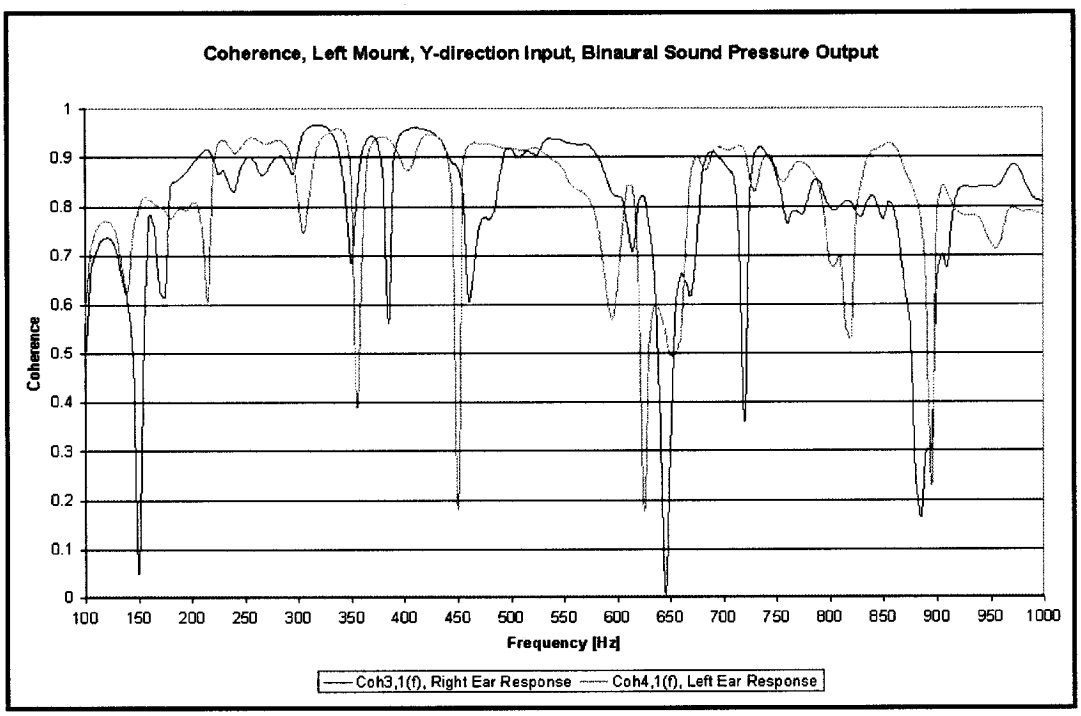

Figure B.20: Coherence, Left Mount, Y-direction Input, Binaural Sound Pressure Output.

Reproduced with permission of the copyright owner. Further reproduction prohibited without permission.

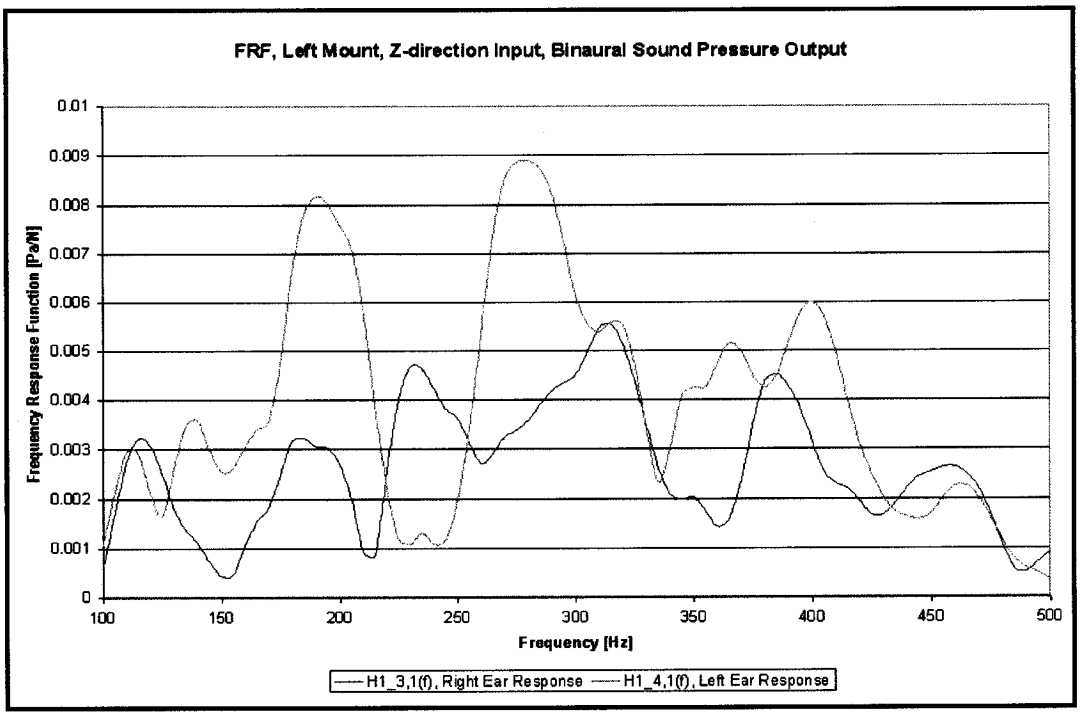

Figure B.21: Frequency Response Function, Left Mount, Z-direction Input, Binaural Sound Pressure Output.

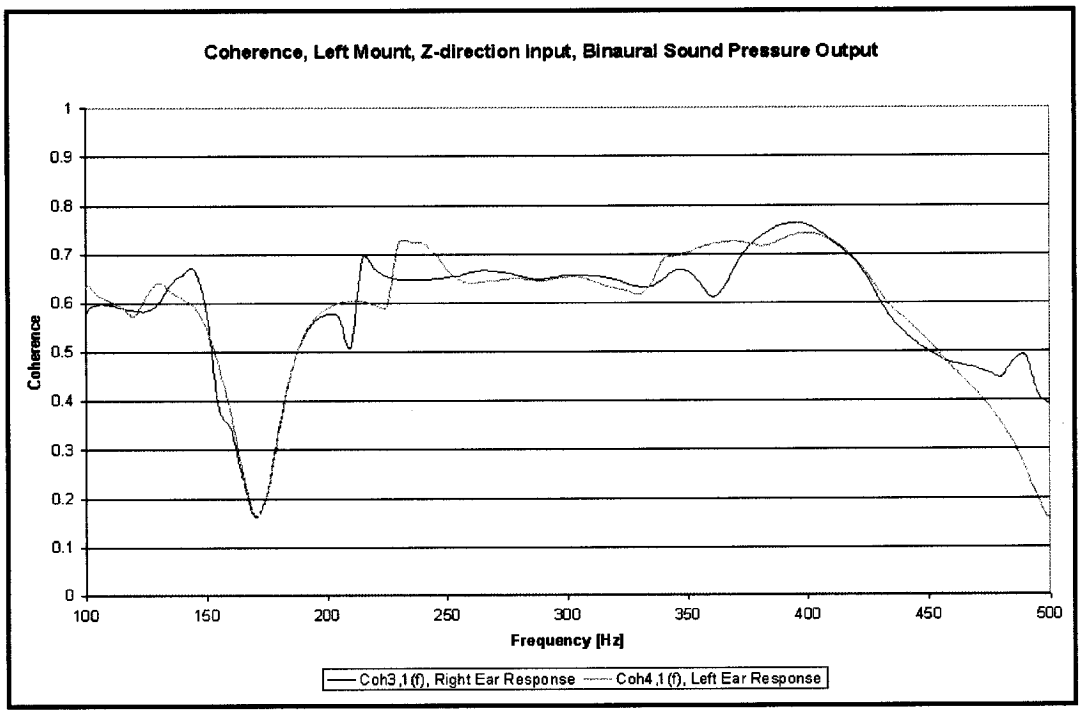

Figure B.22: Coherence, Left Mount, Z-direction Input, Binaural Sound Pressure Output.

Reproduced with permission of the copyright owner. Further reproduction prohibited without permission.

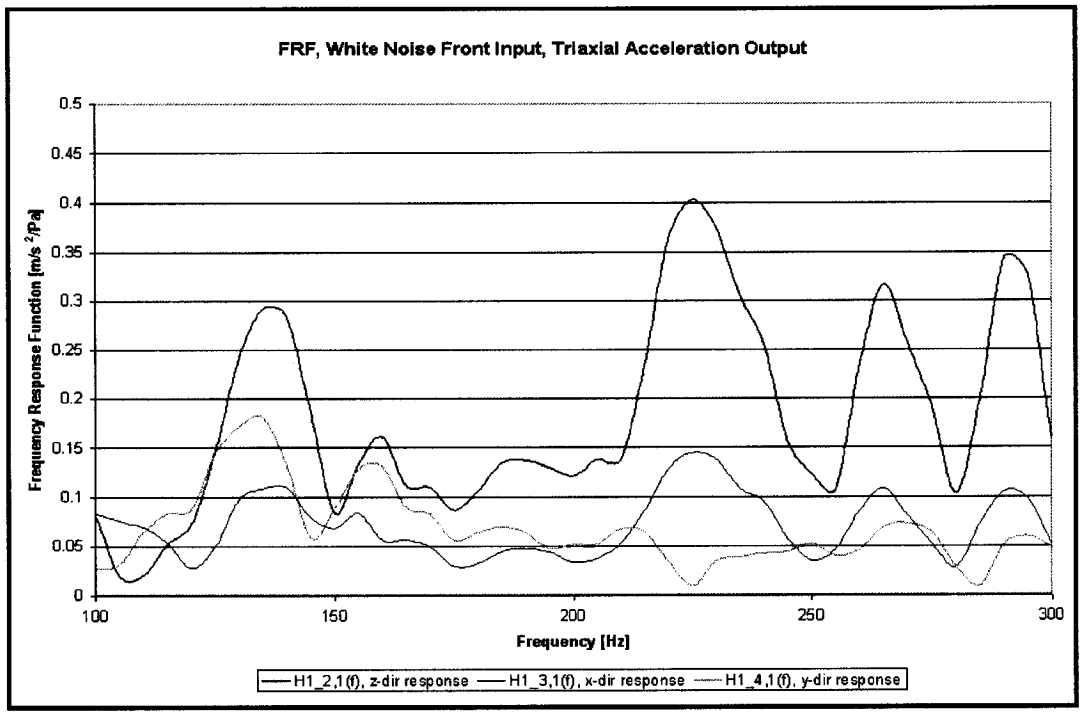

Figure B.23: Frequency Response Function, White Noise Front Input, Triaxial Acceleration Output.

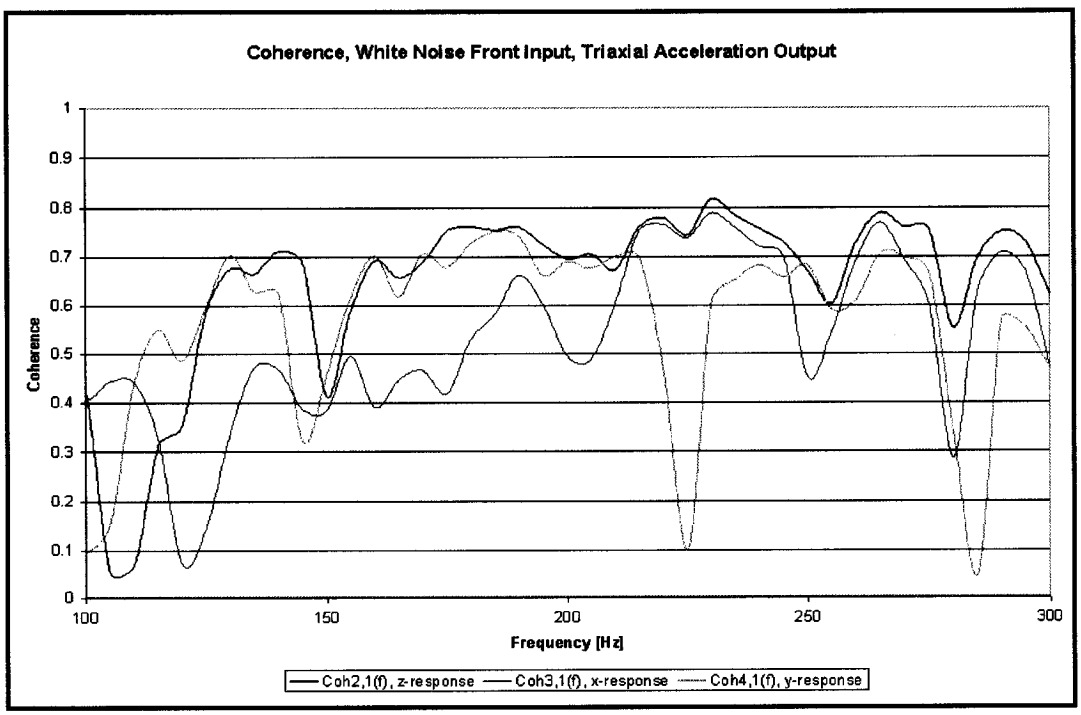

Figure B.24: Coherence, White Noise Front Input, Triaxial Acceleration Output.

Reproduced with permission of the copyright owner. Further reproduction prohibited without permission.

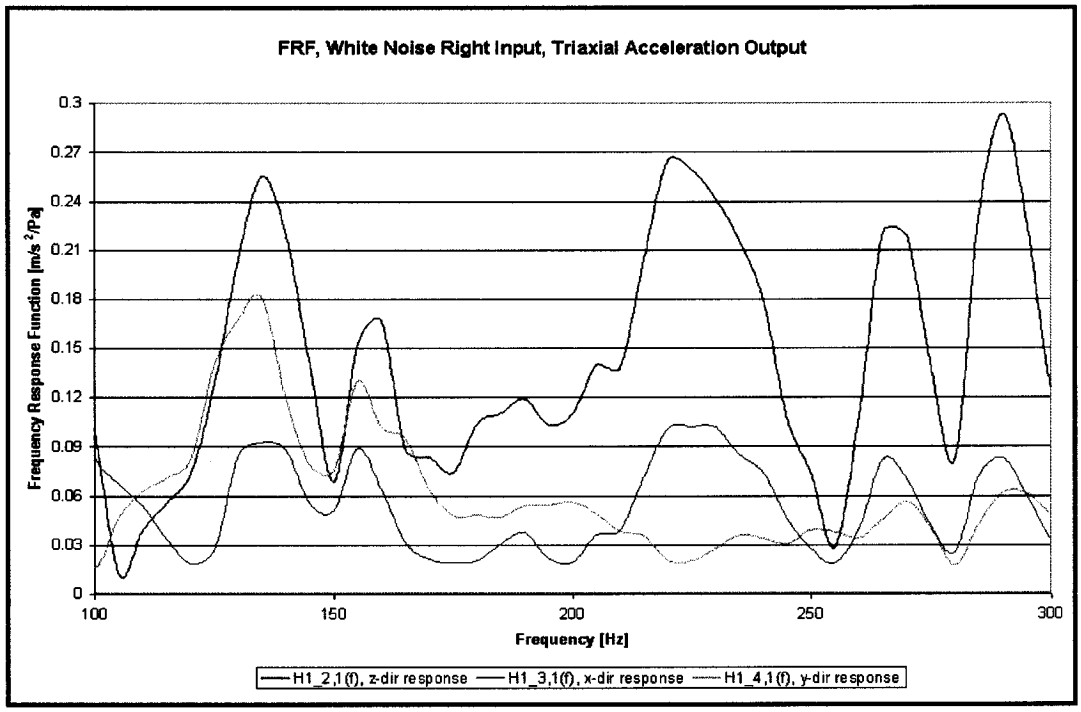

Figure B.25: Frequency Response Function, White Noise Right Input, Triaxial Acceleration Output.

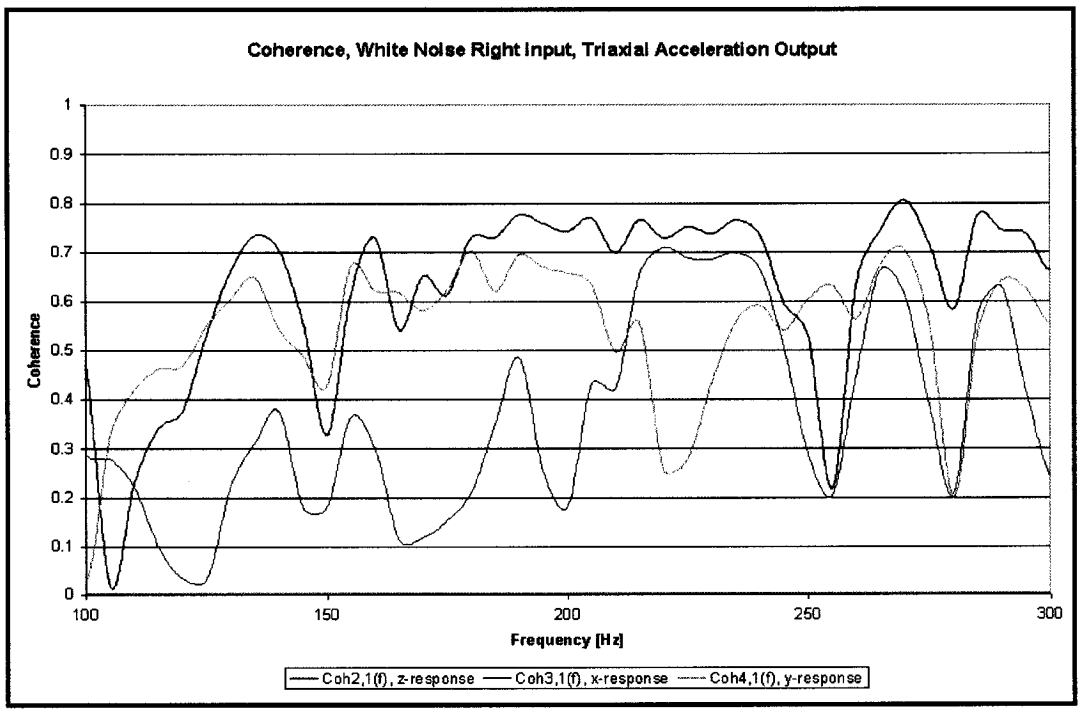

Figure B.26: Coherence, White Noise Right Input, Triaxial Acceleration Output.

Reproduced with permission of the copyright owner. Further reproduction prohibited without permission.

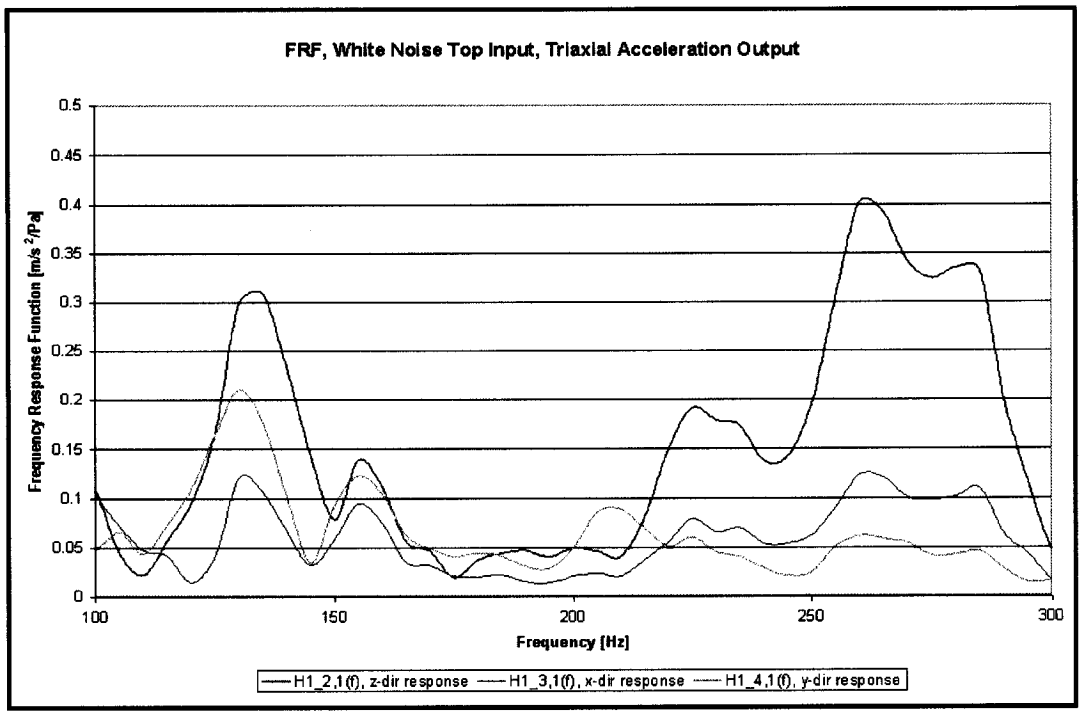

Figure B.27: Frequency Response Function, White Noise Top Input, Triaxial Acceleration Output.

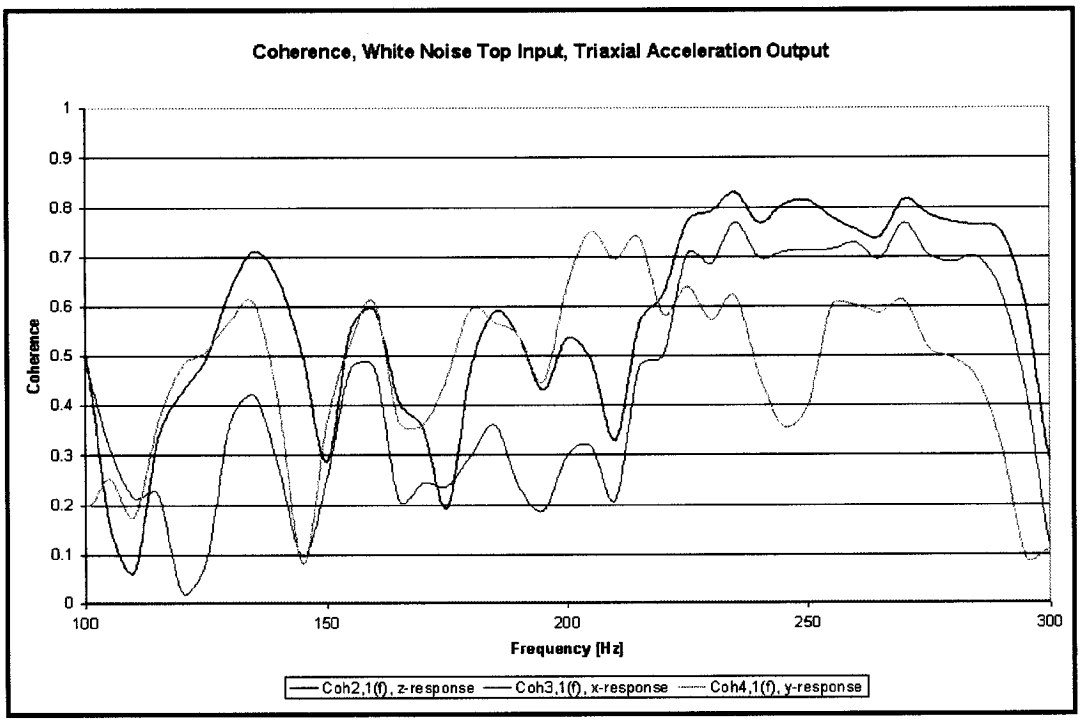

Figure B.28: Coherence, White Noise Top Input, Triaxial Acceleration Output.

Reproduced with permission of the copyright owner. Further reproduction prohibited without permission.

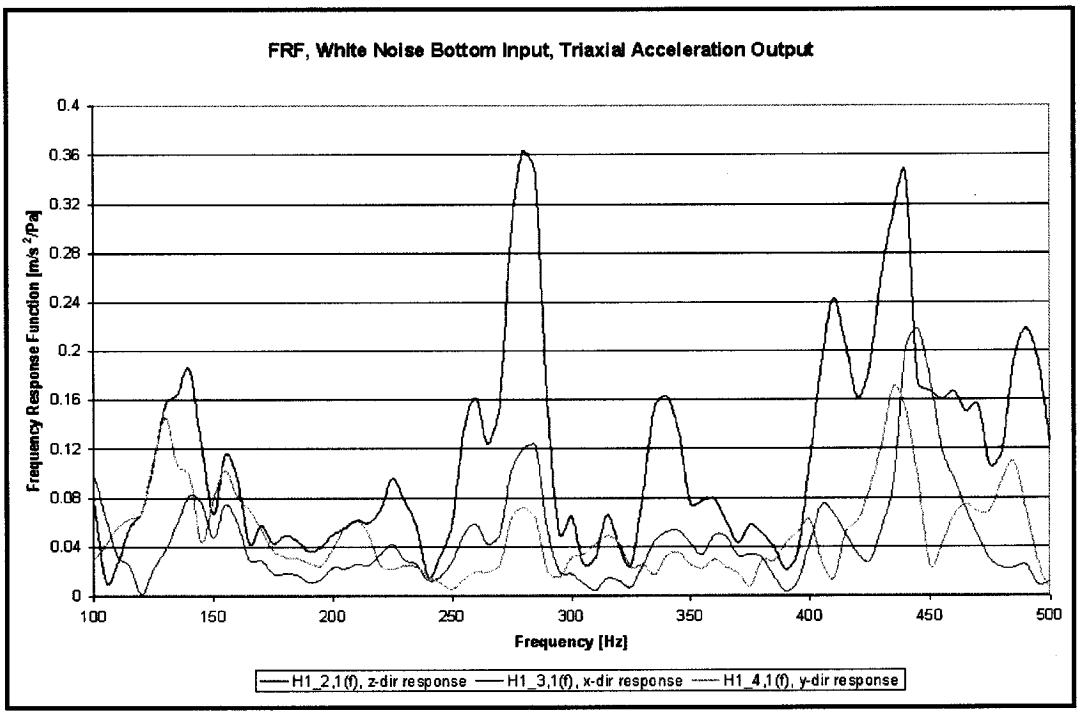

Figure B.29: Frequency Response Function, White Noise Bottom Input, Triaxial Acceleration Output.

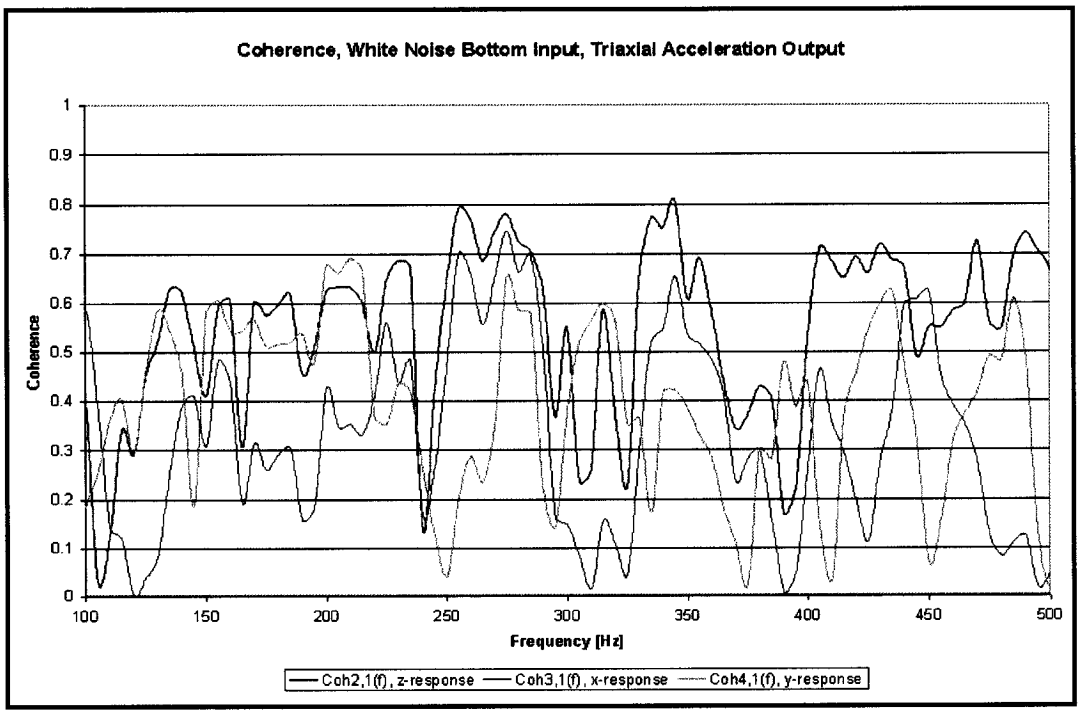

Figure B.30: Coherence, White Noise Bottom Input, Triaxial Acceleration Output.

Reproduced with permission of the copyright owner. Further reproduction prohibited without permission.

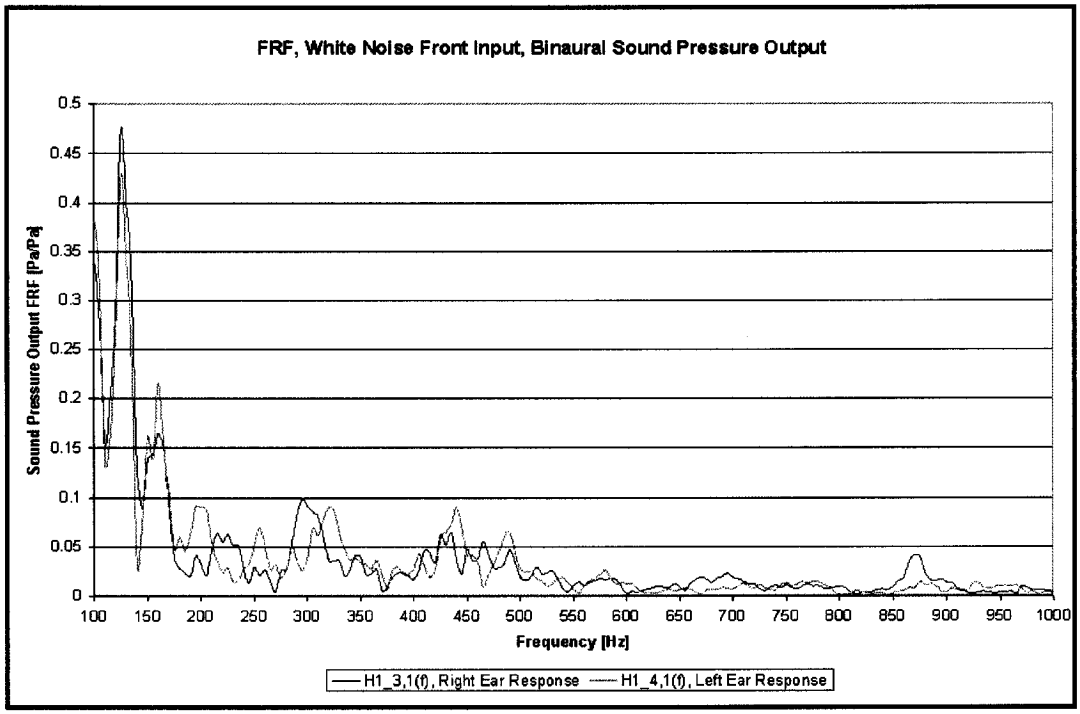

Figure B.31: Frequency Response Function, White Noise Front Input, Binaural Sound Pressure Output.

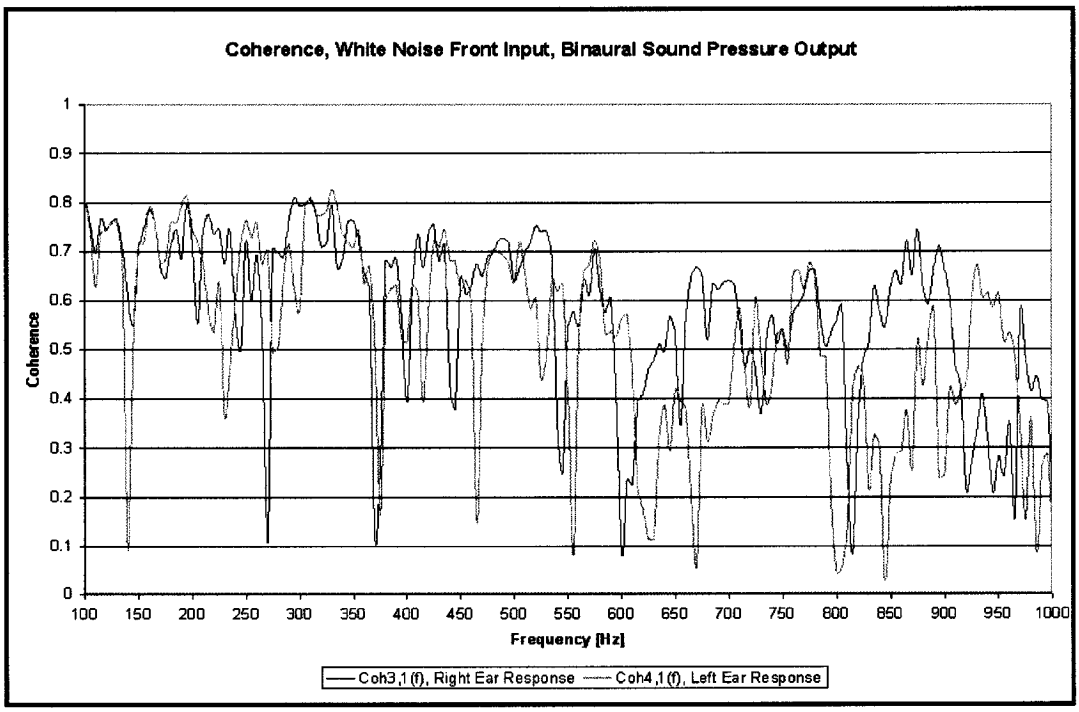

Figure B.32: Coherence, White Noise Front Input, Binaural Sound Pressure Output.

Reproduced with permission of the copyright owner. Further reproduction prohibited without permission.

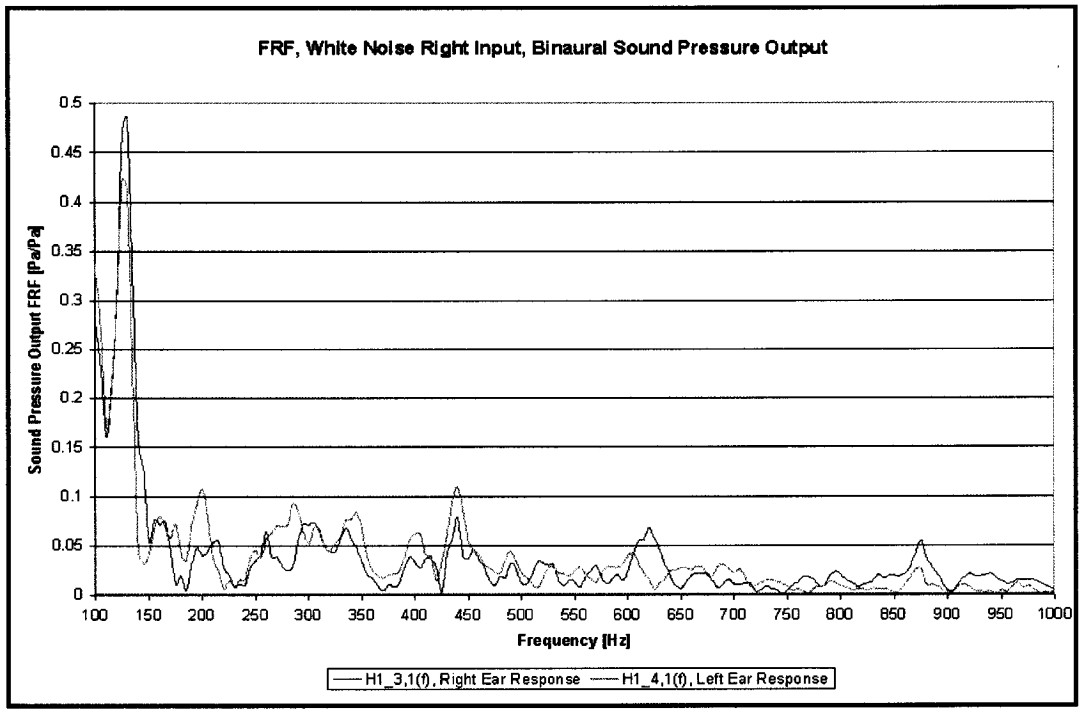

Figure B.33: Frequency Response Function, White Noise Right Input, Binaural Sound Pressure Output.

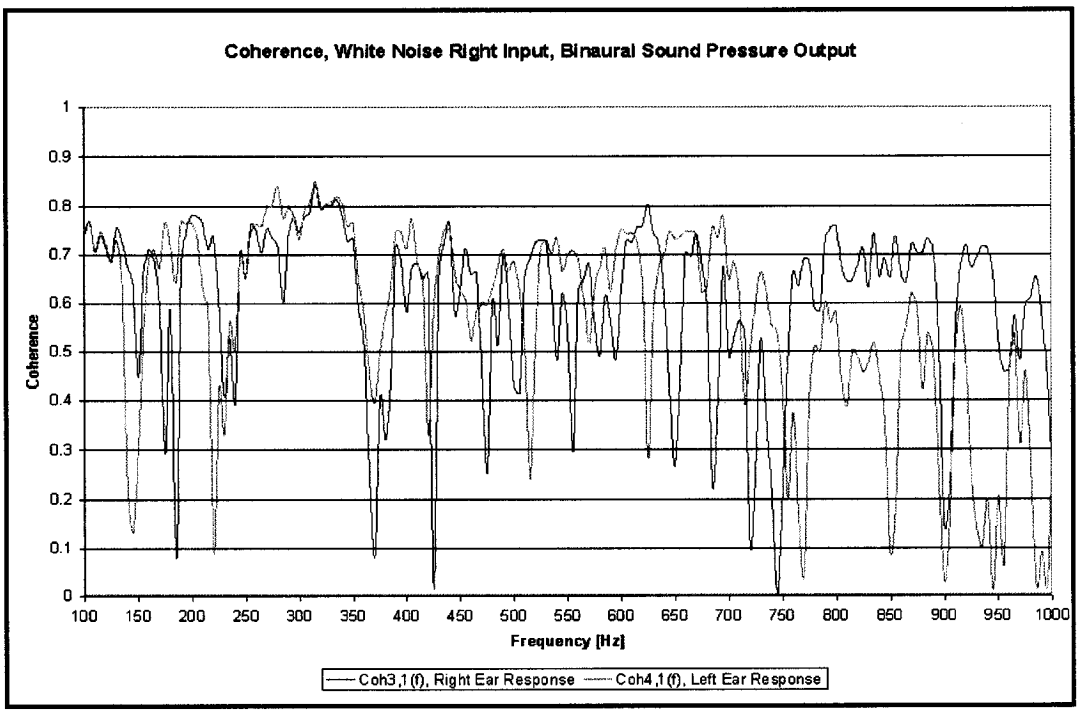

Figure B.34: Coherence, White Noise Right Input, Binaural Sound Pressure Output.

Reproduced with permission of the copyright owner. Further reproduction prohibited without permission.

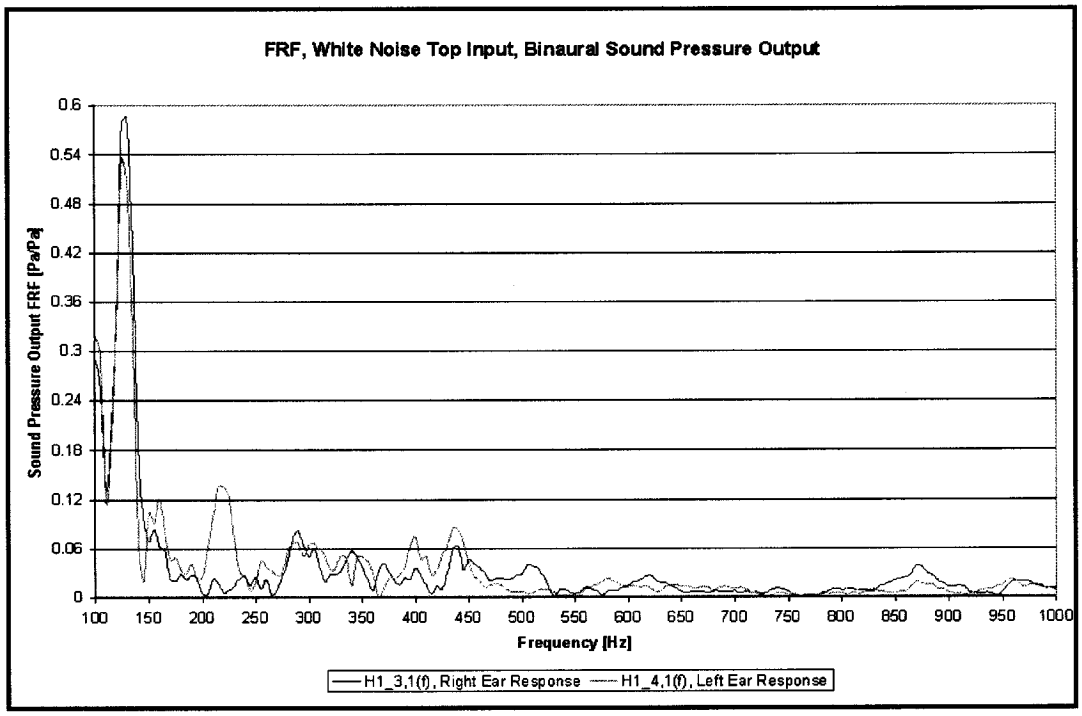

Figure B.35: Frequency Response Function, White Noise Top Input, Binaural Sound Pressure Output.

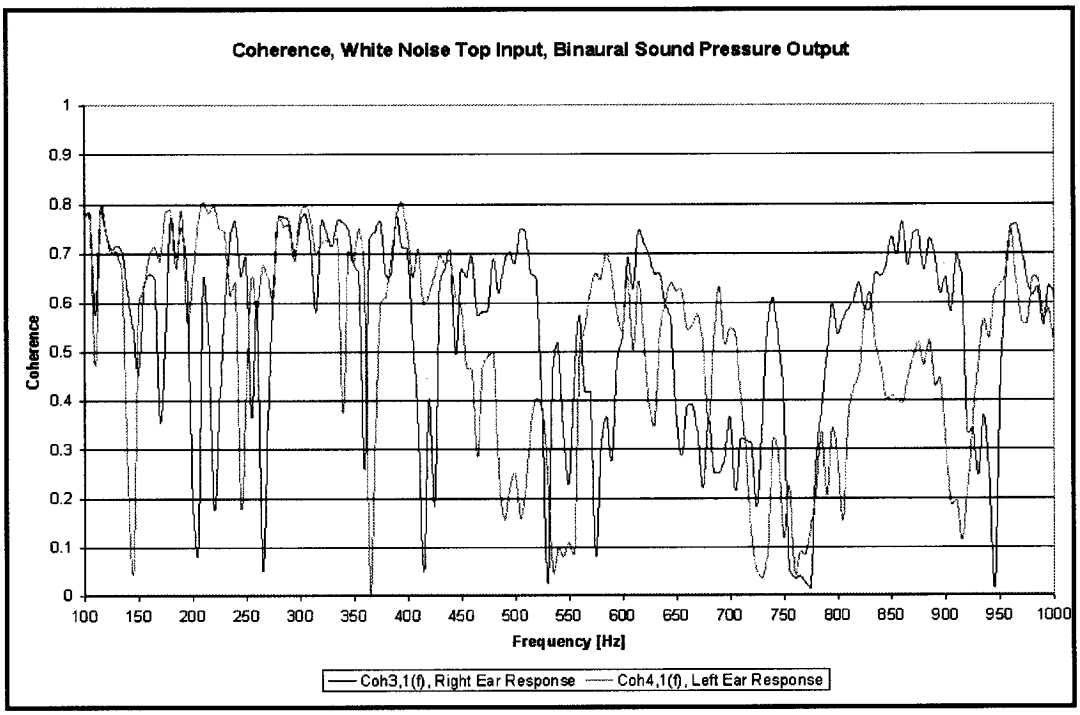

Figure B.36: Coherence, White Noise Top Input, Binaural Sound Pressure Output.

Reproduced with permission of the copyright owner. Further reproduction prohibited without permission.

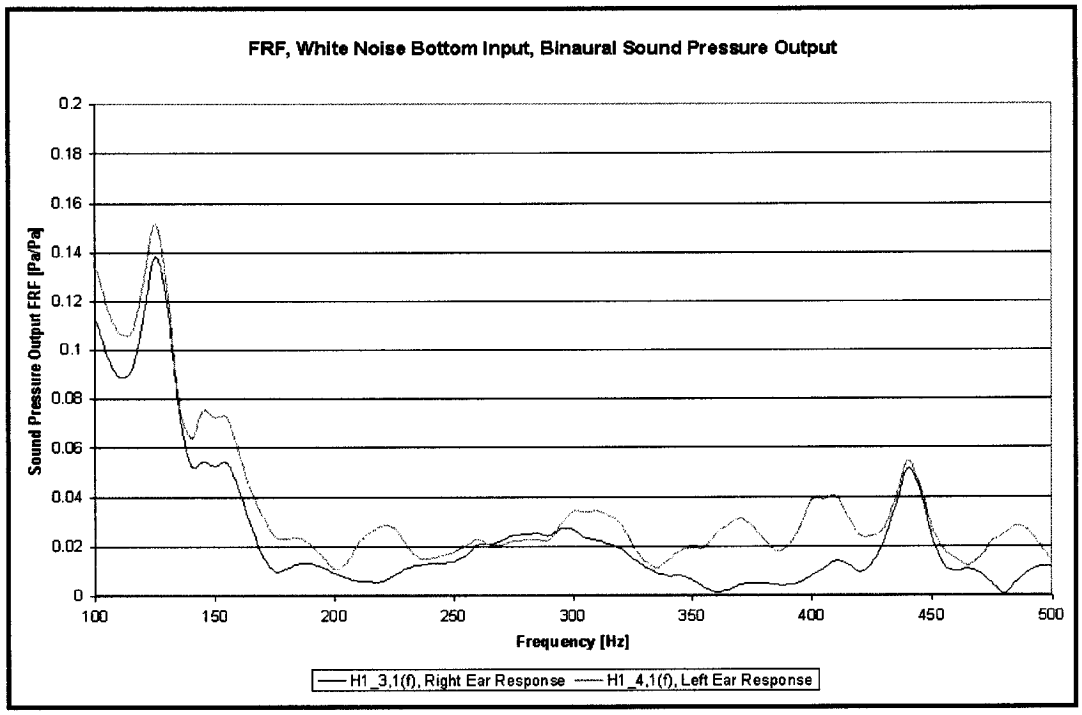

Figure B.37: Frequency Response Function, White Noise Bottom Input, Binaural Sound Pressure Output.

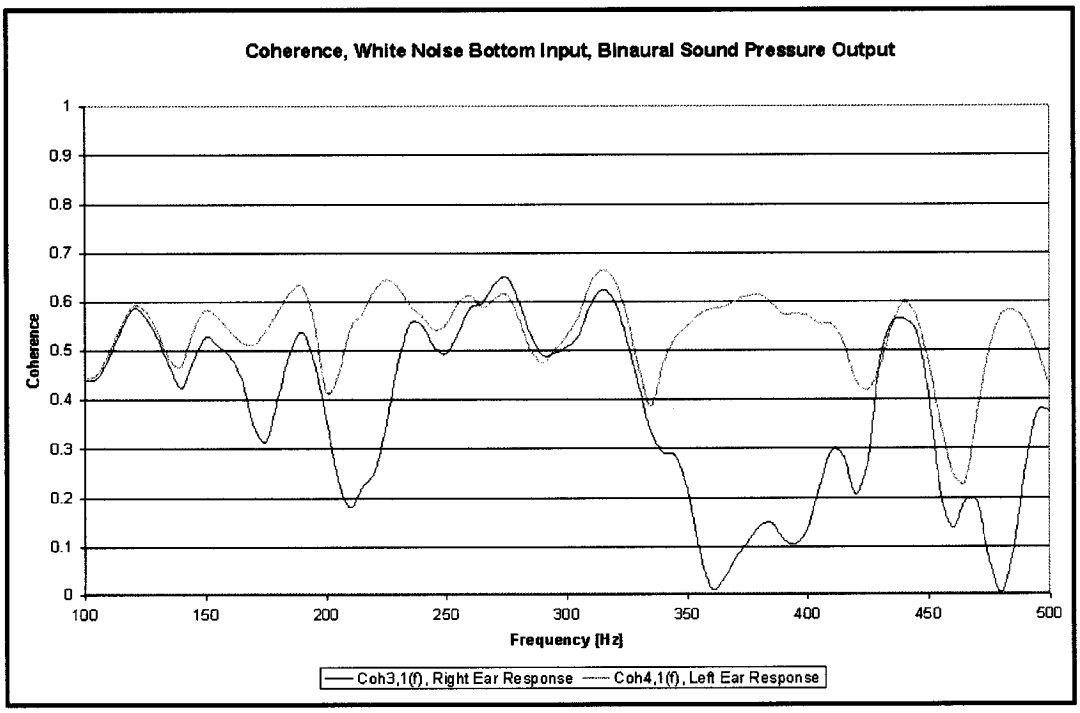

Figure B.38: Coherence, White Noise Top Input, Binaural Sound Pressure Output.

Reproduced with permission of the copyright owner. Further reproduction prohibited without permission.

C. INTERIOR SOUND AND VIBRATION RECEIVER RESULTS

Reproduced with permission of the copyright owner. Further reproduction prohibited without permission.

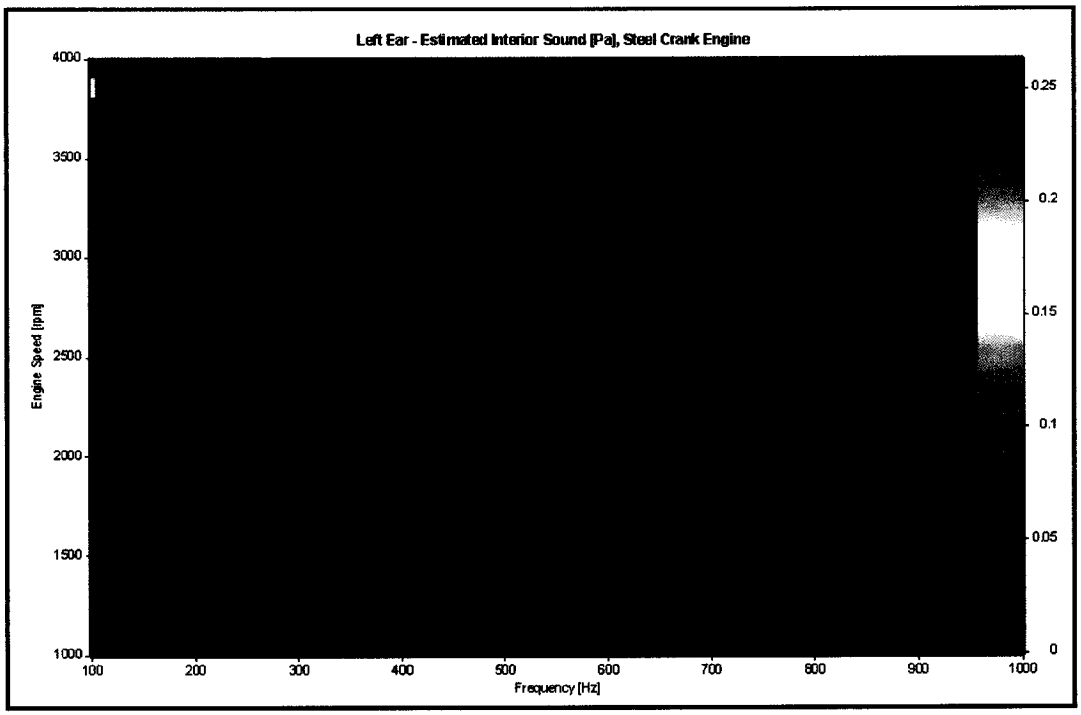

Figure C.1: Estimated Interior Sound [Pa], Left Ear, Steel Crank Engine.

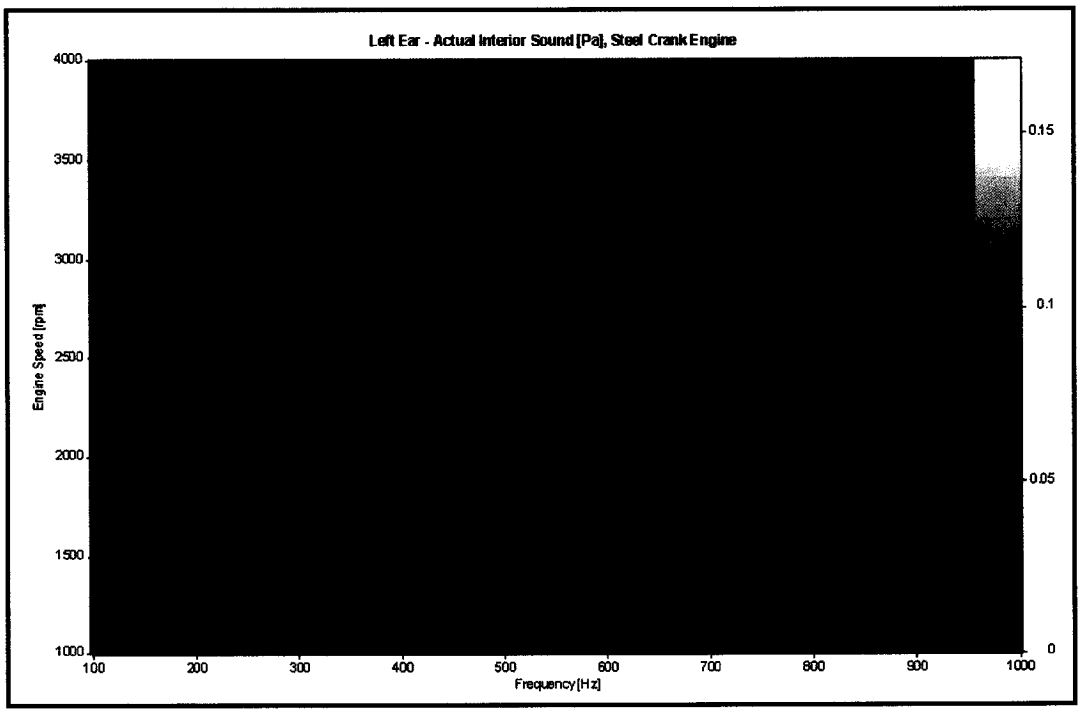

Figure C.2: Actual Interior Sound [Pa], Left Ear, Steel Crank Engine.

Reproduced with permission of the copyright owner. Further reproduction prohibited without permission.

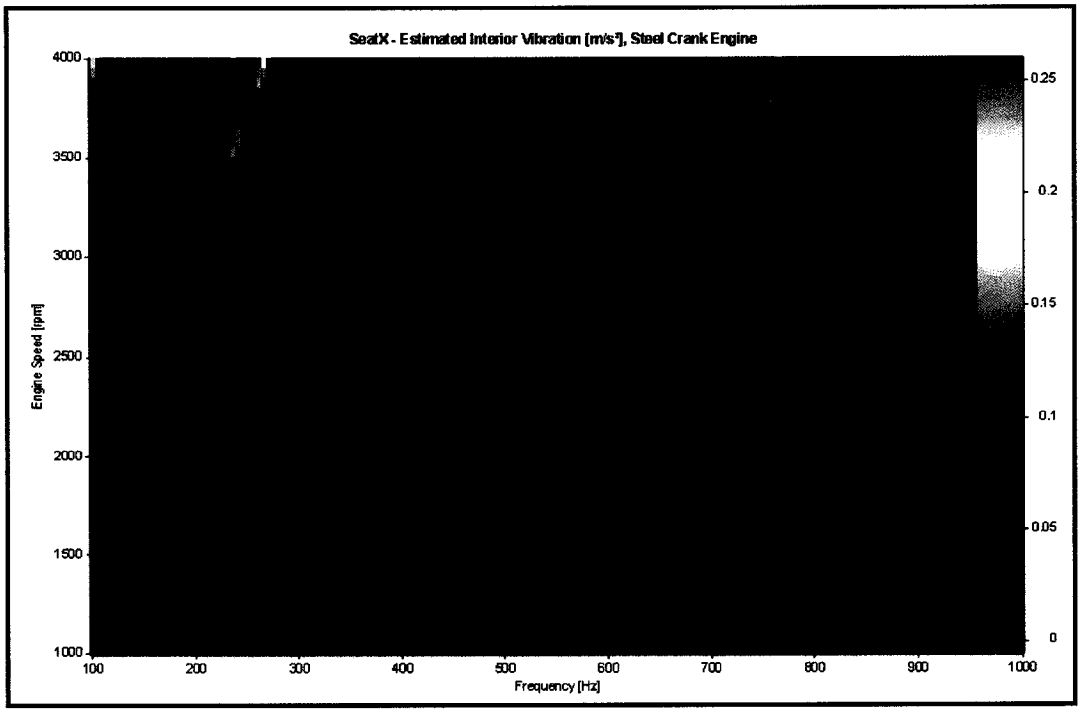

Figure C.3: Estimated Interior Vibration [m/s^2], X-direction, Steel Crank Engine.

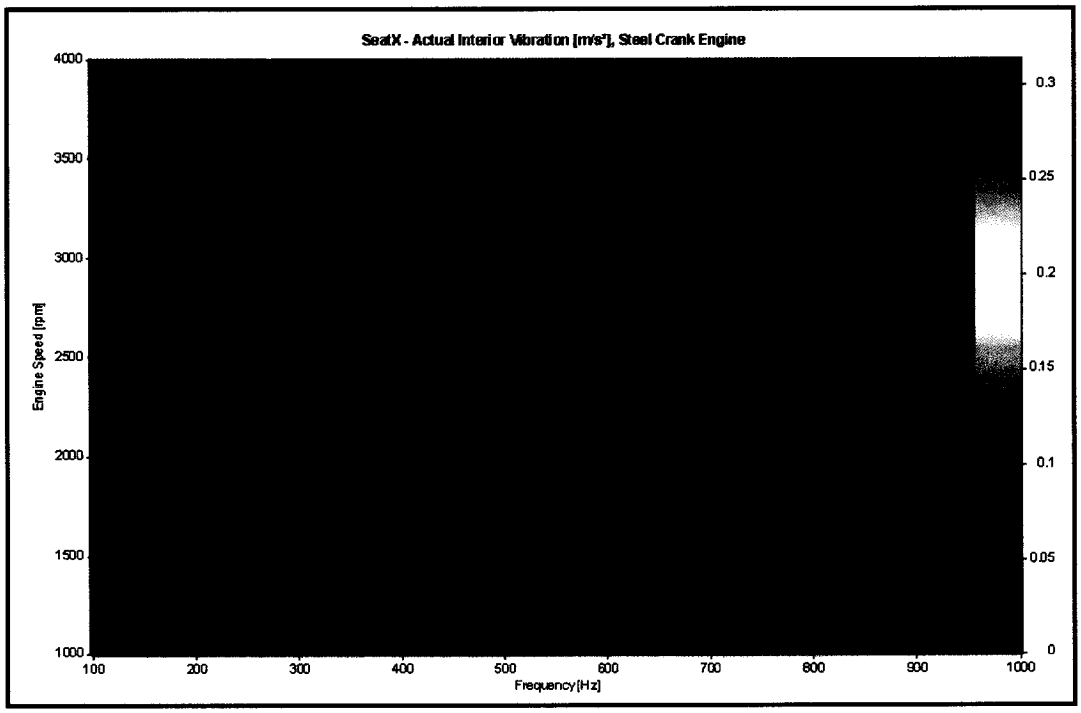

Figure C.4: Actual Interior Vibration [m/s^2], X-direction, Steel Crank Engine.

Reproduced with permission of the copyright owner. Further reproduction prohibited without permission.

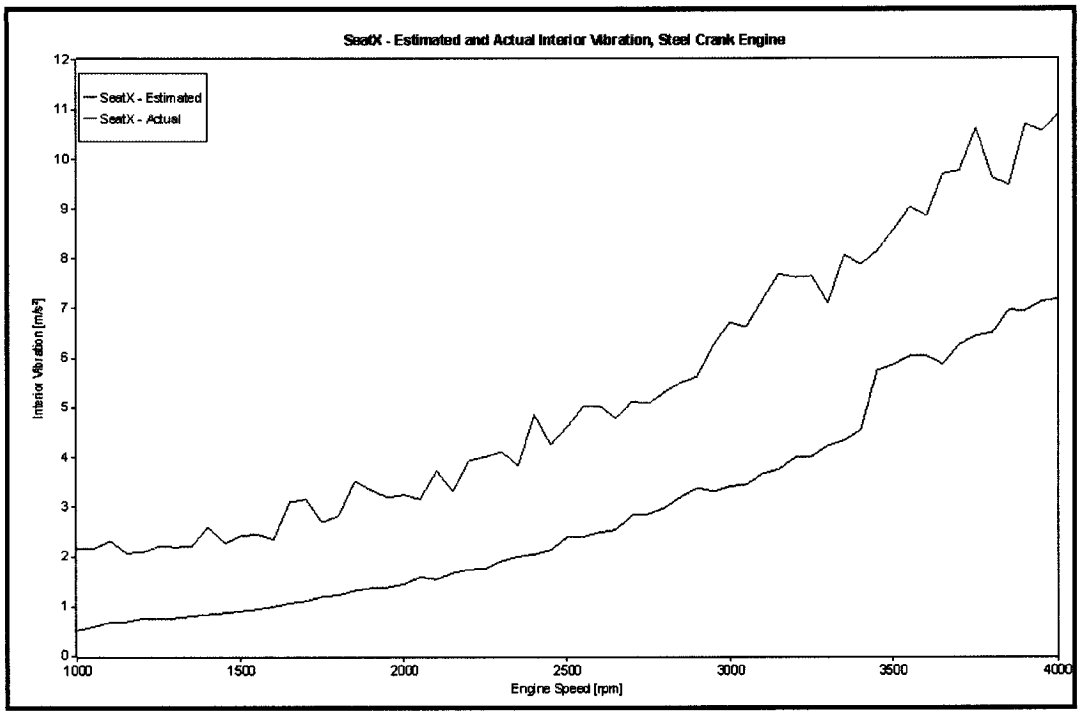

Figure C.5: Estimated and Actual Interior Vibration, X-direction, Steel Crank Engine.

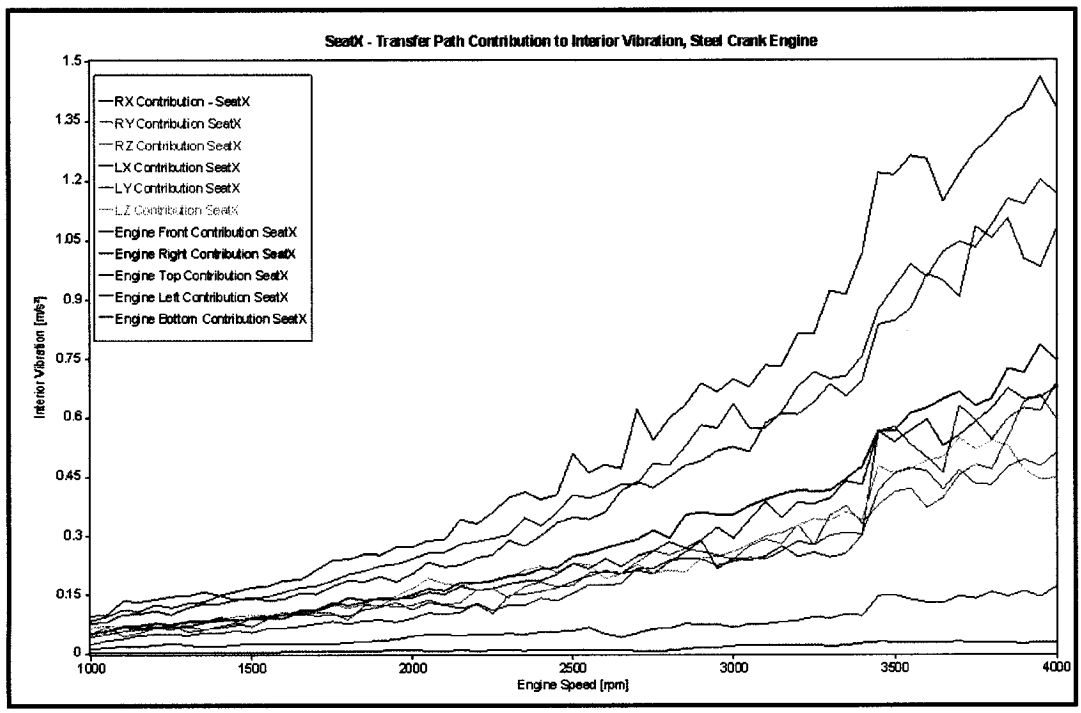

Figure C.6: Transfer Path Contribution to Interior Vibration, X-direction, Steel Crank Engine.

Reproduced with permission of the copyright owner. Further reproduction prohibited without permission.

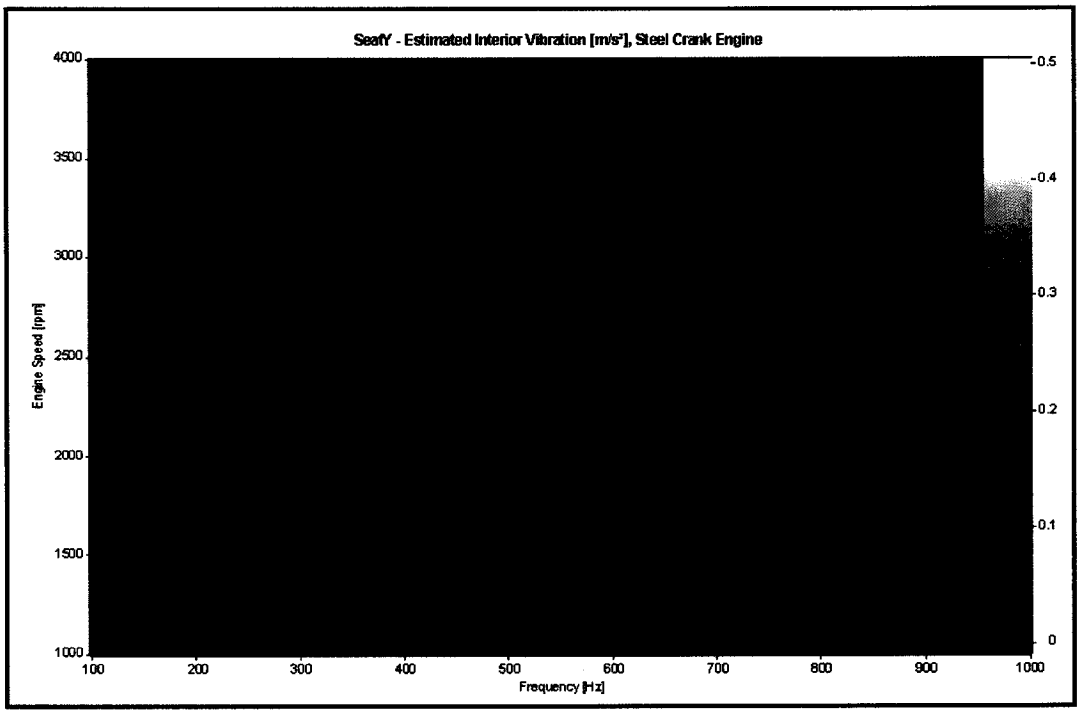

Figure C.7: Estimated Interior Vibration [m/s^2], Y-direction, Steel Crank Engine.

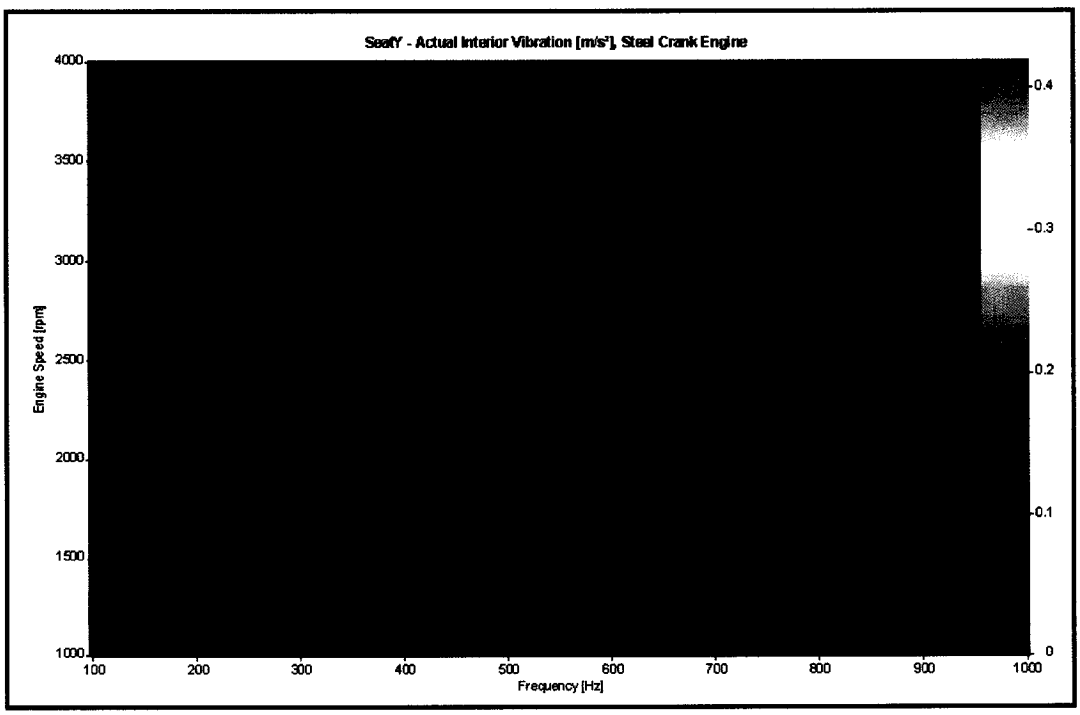

Figure C.8: Actual Interior Vibration [m/s^2], Y-direction, Steel Crank Engine.

Reproduced with permission of the copyright owner. Further reproduction prohibited without permission.

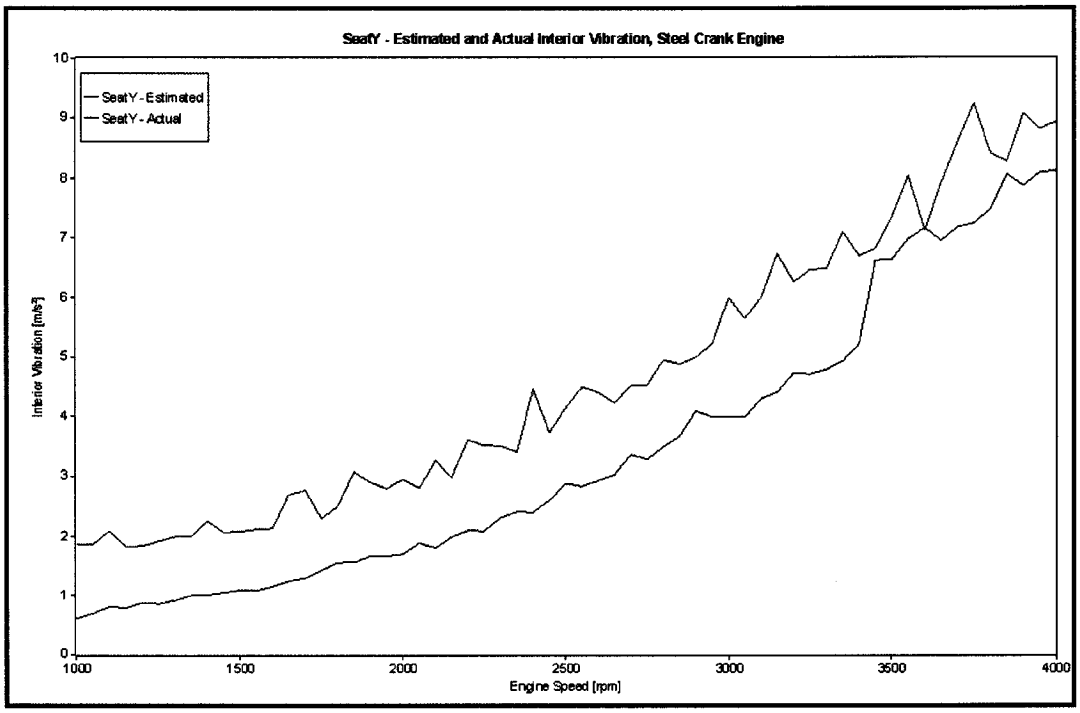

Figure C.9: Estimated and Actual Interior Vibration, Y-direction, Steel Crank Engine.

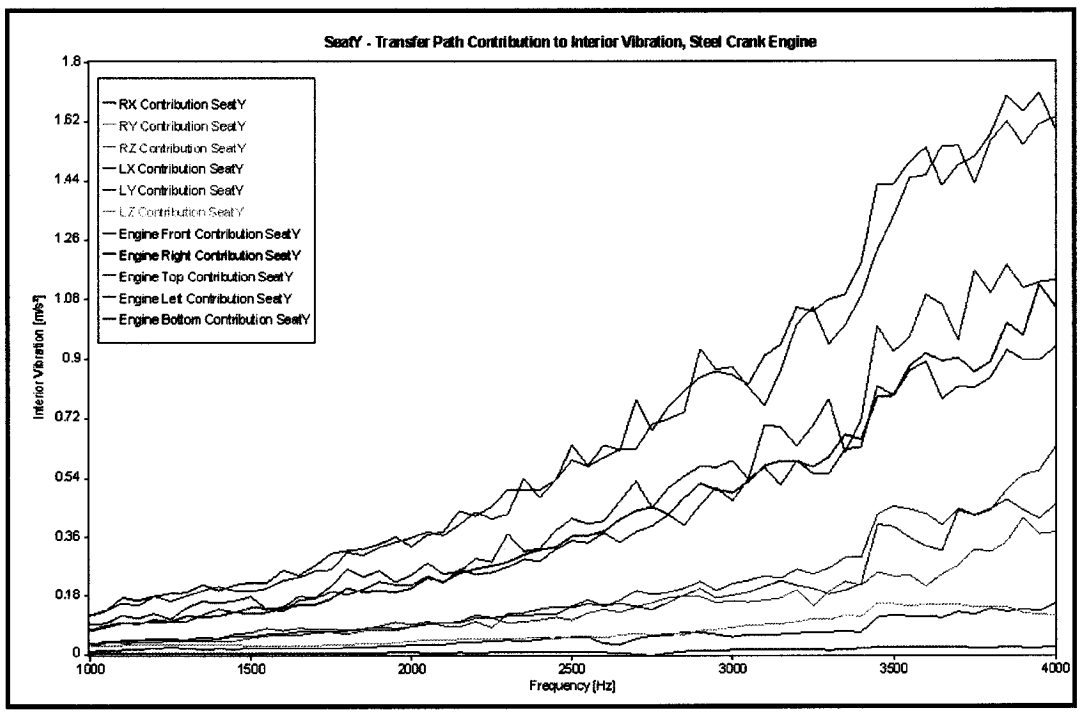

Figure C.10: Transfer Path Contribution to Interior Vibration, Y-direction, Steel Crank Engine.

Reproduced with permission of the copyright owner. Further reproduction prohibited without permission.

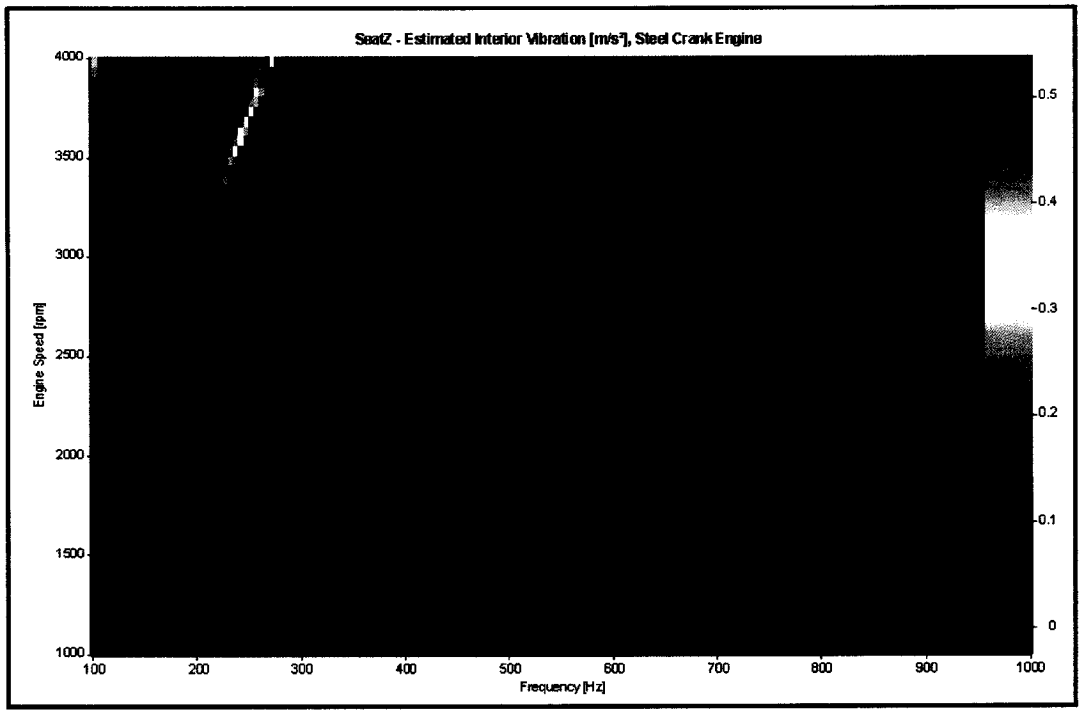

Figure C.11: Estimated Interior Vibration [m/s^2], Z-direction, Steel Crank Engine.

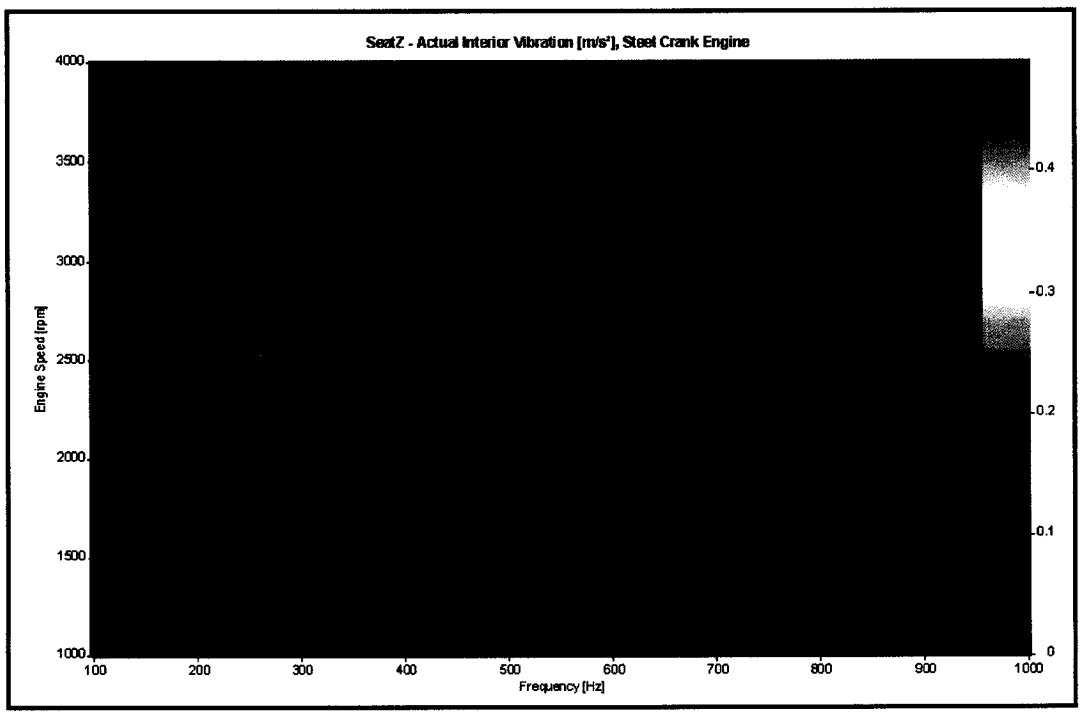

Figure C.12: Actual Interior Vibration [m/s^2], Z-direction, Steel Crank Engine.

Reproduced with permission of the copyright owner. Further reproduction prohibited without permission.

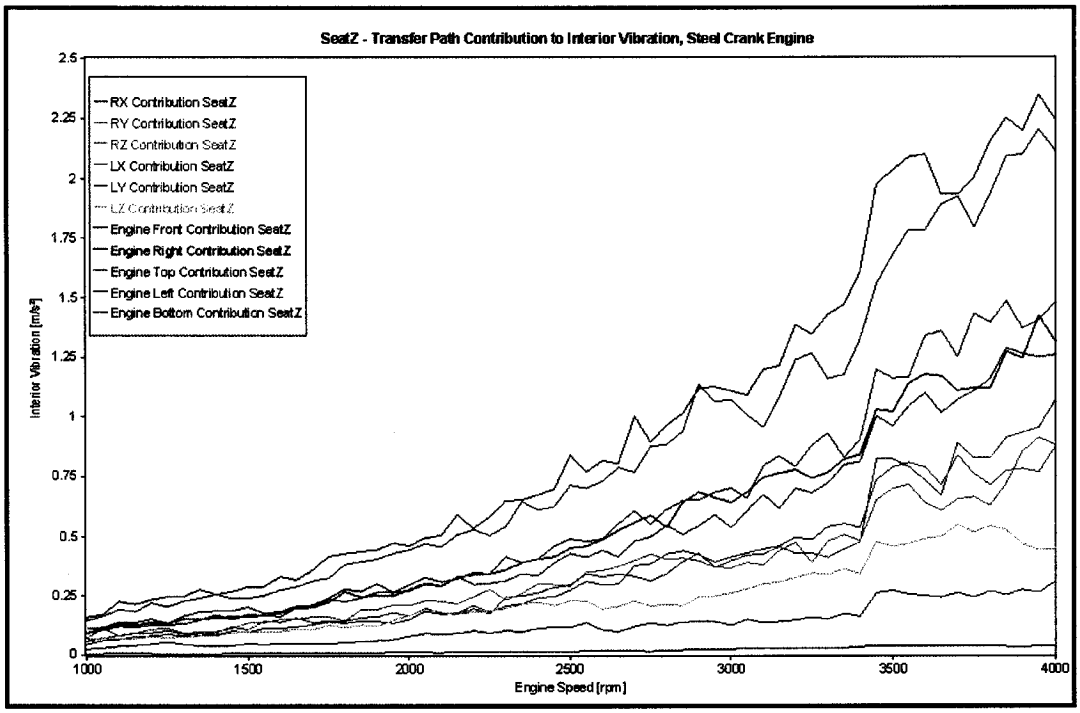

Figure C.13: Transfer Path Contribution to Interior Vibration, Z-direction, Steel Crank Engine.

Reproduced with permission of the copyright owner. Further reproduction prohibited without permission.

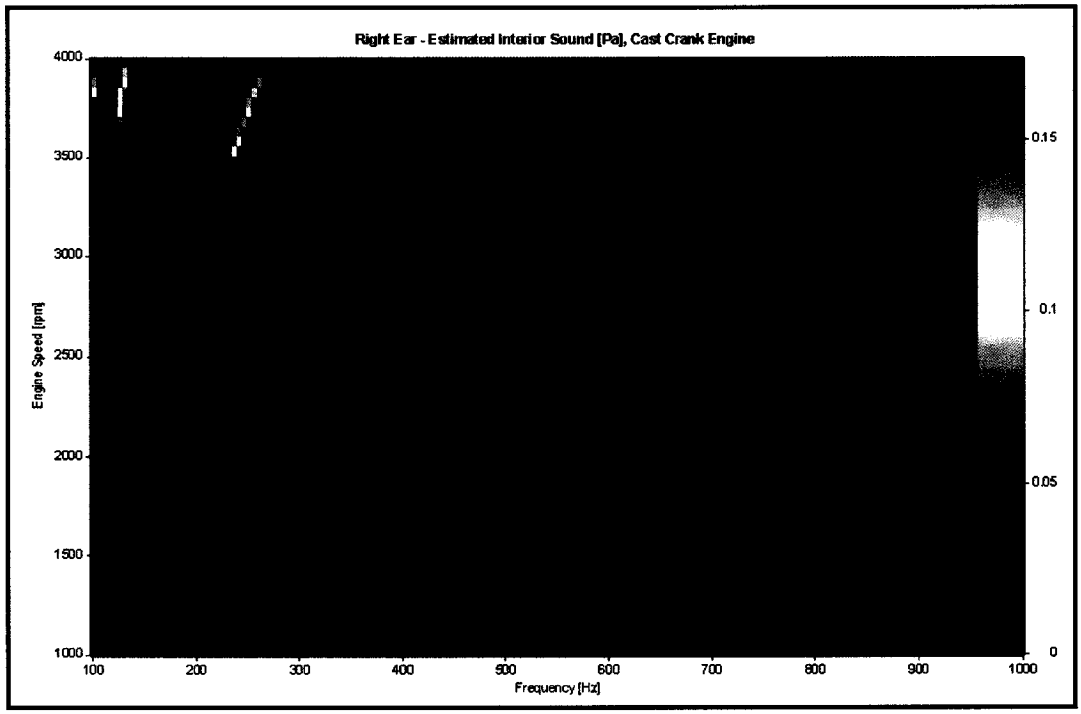

Figure C.14: Estimated Interior Sound [Pa], Right Ear, Cast Crank Engine.

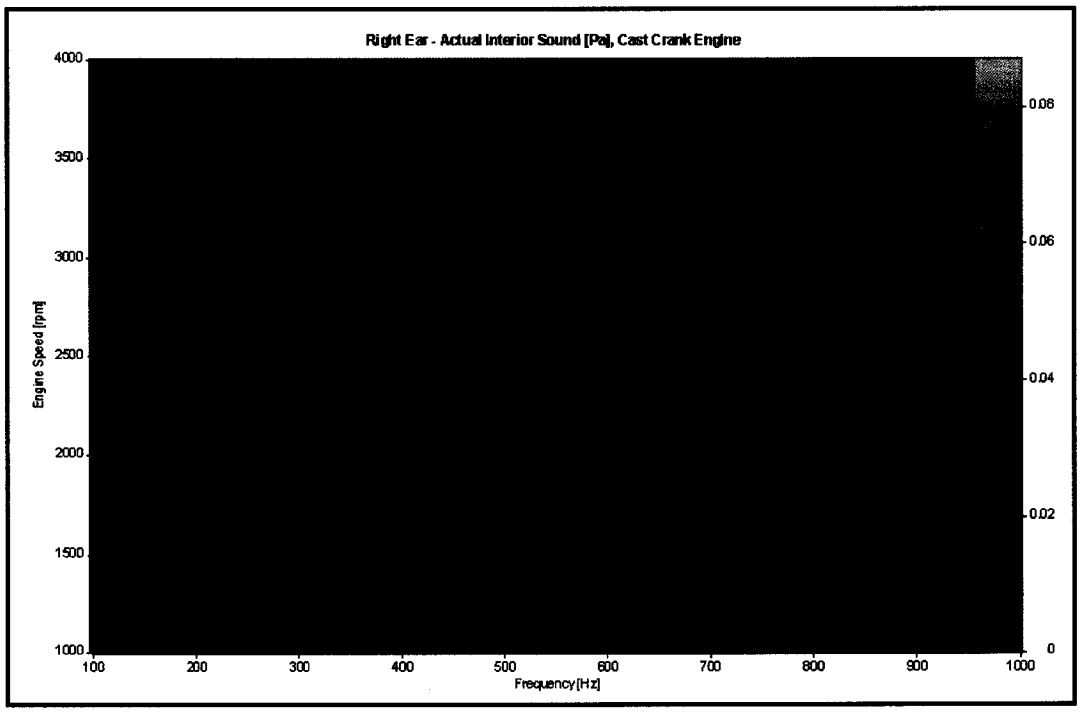

Figure C.15: Actual Interior Sound [Pa], Right Ear, Cast Crank Engine.

Reproduced with permission of the copyright owner. Further reproduction prohibited without permission.

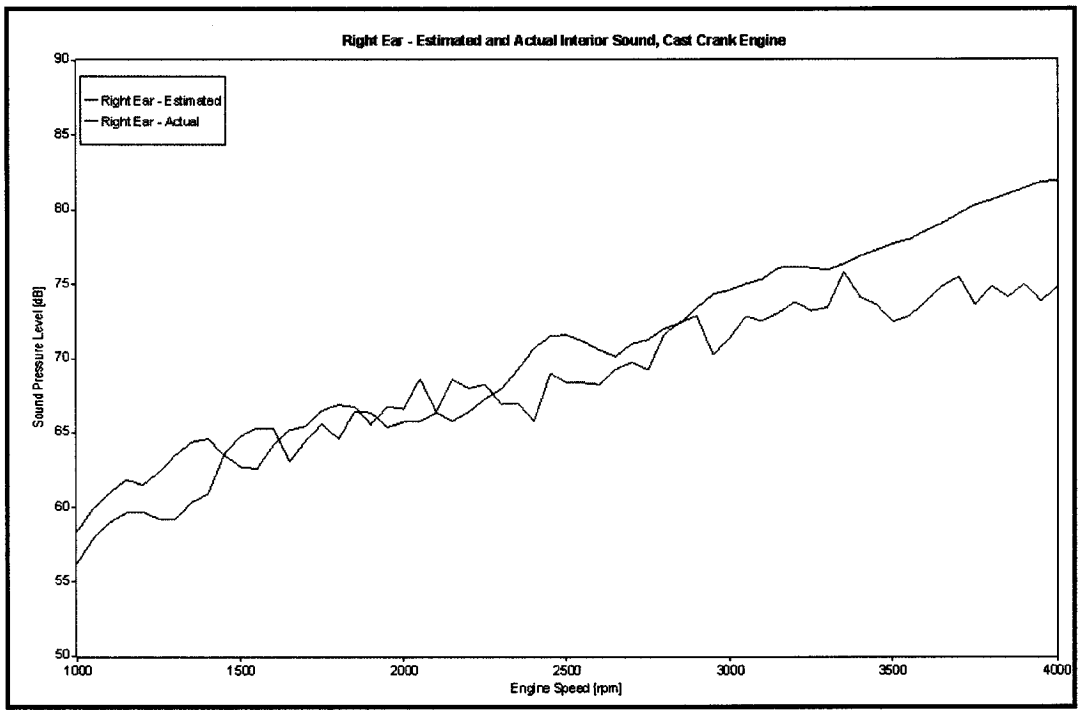

Figure C.16: Estimated and Actual Interior Sound, Right Ear, Cast Crank Engine.

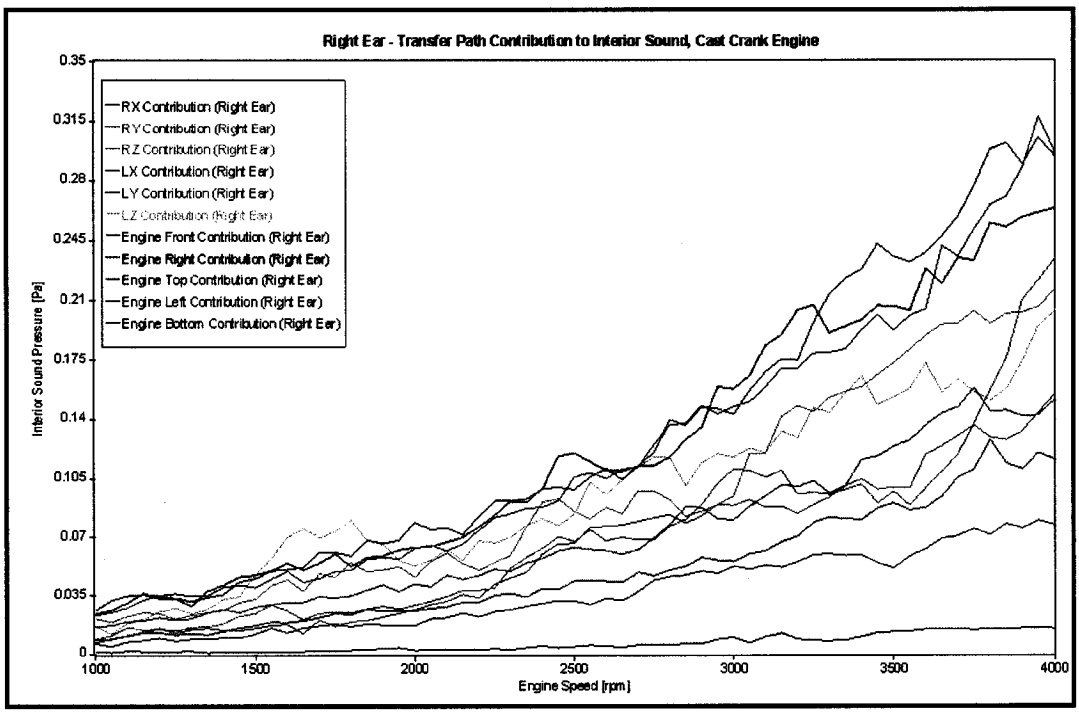

Figure C.17: Transfer Path Contribution to Interior Sound, Right Ear, Cast Crank Engine.

Reproduced with permission of the copyright owner. Further reproduction prohibited without permission.

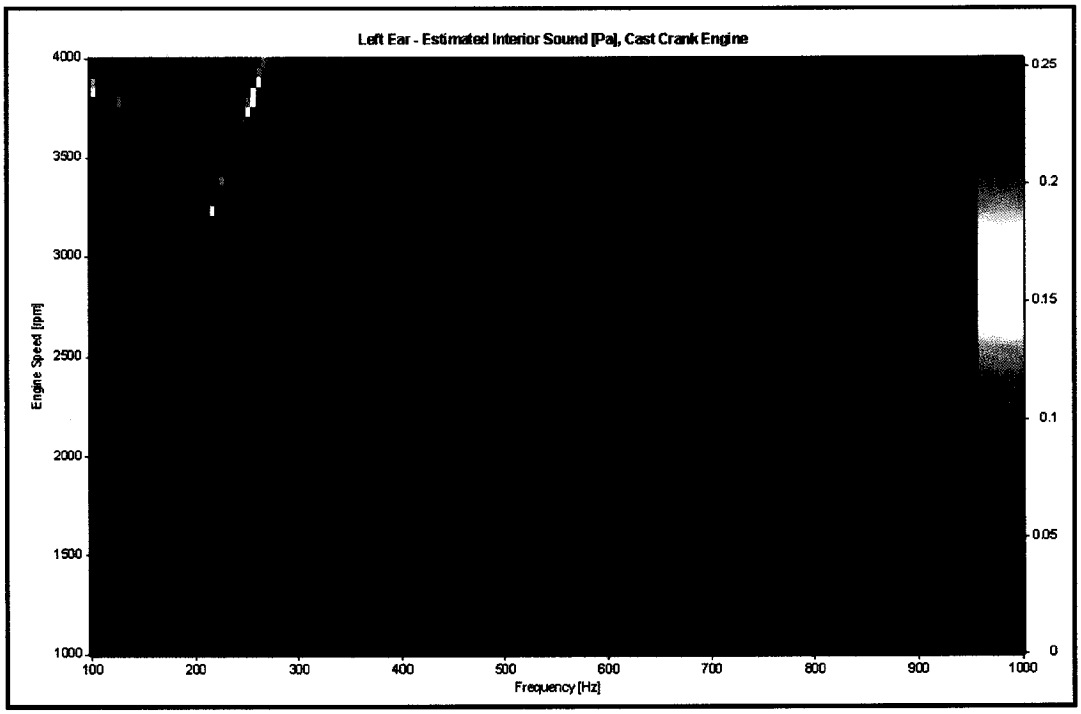

Figure C.18: Estimated Interior Sound [Pa], Left Ear, Cast Crank Engine.

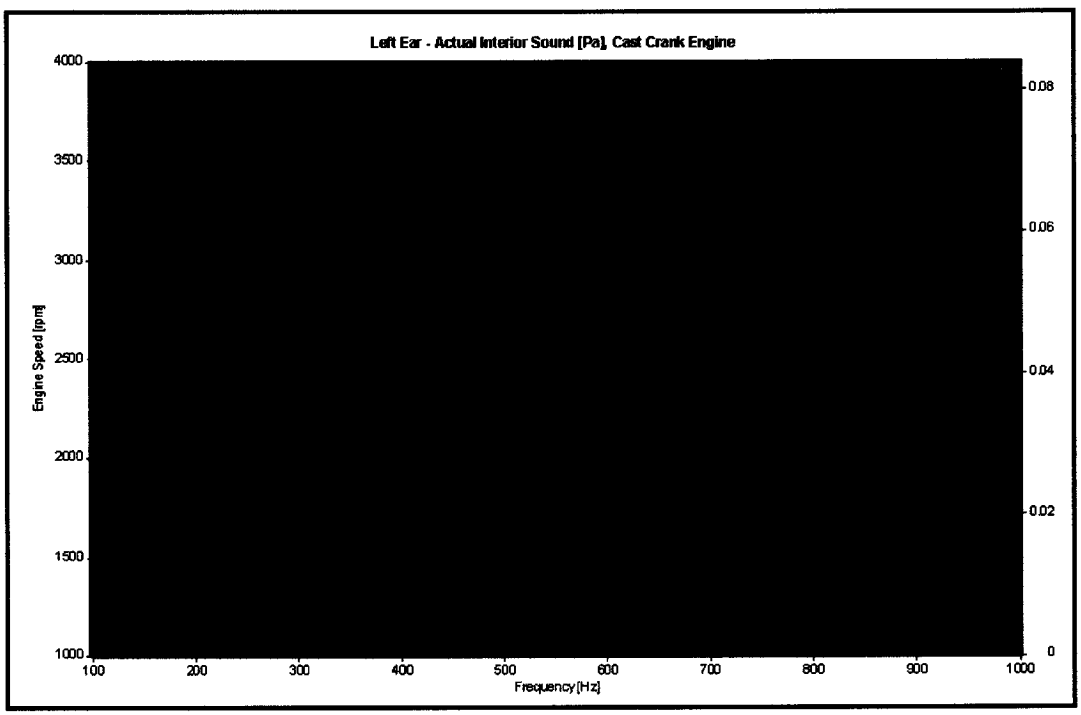

Figure C.19: Actual Interior Sound [Pa], Left Ear, Cast Crank Engine.

Reproduced with permission of the copyright owner. Further reproduction prohibited without permission.

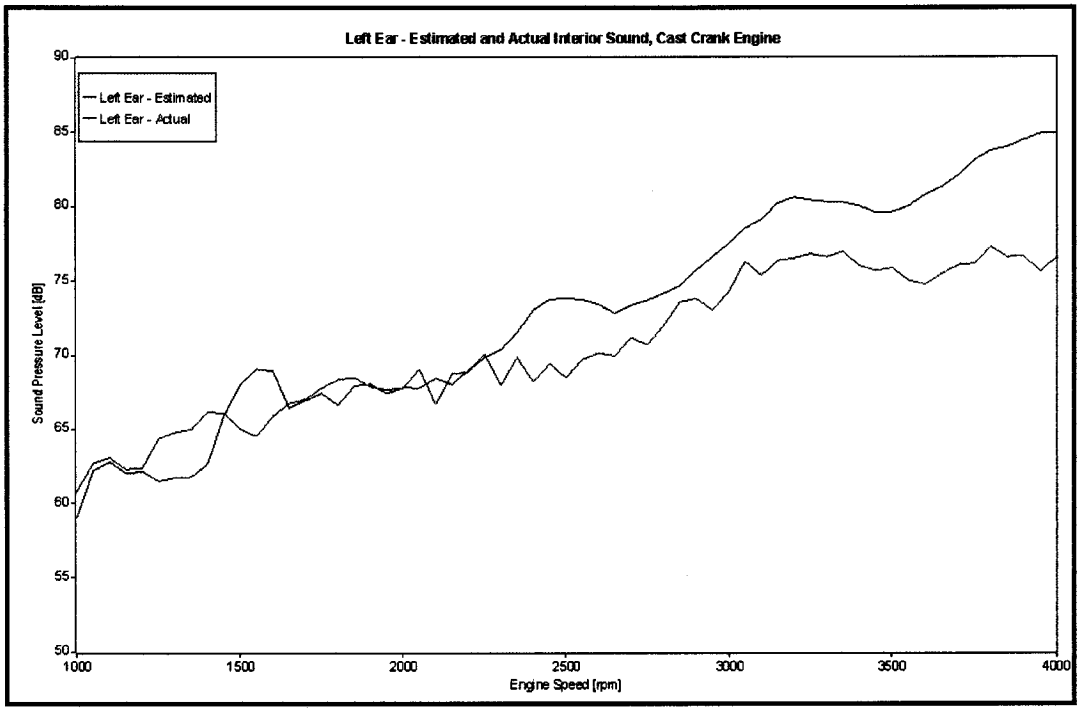

Figure C.20: Estimated and Actual Interior Sound, Left Ear, Cast Crank Engine.

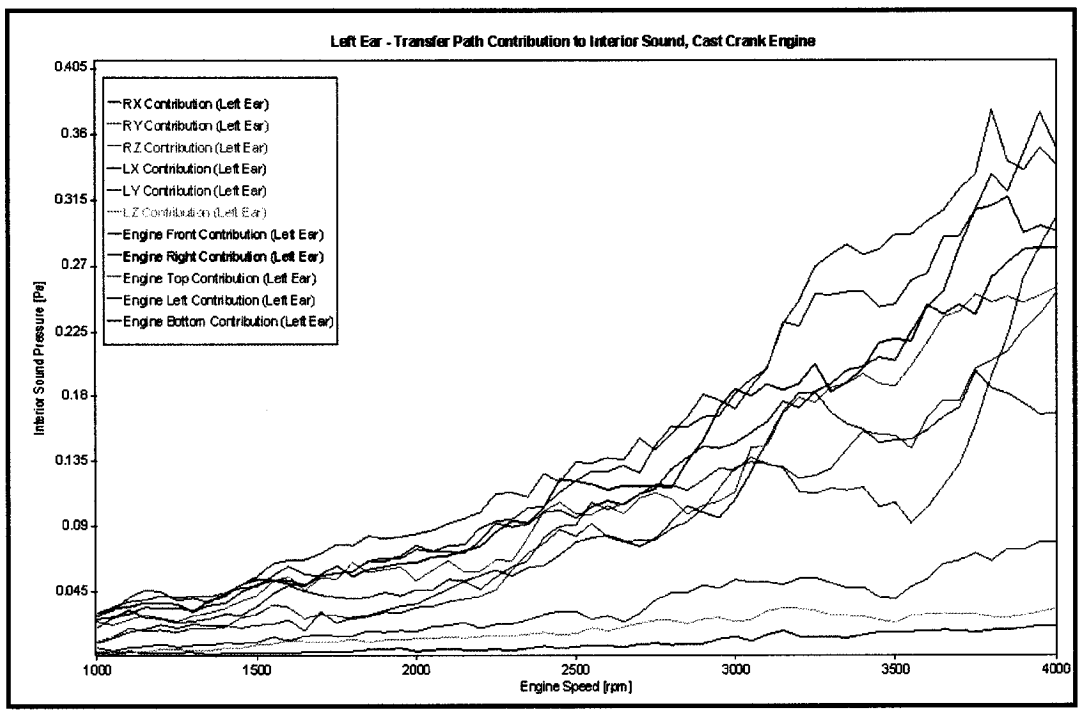

Figure C.21: Transfer Path Contribution to Interior Sound, Left Ear, Cast Crank Engine.

Reproduced with permission of the copyright owner. Further reproduction prohibited without permission.

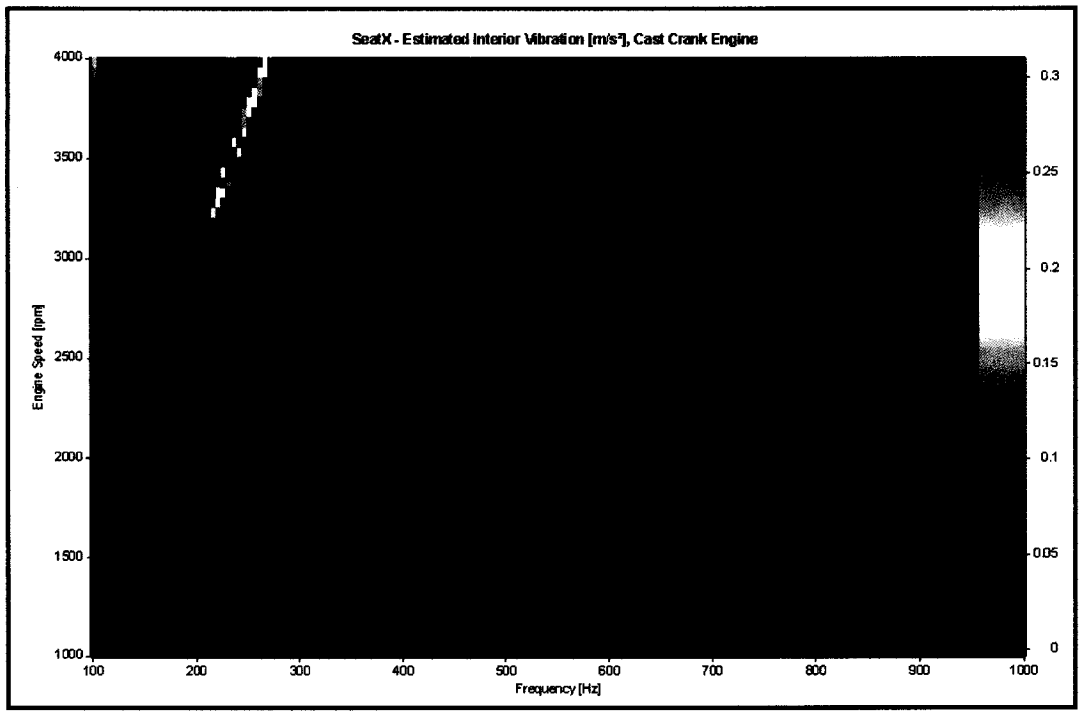

Figure C.22: Estimated Interior Vibration [m/s^2], X-direction, Cast Crank Engine.

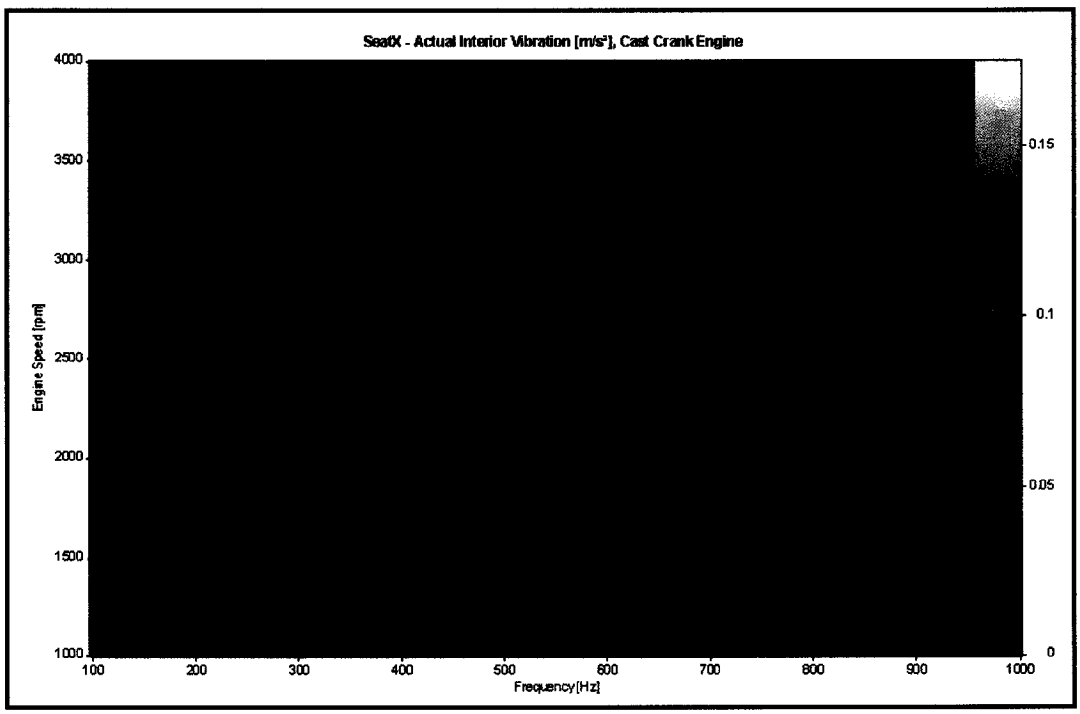

Figure C.23: Actual Interior Vibration [m/s^2], X-direction, Cast Crank Engine.

Reproduced with permission of the copyright owner. Further reproduction prohibited without permission.

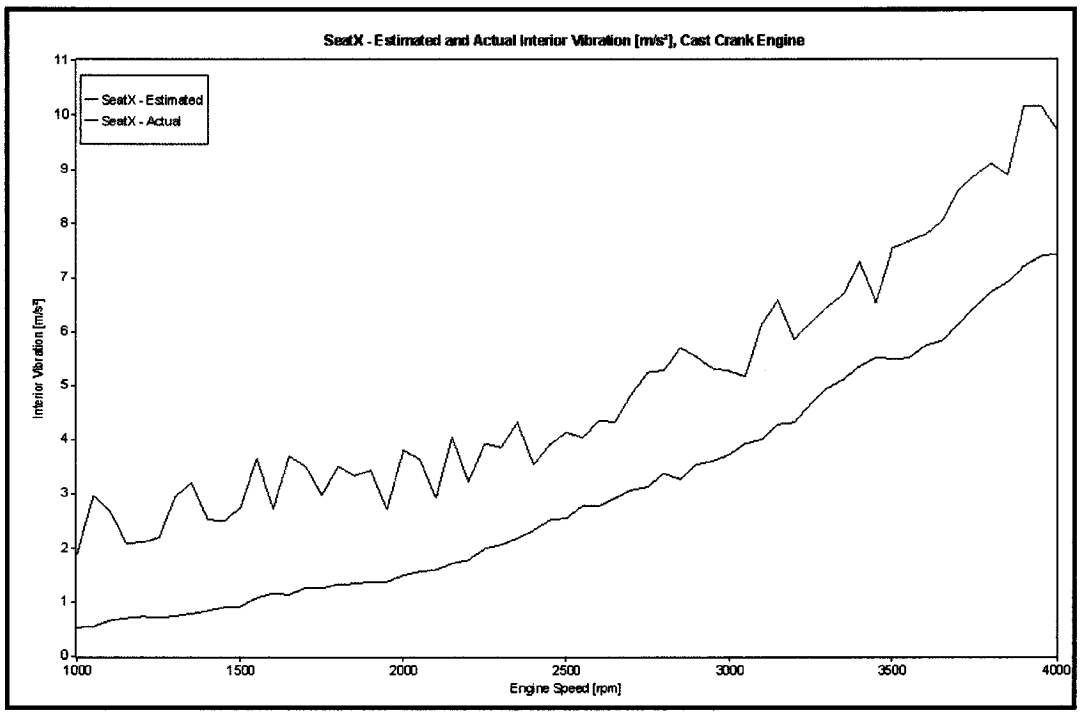

Figure C.24: Estimated and Actual Interior Vibration, X-direction, Cast Crank Engine.

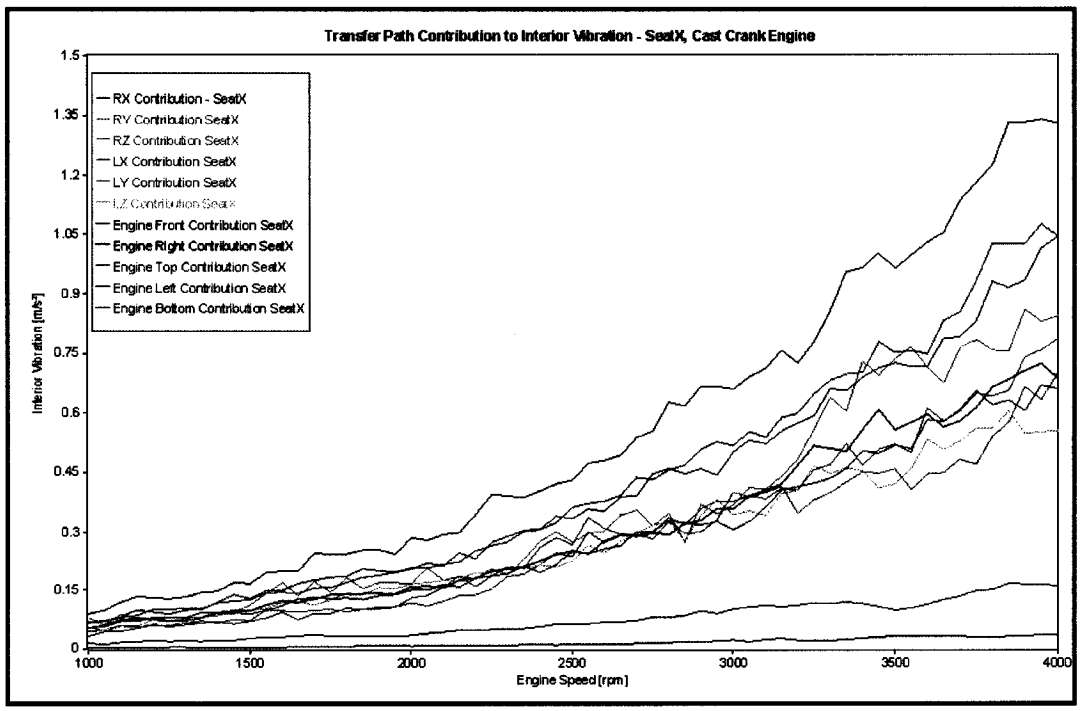

Figure C.25: Transfer Path Contribution to Interior Vibration, X-direction, Cast Crank Engine.

Reproduced with permission of the copyright owner. Further reproduction prohibited without permission.

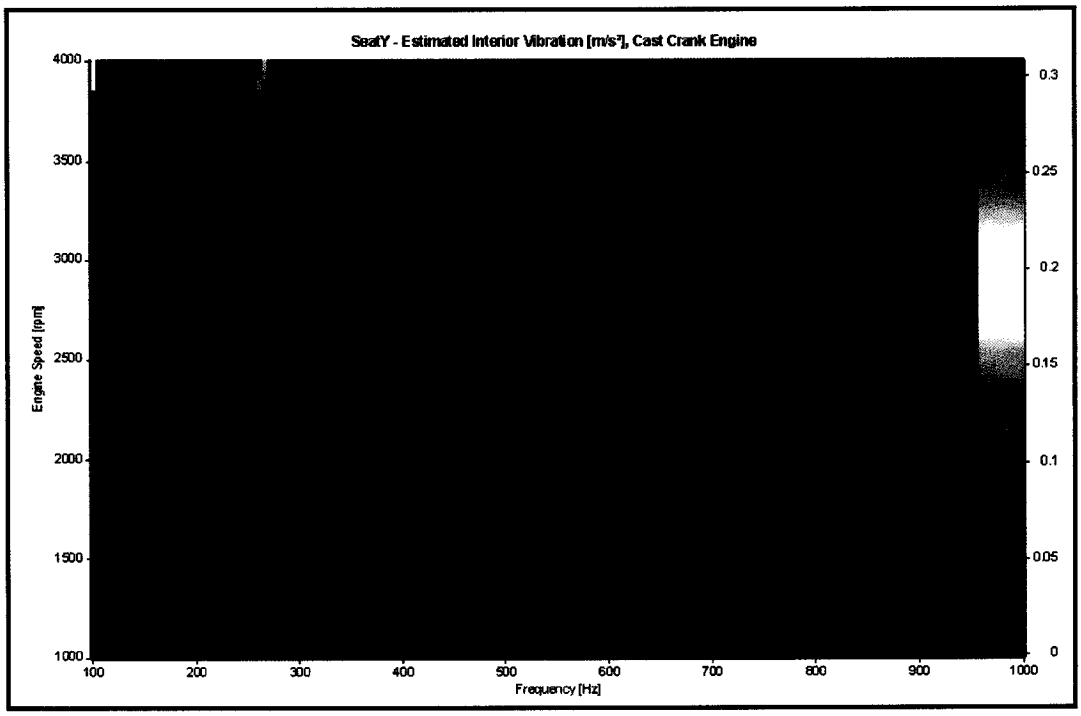

Figure C.26: Estimated Interior Vibration [m/s^2], Y-direction, Cast Crank Engine.

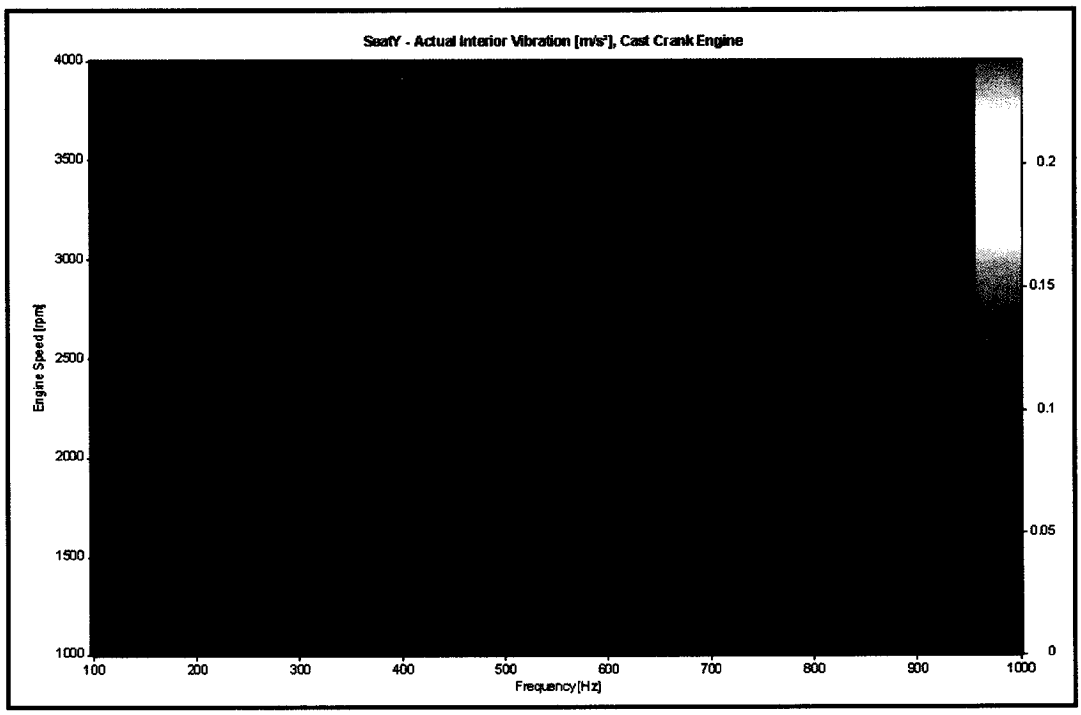

Figure C.27: Actual Interior Vibration [m/s^2], Y-direction, Cast Crank Engine.

Reproduced with permission of the copyright owner. Further reproduction prohibited without permission.

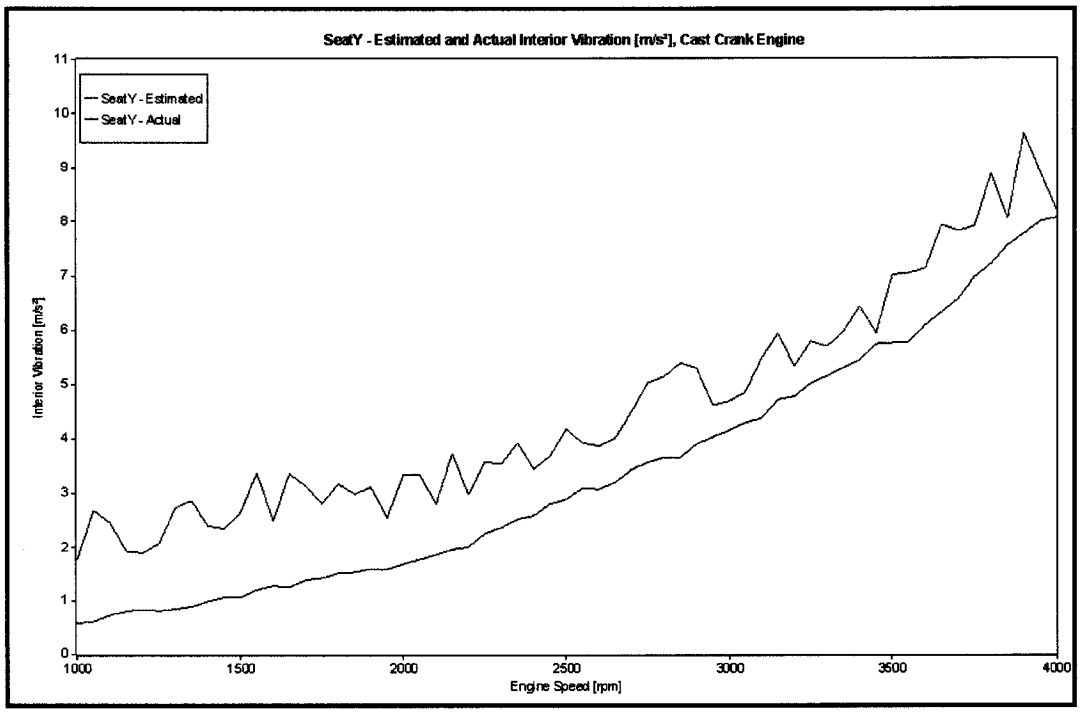

Figure C.28: Estimated and Actual Interior Vibration, Y-direction, Cast Crank Engine.

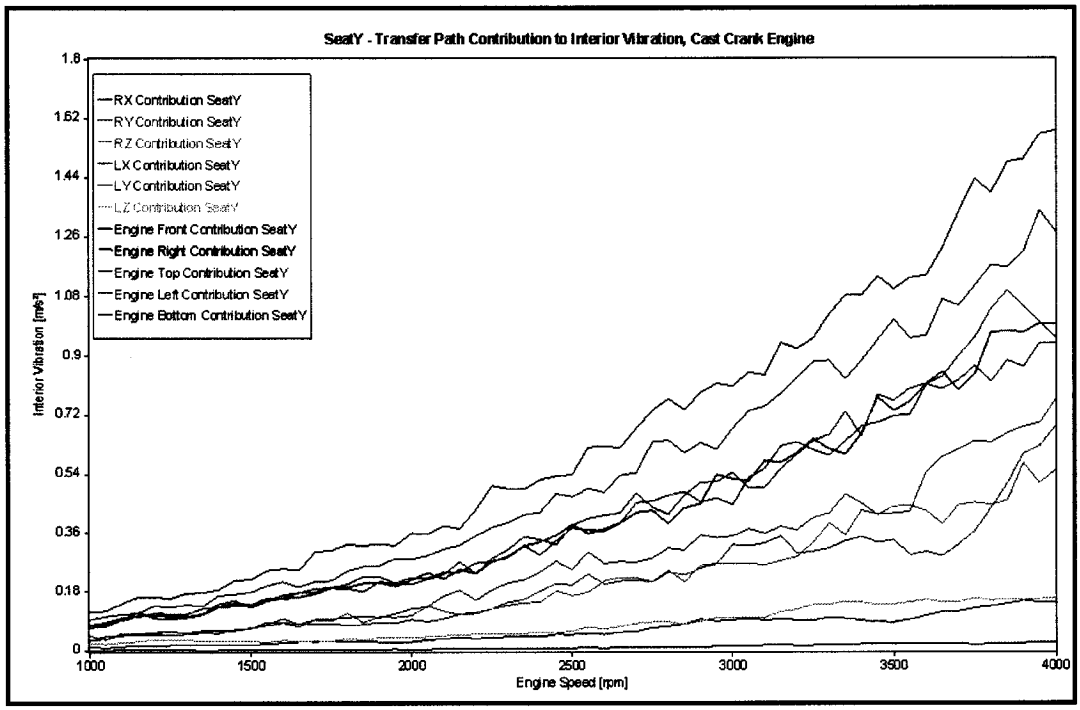

Figure C.29: Transfer Path Contribution to Interior Vibration, Y-direction, Cast Crank Engine.

Reproduced with permission of the copyright owner. Further reproduction prohibited without permission.

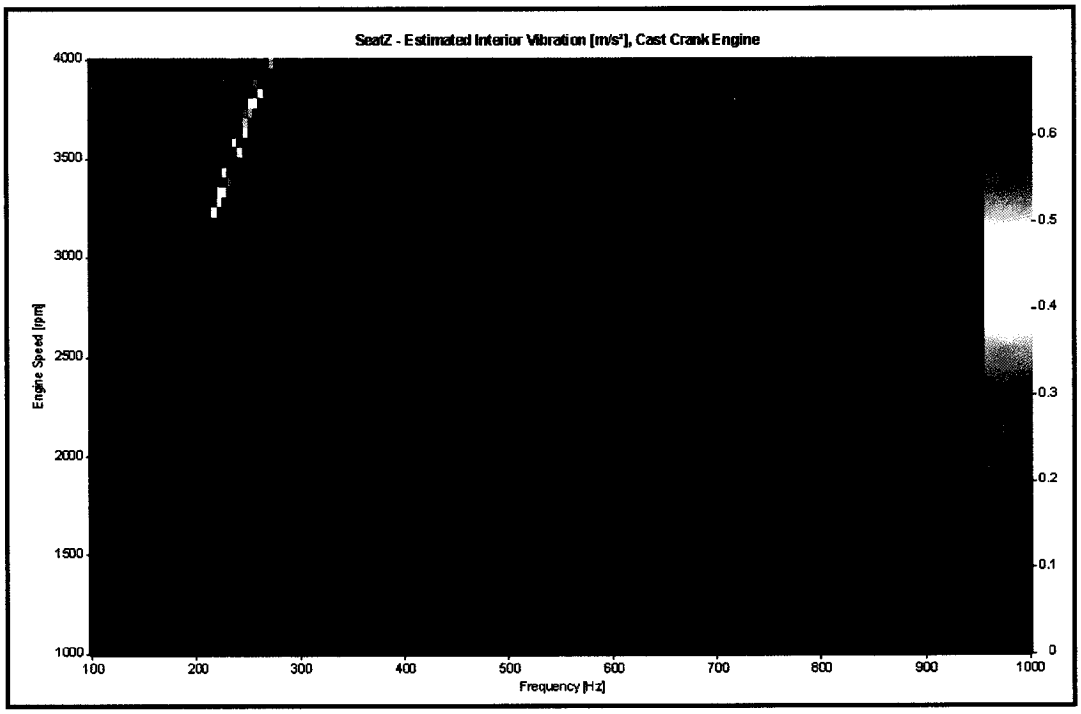

Figure C.30: Estimated Interior Vibration [m/s^2], Z-direction, Cast Crank Engine.

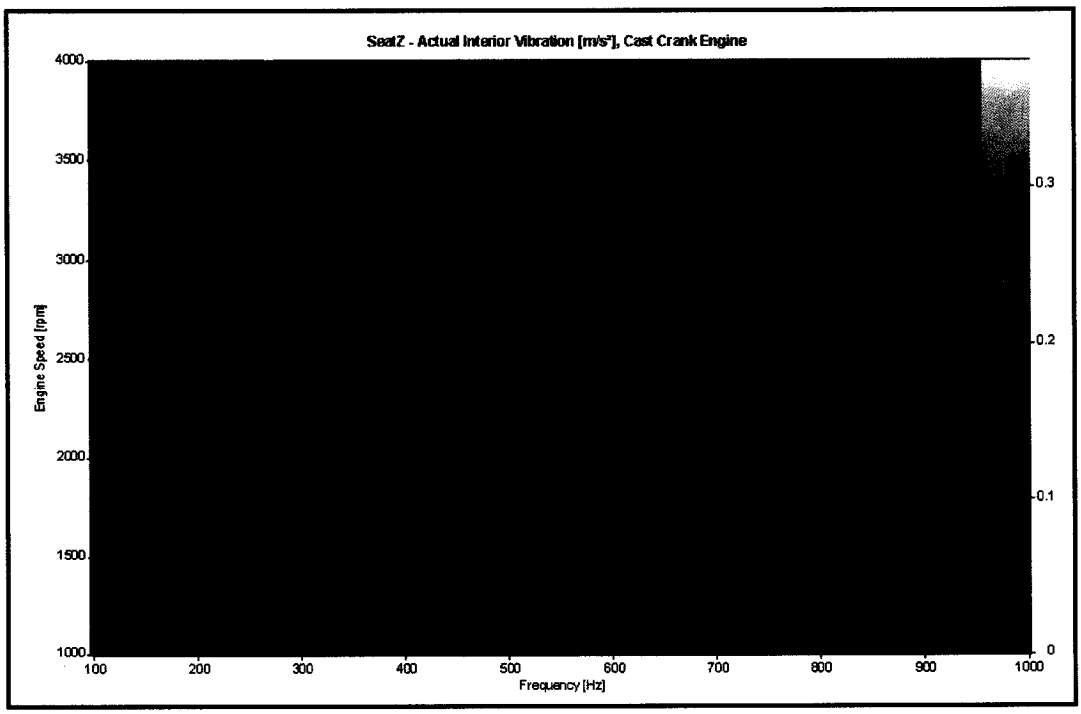

Figure C.31: Actual Interior Vibration [m/s^2], Z-direction, Cast Crank Engine.

Reproduced with permission of the copyright owner. Further reproduction prohibited without permission.

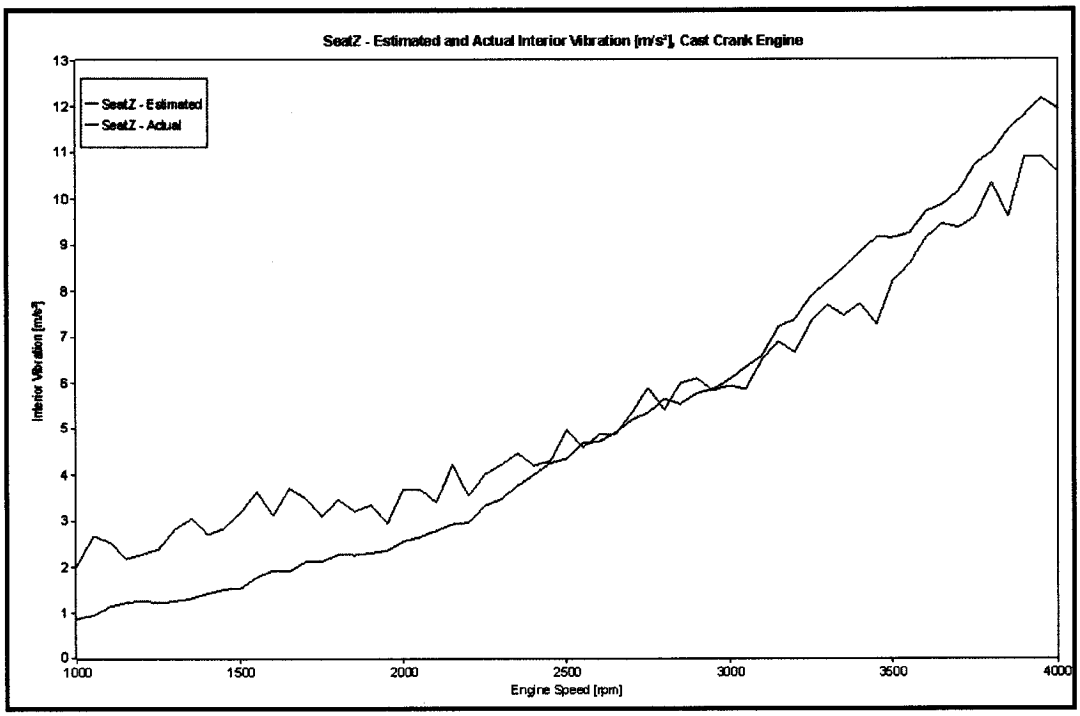

Figure B32: Estimated and Actual Interior Vibration, Z-direction, Cast Crank Engine.

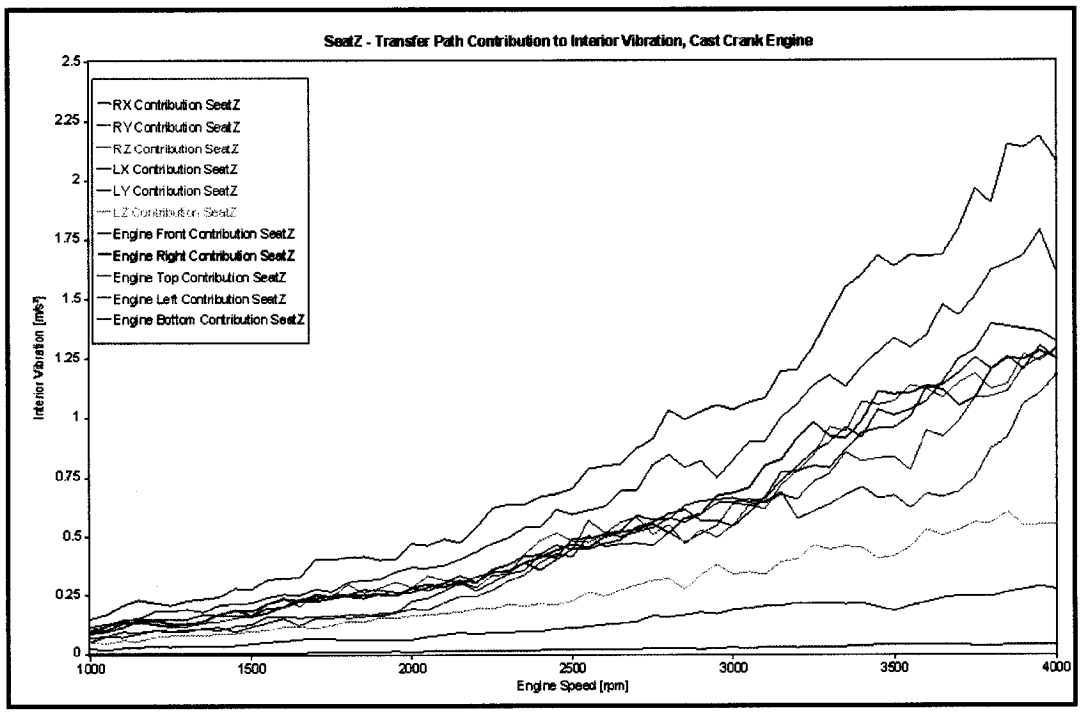

Figure C.33: Transfer Path Contribution to Interior Vibration, Z-direction, Cast Crank Engine.

Reproduced with permission of the copyright owner. Further reproduction prohibited without permission.

D. EQUIPMENT SPECIFICATIONS

Reproduced with permission of the copyright owner. Further reproduction prohibited without permission.

VRS Speed Sensor Model 3010		
Specification	**Value**	**Unit**
Output Voltage	40	V P-P min.
Coil Resistance	45 to 85	Ω
Pole Piece Diameter	2.69	mm
Minimum Surface Speed	0.5	m/s
Inductance	25	mH
Gear Pitch Range	24 or Coarser	DP
Maximum Operating Frequency	50	kHz
Temperature Range	-55 to 120	°C

Figure D.1: Specifications for the VRS 3010 Speed Sensor.

Dytran Triaxial Accelerometer Model 3053B2		
Specification	**Value**	**Unit**
Sensitivity (-10% +15%)	10	mV/g
Range (full scale, each axis)	+/- 500	g
Frequency Range (+/-10%)	2 to 5000	Hz
Resonant Frequency	30	kHz
Linearity (full scale)	1	%
Maximum Transverse Sensitivity	5	%
Maximum Vibration	+/-600	g
Maximum Shock	5000	g
Temperature Range	-50 to +120	°C
Supply Current Range (each axis)	2 to 20	mA
Supply Voltage Range (each axis)	18 to 30	V DC
Output Impedance	100	Ω
Output Bias Voltage	+10	V DC
Discharge Time Constant	0.5	sec
Material, Housing/Connector	Titanium Alloy	
Size (Height x Width x Depth)	13.5 x 12.7 x 12.7	mm
Mass	7.5	grams

Figure D.2: Specifications for the Dytran 3053B2 Triaxial Accelerometer.

Reproduced with permission of the copyright owner. Further reproduction prohibited without permission.

Bruel & Kjaer Calibration Exciter Type 4294		
Specification	**Value**	**Unit**
Frequency (+/-0.02%)	159.15	Hz
Acceleration (+/- 3%)	10	m/s^2 RMS
Velocity (+/- 3%)	10	mm/s RMS
Displacement (+/- 3%)	10	μm RMS
Transverse Amplitude	<5	% of main axis amplitude
Maximum Load	70	grams
Power Supply	9 V alkaline battery	
Size (Length x Diameter)	155 x 52	mm
Mass	500	grams

Figure D.3: Specifications for the Bruel & Kjaer 4294 Calibration Exciter.

HEAD Acoustics Head and Shoulder Unit Model HSU III (Code 1323)		
Specification	**Value**	**Unit**
Microphones	Capacitive Pressure Transducers	
Sensitivity	52.4	mV/Pa
Frequency Range	20 to 20,000	Hz
Polarization Voltage	200	V
Maximum Sound Pressure Level	145	dB
Unweighted Noise Voltage	<3	μV
Analog Output	2 x LEMO 7-pin	
Temperature Range	-20 to +70	°C
Mass	4.3	kg

Figure D.4: Specifications for the HEAD Acoustics HSU III Head and Shoulder Unit.

Reproduced with permission of the copyright owner. Further reproduction prohibited without permission.

Bruel & Kjaer Dual Microphone Supply Type 5935L		
Specification	**Value**	**Unit**
Input Impedance	200	kΩ
Maximum Input Level	5	V RMS
Fixed Gain	0 to 50	dB
Maximum Channel Output Level	5	V RMS
Maximum Channel Output Current	15	mA
Maximum Channel Output Power	20	mW
Frequency Response	0.5 to 100	kHz
Preamplifier Input	LEMO 7-pin socket	
Signal Output	BNC	
Power Supply	3 x 1.5V alkaline battery	
Size (Height x Width x Depth)	132.6 x 69.5 x 200	mm
Mass	1.1	kg

Figure D.5: Specifications for the Bruel & Kjaer 5935L Dual Microphone Supply.

GRAS ½-inch Free-Field Microphone Type 40AF		
Specification	**Value**	**Unit**
Sensitivity	50	mV/Pa
Frequency Response	3.15 to 20,000	Hz
Polarization Voltage	200	V
Upper Limit	148	dB
Capacitance	17	pF
Temperature Range	-40 to +150	°C
Mass	7	grams

Figure D.6: Specifications for the GRAS 40AF ½-inch Free-Field Microphone.

GRAS ½-inch Preamplifier Type 26AJ		
Specification	**Value**	**Unit**
Frequency Response	2 to 200,000	Hz
Input Impedance	20	GΩ
Output Impedance	55	Ω
Output Connector	LEMO 7-pin	
Noise	<6	μV RMS
Power Supply	28 to 120	V
Maximum Signal Output Voltage	+/-10 to +/-50	V
Temperature Range	-30 to +70	°C

Figure D.7: Specifications for the GRAS 26AJ ½-inch Preamplifier.

Reproduced with permission of the copyright owner. Further reproduction prohibited without permission.

GRAS Power Module Type 12AG		
Specification	**Value**	**Unit**
Output Voltage / Preamplifier Supply	28 or 120	V
Polarization Voltage	0 or 200	V
Frequency Response	20 to 20,000	Hz
Inherent Noise	<5.6	μV
Output Impedance	30	Ω
Input Connector	LEMO 7-pin	
Output Connector	BNC	
Temperature Range	-10 to +50	°C
Size (Height x Width x Depth)	132.6 x 215.0 x 196.0	mm
Mass	2.5	kg

Figure D.8: Specifications for the GRAS 12AG Power Module.

Bruel & Kjaer Sound Level Calibrator Type 4321		
Specification	**Value**	**Unit**
Sound Pressure Level	94+/-0.2	dB
Frequency (+/- 0.1%)	1	kHz
Power Supply	2 x 1.5V alkaline battery	
Temperature Range	-25 to +70	°C
Size (Height x Width x Depth)	40 x 72 x 72	mm
Mass	150	grams

Figure D.9: Specifications for the Bruel & Kjaer 4321 Sound Level Calibrator.

Reproduced with permission of the copyright owner. Further reproduction prohibited without permission.

PCB Impact Hammer Model 086D20		
Specification	**Value**	**Unit**
Sensitivity (+/-15%)	0.23	mV/N
Range	+/-22,000	N
Frequency Range (Hard Tip)	1	kHz
Resonant Frequency	>12	kHz
Non-Linearity	<1	%
Excitation Voltage	18 to 30	V DC
Constant Current Excitation	2 to 20	mA
Output Impedance	<100	W
Discharge Time Constant	>1400	sec
Sensing Element	Quarts	
Electrical Connector	BNC	
Head Diameter	51	mm
Tip Diameter	51	mm
Hammer Length	370	mm

Figure D.10: Specifications for the PCB 086D20 Impact Hammer.

Harman/Kardon Loudspeakers Model HK395		
Specification	**Value**	**Unit**
Speakers	3 (2 satellites and 1 subwoofer)	
Total Power	30	W
Input Sensitivity	380	mV RMS
Signal/Noise Ratio	>80	dBA
Frequency Response	45 to 20,000	Hz
Subwoofer Frequency Response	45 to 250	Hz
Satellite Frequency Response	250 to 20,000	Hz
Subwoofer Power	18	W
Satellite Power	6	W
Subwoofer Mass	4.62	kg
Satellite Mass	0.75	kg
Subwoofer Size (Height x Width x Depth)	310 x 160 x 270	mm
Satellite Size (Height x Width x Depth)	124 x 86 x 111.5	mm

Figure D.11: Specifications for the Harman/Kardon HK395 Loudspeakers.

Reproduced with permission of the copyright owner. Further reproduction prohibited without permission.

DACTRON Photon Portable Dynamic Signal Analyzer		
Specification	**Value**	**Unit**
Analog channels	4	
Electronics	Differential amplifier, programmable gain amplifier, anti-aliasing filter, and 24-bit Analog to Digital Converter (ADC).	
Filtering	An analog filter at 300 kHz plus a 160 dB/octave linear-phase digital filter prevent aliasing and phase distortion.	
Frequency range	21	kHz
Voltage Range	+/-10	V
Signal Conditioning	Voltage or ICP sensor	
Resolution	24-bit	
Dynamic Range	110	dBfs
Accuracy	+/-0.15	dB
Signal-to-noise	>95	dB

Figure D.12: Specifications for the DACTRON Photon Portable Dynamic Signal Analyzer.

Prosig P5600 Data Acquisition System		
Specification	**Value**	**Unit**
Analog channels	8	
Anti-alias filter	Butterworth low pass, 48 dB/octave	
Sampling rate	100	kHz
Voltage Range	+/-10V to +/-1.25mV	
Signal Inputs	Direct voltage, ICP, strain gage	
Resolution	16-bit	
Overall Accuracy	+/-10% full scale at gain <1000	

Figure D.13: Specifications for the Prosig P5600 Data Acquisition System.

Reproduced with permission of the copyright owner. Further reproduction prohibited without permission.

VITA AUCTORIS

Nikolina Kojovic was born on November 3, 1980 in Sarajevo, Bosnia and Herzegovina. She graduated from Interlochen Arts Academy, Interlochen, Michigan in 1998. She attended the University of Windsor, Windsor, Ontario where she received the Bachelor of Applied Science in Mechanical Engineering with Automotive Option degree in 2002. Nikolina is currently a member of Ford Powertrain Engineering Research and Development Group and a candidate for the Masters of Applied Science degree in Mechanical Engineering at the University of Windsor.

Reproduced with permission of the copyright owner. Further reproduction prohibited without permission.